



uOttawa

L'Université canadienne
Canada's university

**FACULTÉ DES ÉTUDES SUPÉRIEURES
ET POSTDOCTORALES**



**FACULTY OF GRADUATE AND
POSTDOCTORAL STUDIES**

Ratnambikai Shankar

AUTEUR DE LA THÈSE / AUTHOR OF THESIS

Ph.D. (Electrical Engineering)

GRADE / DEGREE

School of Information Technology and Engineering

FACULTÉ, ÉCOLE, DÉPARTEMENT / FACULTY, SCHOOL, DEPARTMENT

Scalable Optical Switches: Architectures and Physical Layer Characterization

TITRE DE LA THÈSE / TITLE OF THESIS

Trevor J. Hall

DIRECTEUR (DIRECTRICE) DE LA THÈSE / THESIS SUPERVISOR

CO-DIRECTEUR (CO-DIRECTRICE) DE LA THÈSE / THESIS CO-SUPERVISOR

EXAMINATEURS (EXAMINATRICES) DE LA THÈSE / THESIS EXAMINERS

John Cartledge

Robert Gauthier

Gregor Bochmann

Alex Vukovic

Gary W. Slater

Le Doyen de la Faculté des études supérieures et postdoctorales / Dean of the Faculty of Graduate and Postdoctoral Studies

Scalable Optical Switches: Architectures and Physical Layer Characterization

Rathy Shankar

Thesis submitted to the
Faculty of Graduate and Postdoctoral Studies
In partial fulfillment of the requirements
For the PhD degree in Electrical Engineering

Ottawa-Carleton Institute for Electrical and Computer Engineering
School of Information Technology and Engineering
Faculty of Engineering
University of Ottawa

© Rathy Shankar, Ottawa, Canada, 2008



Library and
Archives Canada

Bibliothèque et
Archives Canada

Published Heritage
Branch

Direction du
Patrimoine de l'édition

395 Wellington Street
Ottawa ON K1A 0N4
Canada

395, rue Wellington
Ottawa ON K1A 0N4
Canada

Your file Votre référence
ISBN: 978-0-494-48669-6
Our file Notre référence
ISBN: 978-0-494-48669-6

NOTICE:

The author has granted a non-exclusive license allowing Library and Archives Canada to reproduce, publish, archive, preserve, conserve, communicate to the public by telecommunication or on the Internet, loan, distribute and sell theses worldwide, for commercial or non-commercial purposes, in microform, paper, electronic and/or any other formats.

The author retains copyright ownership and moral rights in this thesis. Neither the thesis nor substantial extracts from it may be printed or otherwise reproduced without the author's permission.

AVIS:

L'auteur a accordé une licence non exclusive permettant à la Bibliothèque et Archives Canada de reproduire, publier, archiver, sauvegarder, conserver, transmettre au public par télécommunication ou par l'Internet, prêter, distribuer et vendre des thèses partout dans le monde, à des fins commerciales ou autres, sur support microforme, papier, électronique et/ou autres formats.

L'auteur conserve la propriété du droit d'auteur et des droits moraux qui protègent cette thèse. Ni la thèse ni des extraits substantiels de celle-ci ne doivent être imprimés ou autrement reproduits sans son autorisation.

In compliance with the Canadian Privacy Act some supporting forms may have been removed from this thesis.

Conformément à la loi canadienne sur la protection de la vie privée, quelques formulaires secondaires ont été enlevés de cette thèse.

While these forms may be included in the document page count, their removal does not represent any loss of content from the thesis.

Bien que ces formulaires aient inclus dans la pagination, il n'y aura aucun contenu manquant.

■*■
Canada

Abstract

Optical switches are the key components in realizing reconfigurable all optical networks. The deployment of optical switches (replacing the conventional electronic switches) at the network nodes enables increased switching capacity and flexibility to data rate, format, and protocol. The scaling of optical networks, while benefiting from optical transparency is however influenced by the accumulations of certain physical impairments, such as interference (crosstalk) and amplifier noises that cannot be entirely eliminated or compensated without the need for signal regeneration.

The objective of this work is to investigate the scalability of various optical switches and networks by using theoretical and experimental models. Integrated directional coupler switches are studied by developing an improved numerical model taking into account of all possible impairments for more accurate representation. New architectural options for large port count wavelength add/drop switches that are modular and cost effective are explored and accessed by making use of the experimental characterization results on the switch modules. Further, the performance aspects of cascading of switches in periodic networks are investigated experimentally by using a re-circulating test bed in the presence of combined physical impairments, and their impact on the tolerance to the switch crosstalk is revealed. Architectural options for the next generation of multi-granularity switching node, consisting of wavelength switches and semiconductor optical amplifier gates, are also explored and their physical layer performance in single and cascaded stages are experimentally characterized for optimum operating conditions.

The models, experimental and numerical, presented in this thesis, can be used to understand and predict the limitations due to various impairments in optical switches and networks and to design those systems by comparing different switching configurations and system parameters for an optimized performance, for any given set of requirements.

Contents

| | |
|---|-------------|
| Abstract | i |
| List of Tables..... | vii |
| List of Figures..... | viii |
| List of Acronyms..... | xii |
| Acknowledgements..... | .xv |
| | |
| 1 Introduction..... | 16 |
| 1.1 Objective and motivation..... | 17 |
| 1.2 Thesis organization..... | 18 |
| | |
| 2 Optical switching: background and state of the art | 20 |
| 2.1 Elements of an optical network | 20 |
| 2.1.1 OLT..... | 21 |
| 2.1.2 OADM..... | 21 |
| 2.1.3 OXC..... | 22 |
| 2.2 Optical switching: classification and applications..... | 23 |
| 2.2.1 Fiber or space switching | 23 |
| 2.2.2 Wavelength switching | 23 |
| 2.2.3 Packet switching | 24 |
| 2.2.4 Multi-granularity switching..... | 24 |
| 2.3 Characteristics of OXCs | 24 |
| 2.3.1 Blocking characteristics..... | 24 |
| 2.3.2 Optical performance | 25 |
| 2.4 Switch architectures..... | 26 |
| 2.4.1 Wave path architectures..... | 26 |
| 2.4.1.1 Wavelength layered switch..... | 27 |
| 2.4.1.2 Broadcast and select switches..... | 27 |
| 2.4.2 Virtual wave path architectures | 28 |
| 2.5 Switch technologies | 29 |
| 2.6 Wavelength conversion technologies | 31 |
| 2.7 Scalability | 31 |

| | | |
|----------|--|-----------|
| 2.7.1 | Crosstalk or interferometric noise | 32 |
| 2.7.2 | Insertion loss..... | 33 |
| 3 | Core switch architectures for Agile All Photonic Network | 34 |
| 3.1 | Agile All Photonic Network | 34 |
| 3.2 | Core node: functions and requirements | 35 |
| 3.3 | Switch architectures..... | 37 |
| 3.3.1 | DC switch | 37 |
| 3.3.2 | Broadcast and select (B&S) switch | 37 |
| 3.3.2.1 | Multistage options | 40 |
| 3.3.3 | AWG and TWC | 42 |
| 3.4 | Scalability of the switches | 43 |
| 3.4.1 | Crosstalk model | 43 |
| 3.4.2 | Wavelength layered switch..... | 44 |
| 3.4.3 | B&S switch..... | 45 |
| 3.4.4 | AWG and TWC | 46 |
| 3.5 | Performance evaluation and comparison..... | 46 |
| 3.5.1 | Wavelength layered switch..... | 46 |
| 3.5.2 | Broadcast and select switch..... | 48 |
| 3.5.3 | AWG and TWC | 49 |
| 3.5.4 | Architectural choices for different switch scales..... | 50 |
| 3.6 | Summary..... | 50 |
| 4 | Performance analysis and scalability of directional coupler switches..... | 52 |
| 4.1 | Directional coupler switches: state of the art..... | 53 |
| 4.1.1 | DC element | 54 |
| 4.1.2 | Sources of loss and crosstalk in DC based switches..... | 54 |
| 4.2 | Switch architectures for DC based switches..... | 56 |
| 4.2.1 | Crossbar and Double cross bar | 56 |
| 4.2.2 | Clos..... | 57 |
| 4.2.3 | Spanke..... | 59 |
| 4.2.4 | Modified binary tree or Omega | 60 |
| 4.3 | Performance comparison of DC switch architectures | 61 |
| 4.3.1 | Switch elements | 62 |

| | | |
|----------|---|-----------|
| 4.3.2 | Switch insertion loss | 62 |
| 4.4 | Noise analysis | 64 |
| 4.4.1 | In-band crosstalk | 65 |
| 4.4.2 | ASE noise | 65 |
| 4.4.2.1 | Amplifier model..... | 65 |
| 4.4.2.2 | Beat noise variances due to ASE | 66 |
| 4.5 | BER and power penalty calculations | 66 |
| 4.5.1 | BER by weighted averaging | 67 |
| 4.5.2 | Thermal and shot noise detection | 67 |
| 4.5.3 | ASE noise limited detection | 69 |
| 4.5.3.1 | Impact of decision threshold on ASE induced penalty..... | 69 |
| 4.5.3.2 | Impact of decision threshold on the tolerance to crosstalk in the presence of ASE. 70 | |
| 4.6 | DC switch design: an example | 71 |
| 4.7 | Summary..... | 73 |
| 5 | ROADMs based on wavelength selective switches: architectures for multi-degree ROADMs and performance characterization in terms of crosstalk..... | 75 |
| 5.1 | Introduction..... | 76 |
| 5.1.1 | ROADM architectures and technologies..... | 76 |
| 5.1.2 | ROADM performance in terms of crosstalk..... | 77 |
| 5.1.3 | Organization of this work | 77 |
| 5.2 | WSS-based ROADM configurations..... | 78 |
| 5.3 | Crosstalk analysis applied to different WSS-based ROADM configurations | 79 |
| 5.4 | Experiments | 81 |
| 5.4.1 | Crosstalk measurements | 81 |
| 5.4.2 | Measurements of BER and power penalty estimation..... | 83 |
| 5.5 | Large degree ROADM or WXC..... | 85 |
| 5.5.1 | Crosstalk performance | 87 |
| 5.6 | Summary..... | 90 |
| 6 | Scaling limitations of NZ-DSF ring networks constructed with WSS-based ROADMs | 91 |
| 6.1 | Introduction..... | 91 |
| 6.2 | Re-circulating loop | 92 |

| | | |
|----------|---|------------|
| 6.2.1 | Experimental set up | 93 |
| 6.2.2 | Loop Operation | 94 |
| 6.2.3 | Simulation Model/Numerical modeling | 95 |
| 6.2.4 | Results and discussion | 98 |
| 6.2.5 | Analytical modeling..... | 100 |
| 6.3 | Numerical study on the cascadability of WSS by using the RCL | 102 |
| 6.3.1 | Network model | 102 |
| 6.3.2 | Simulation model: periodic add/drop | 103 |
| 6.3.3 | Simulation results | 104 |
| 6.3.3.1 | The impact of fiber dispersion on the tolerance to WSS crosstalk..... | 104 |
| 6.3.3.2 | Large degree WSS-based ROADMs..... | 107 |
| 6.3.3.3 | The impact of channel filtering on the cascadability..... | 109 |
| 6.4 | Summary..... | 110 |
| 7 | Physical layer characterization of optical transport networks supporting heterogeneous switch architectures..... | 112 |
| 7.1 | Introduction..... | 113 |
| 7.2 | Heterogeneous switch architecture | 114 |
| 7.3 | SOA technology..... | 116 |
| 7.3.1 | SOA structure | 116 |
| 7.3.2 | Polarization issues and techniques for compensation..... | 117 |
| 7.3.3 | Multiple quantum- well (MQW) SOAs..... | 118 |
| 7.3.4 | Quantum dot (QD) SOAs | 118 |
| 7.3.5 | Gain-clamped SOAs (GC-SOA)..... | 119 |
| 7.4 | Characterization of SOA..... | 119 |
| 7.4.1 | SOA and driver unit..... | 119 |
| 7.5 | Characterization of the heterogeneous switch in systems | 122 |
| 7.5.1 | Single channel configuration | 123 |
| 7.5.1.1 | The impact of gain compression and gain dynamics..... | 123 |
| (b) | 125 | |
| 7.5.2 | Multi-channel systems | 125 |
| 7.5.2.1 | FWM..... | 126 |
| 7.5.2.2 | Cross gain modulation (XGM) | 127 |
| 7.5.2.3 | Penalty due to gain compression for multiple channel operation..... | 128 |
| 7.5.3 | Dynamic routing | 130 |

| | | |
|----------|--|------------|
| 7.5.4 | The effect on cascading of SOA gates in periodic networks..... | 133 |
| 7.5.5 | Summary and discussion on switch characterization | 135 |
| 7.5.6 | Performance comparison between SOA switch structures | 136 |
| 7.6 | Summary..... | 137 |
| 8 | Conclusions and future directions..... | 139 |
| 8.1 | Conclusions..... | 139 |
| 8.2 | Original contributions..... | 142 |
| 8.3 | Future directions | 143 |
| | References..... | 144 |

List of tables

| | |
|---|-----|
| Table 3.1. Core node details and switch technologies..... | 50 |
| Table 4.1. Expressions of switch characteristics for the architecture types discussed in Sec. 4.2. N is the switch dimension, l_c DC IL, l_x the waveguide crossover loss, l_{w-f} fiber-to-waveguide loss, x_c DC crosstalk, and x_x is crossover crosstalk..... | 61 |
| Table 4.2. Worst case IL and crosstalk. l_c and X_c are the losses of DC and crossover, respectively, in dB; l_x and X_x are the crosstalk of DC and crossover, respectively, in dB. | 72 |
| Table 5.1 ROADM configurations and their features | 76 |
| Table 5.2. Total in-band crosstalk in an eight degree ROADM..... | 83 |
| Table 5.3. Equations for the number of WSSs required, insertion loss, and in-band crosstalk of a WXC node..... | 86 |
| Table 5.4. Total crosstalk of a signal traversing S number of nodes..... | 89 |
| Table 6.1. The components and their key parameters that are used for the numerical model. | 96 |
| Table 7.1. Comparison of main parameters from different SOA structures..... | 119 |
| Table 7.2. Power penalties incurred at different input powers for bit rates of 2.5 Gb/s and 622 Mb/s..... | 124 |
| Table 7.3. A comparison between the two SOA switch structures. | 137 |

List of Figures

| | |
|---|----|
| Fig. 2.1. Optical network: a generic example..... | 20 |
| Fig. 2.2. Wavelength layered switch. | 27 |
| Fig. 2.3. B&S architecture. | 28 |
| Fig. 2.4. VWP switch realized using AWG and TWC | 28 |
| Fig. 3.1. AAPN topology: overlaid star..... | 35 |
| Fig. 3.2. Spanke-Benes structure: partitioned 16×16 rearrangeable nonblocking switch [53]. | 37 |
| Fig. 3.3 The architecture of the B&S switch [26]..... | 38 |
| Fig. 3.4. Architectural options for the selection stage. (a) SOAs with combiner and demultiplexer; (b) SOA s with AWG..... | 39 |
| Fig. 3.5. Causes of coherent crosstalk (main signal- solid line, crosstalk- broken line). | 39 |
| Fig. 3.6. Rearrangeable nonblocking three stage Clos architecture | 40 |
| Fig. 3.7. Total number of SOAs required as a function of number of wavelengths per fiber. | 41 |
| Fig. 3.8. Three stage Clos architecture by using AWGs and TWCs. | 42 |
| Fig. 3.9. Power penalty vs element crosstalk for $Q=7$ (BER =10 ⁻¹²) and extinction ratio, $r=20$ | 47 |
| Fig. 3.10. Element crosstalk vs switch port counts for single stage and multistage switches. | 48 |
| Fig. 3.11. Component crosstalk requirement as function of fiber port counts. | 49 |
| Fig. 4.1. Directional coupler | 54 |
| Fig. 4.2. Sources of insertion loss and crosstalk in a DC based optical switch..... | 55 |
| Fig. 4.3. Switch architectures (a) Crossbar (b) Double crossbar | 56 |
| Fig. 4.4. Clos architecture..... | 57 |
| Fig. 4.5. Spanke architecture (a) type I (b) type II | 59 |
| Fig. 4.6. Construction of Omega architecture from binary tree. (a) 4 x 4 binary tree (b) Rearranged layout of 4 x 4 binary tree (c) 4 x 4 Omega architecture (d) Configuration of an $N \times N$ Omega architecture..... | 60 |
| Fig. 4.7. Total number of switching elements required versus switch dimension..... | 62 |
| Fig. 4.8. Worst case IL versus switch dimension. DC IL = 0.5 dB, and fiber-to- waveguide loss =1 dB (a) Crossover loss = 0.2 dB (b) Crossover loss =0 dB | 63 |

| | |
|---|----|
| Fig. 4.9. Single crossover loss needed versus switch dimension for a given total IL of -30 dB, DC IL = -0.5 dB, and fiber- to-waveguide loss = -1 dB..... | 64 |
| Fig. 4.10. PP versus element crosstalk. | 68 |
| Fig. 4.11. (a) PP versus normalized decision threshold: single amplifier-IL= 10 dB (solid lines) and 17 dB (dashed lines) for $r=0.02$ ('+') and $r=0.1$ ('□'); two amplifiers for IL= 17 dB and $r=0.1$ (dash-dot line). (b) Receiver loss versus normalized decision threshold. | 70 |
| Fig. 4.12. PP versus element crosstalk. | 71 |
| Fig. 4.13. PP versus element crosstalk. | 73 |
| Fig. 5.1. Two degree ROADM module constructed using two WSS, each for add and drop. | 78 |
| Fig. 5.2. Multiple-degree ROADM architectures: (a) WSSs for add and drop; (b) Splitters for drop and WSSs for add; (c) WSSs for drop and combiners for add..... | 79 |
| Fig. 5.3. The functional diagram of the WSS [19], consisting a 2-layer stack of arrays of waveguide gratings, lenses and MEMS array. Thick gray line indicates the main signal, switched to the selected port, 'S', and the broken and dash and dot lines indicate crosstalk to non-selected ports, 'x1' and 'x2', respectively. | 79 |
| Fig. 5.4. Crosstalk in WSS-based ROADM: (a) WSSs for add and drop; (b) Splitters for drop and WSS for add; (c) WSS for drop and combiners for add. Thick gray lines indicate the main signal and the broken lines indicate the interfering signals or crosstalk..... | 80 |
| Fig. 5.5. Experimental setups for measuring crosstalk powers and BER of a WSS: (a) passive split and WSS add; (b) WSS drop and passive combine..... | 82 |
| Fig. 5.6. BER measurements: (a) WSS add, set up as in Fig. 5.5(a); (b) WSS drop, set up as in Fig. 5.5(b)..... | 84 |
| Fig. 5.7. Large degree WXC architecture. | 85 |
| Fig. 5.8. Power penalty as function of WXC node degree. (a) Optimum decision threshold; (b) Midway decision threshold..... | 88 |
| Fig. 5.9. WSS crosstalk as function of node degree at 1 dB of penalty. | 89 |
| Fig. 6.1 (a) Experimental set up (b) The timing diagram..... | 93 |
| Fig. 6.2. RCL model implemented with VPI..... | 95 |
| Fig. 6.3. EDFA gain and NF vs input power. | 97 |
| Fig. 6.4. WSS filtering characteristics; amplitude and group delay as a function of frequency. | 97 |
| Fig. 6.5. Experimental (closed symbol) Vs theoretical results (open symbols) of the recirculating loop..... | 98 |
| Fig. 6.6. The measured eye diagrams of the signal at various distances: At transmitter, 12 , 18 , 22 , and 28 loops. | 99 |

| | |
|--|-----|
| Fig. 6.7. The eye diagram at 22 loops at 622 Mb/s. | 100 |
| Fig. 6.8. Power budget diagram of the RCL..... | 101 |
| Fig. 6.9. OSNR degradation as function of number of loops, theory ('+') and modeling ('o')..... | 102 |
| Fig. 6.10. Generic optical network consisting a metro rings, interconnecting ring, and long haul. | 103 |
| Fig. 6.11. The implementation of crosstalk sources in an add/drop node | 103 |
| Fig. 6.12. BER as function of number of loops for a WSS crosstalk of -40 dB with and without fiber dispersion..... | 105 |
| Fig. 6.13. Number of WSS cascades as a function of WSS crosstalk at varying fiber dispersion. | 106 |
| Fig. 6.14. The power penalty (due to crosstalk) calculated as function of fiber dispersion for a ring network with 16 nodes. | 106 |
| Fig. 6.15. Number of cascades as a function of WSS crosstalk. | 107 |
| Fig. 6.16. Power penalty as a function of node degree of a single stage WSS-based ROADM node. | 108 |
| Fig. 6.17. Number of loops as function of center frequency detuning. | 110 |
| Fig. 6.18. The channel shapes of WSS (broken line) and AWG (solid line)..... | 110 |
| Fig. 7.1. Heterogeneous switch employing WSSs and SOA switch. | 115 |
| Fig. 7.2. SOA switch: (a) Structure that can handle wavelength and time domain switching; (b) Structure that can handle time domain (wavelength stripped) switching..... | 115 |
| Fig. 7.3. Schematic of a double-heterostructure SOA. | 116 |
| Fig. 7.4. SOA mounted on the evaluation board. | 120 |
| Fig. 7.5. SOA gain vs drive current at a signal input power of -10 dBm at a wavelength of 1561.4 nm..... | 121 |
| Fig. 7.6. SOA gain vs wavelength (a); ASE spectrum (b)..... | 121 |
| Fig. 7.7. Gain as a function of input power at a wavelength of 1561.4 nm at drive current of 100 mA. | 122 |
| Fig. 7.8. Experimental setup for single channel operation. | 123 |
| Fig. 7.9. Ber vs received power at 2.5 Gb/s (left) and 622 Mb/s (right) at different input powers. | 124 |
| Fig. 7.10. Received eye diagrams at input powers of -10 dBm (a) and 3 dBm (b). | 125 |
| Fig. 7.11. Experimental setup. | 126 |
| Fig. 7.12. Spectra of FWM at the output of SOA..... | 127 |
| Fig. 7.13. BER vs received power measurements as a function of number of channels with SOA in saturation. | 128 |

| | |
|--|-----|
| Fig. 7.14. The experimental set up used to measure the penalty due to gain compression in multi-wavelength operation..... | 129 |
| Fig. 7.15. Multi-channel input spectrum at the input of SOA. | 129 |
| Fig. 7.16. Power penalty and the SOA gain as a function of number of channels. | 130 |
| Fig. 7.17. 17. Details on drive electronics. | 131 |
| Fig. 7.18. BER as a function of received power for the SOA under static (solid line), and dynamic (broken lines) switching conditions..... | 131 |
| Fig. 7.19. Received eye diagrams for SOA. | 132 |
| Fig. 7.20. Switch configurations for characterizing the wavelength and packet paths. | 133 |
| Fig. 7.21. Number of loops as a function of loop input power (per channel) of the wavelength path..... | 134 |
| Fig. 7.22. BER as a function of number of loops for the packet path. | 134 |
| Fig. 7.23. Eye diagrams: (a) wavelength path, five channels, at 22 loops; (b) packet path, five channels, at 5 loops. | 135 |

List of acronyms

| | |
|--------|--|
| AAPN | agile all photonic network |
| AWG | arrayed waveguide grating |
| ASE | amplified spontaneous emission |
| BER | bit error rate |
| BERT | bit error rate tester |
| B&S | broadcast and select |
| CW | continuous wave |
| CDR | clock data recovery |
| DC | directional coupler |
| DF | de-correlating fiber |
| DeMUX | de-multiplexer |
| EDFA | erbium doped fiber amplifier |
| FPGA | field programmable gate array |
| FWC | fixed wavelength converter |
| FWM | four wave mixing |
| GC-SOA | gain-clamped semiconductor amplifier |
| IL | insertion loss |
| iPLC | integrated planar lightwave circuits |
| iPLT | integrated planar lightwave technology |
| MAN | metropolitan area network |
| MEMS | micro electro mechanical systems |
| MQW | multiple quantum well |
| MOD | modulator |
| MUX | multiplexer |
| MZI | Mach-Zehnder interferometer |
| NF | noise figure |
| NRZ | non return to zero |
| NZ-DSF | non zero dispersion shifted fiber |
| OADM | optical add-drop multiplexer |

| | |
|-------|---|
| O-E-O | optical-electrical-optical |
| OLT | optical line terminal |
| OSA | optical spectrum analyzer |
| OSC | optical supervisory channel |
| OSNR | optical signal to noise ratio |
| OXC | optical crossconnect |
| PC | polarization controller |
| PDF | probability density function |
| PDG | polarization dependant gain |
| PDL | polarization dependent loss |
| PP | power penalty |
| PRBS | pseudo random bit sequence |
| QD | quantum dot |
| RCL | re-circulating loop |
| RIN | relative intensity noise |
| ROADM | reconfigurable optical add-drop multiplexer |
| RX | receiver |
| SFP | small field pluggable |
| SGDBR | sample grating distributed Bragg reflector |
| SSA | small switch array |
| SW | switch |
| TE | transverse electric |
| TM | transverse magnetic |
| TWC | tunable wavelength converter |
| TX | transmitter |
| WAN | wide area network |
| WB | wavelength blocker |
| WDM | wavelength division multiplexing |
| WP | wave path |
| WSS | wavelength selective switch |
| WXC | wavelength crossconnect |

| | |
|------------|------------------------------------|
| VOA | variable optical attenuator |
| VWP | virtual wave path |
| XGM | cross gain modulation |

Acknowledgements

Firstly, I would like to express my deepest gratitude to my supervisor, Dr. T. J. Hall, for his support and guidance throughout my program. I thank him for his kindness, freedom he offered me to choose my own path, and his encouragement and help to get back on track when I got lost.

I thank Dr. A. Vukovic and his team at the Communication Research Center, for their generous support in allowing me to carry out some of my experiments using their optical network testing laboratory.

Many thanks go to the members, past and present, at the Center for Research in Photonics, for their help in numerous ways and friendship during my stay at the University of Ottawa.

I am so grateful to my parents, brother, and sisters for their love and mental support throughout my journey in life.

Finally, I thank my loving husband, Kana, for his understanding and patience in supporting me while completing this thesis and my lovely daughter, Cynthia, the best I had during my thesis mission, for fulfilling our life with joy.

This work was supported by the Natural Sciences and Engineering Research Council (NSERC) of Canada and industrial and government partners, through the Agile All-Photonic Networks (AAPN) Research Network; NSERC Strategic Project Grant STPGP 306932-04; and the Ontario Centres of Excellence OCE/CITO Research Partnerships Program.

1 Introduction

To meet the ever increasing demand for transmission bandwidth, a bandwidth revolution took place in telecommunications networks with the invention of low-loss optical fiber. Introduction of narrow line-width lasers together with erbium-doped fiber amplifiers (EDFAs) accelerated the growth of optical communication systems improving the capacity and reach of the signal transmission. By employing wavelength division multiplexing (WDM) technology, capacities in few tens of Tb/s has been demonstrated, to date, in a single transmission fiber [1].

Traditionally, optics has been used to provide transmission and to increase the capacity in point-to-point links of the backbone network. At the end of the links, called nodes, all functions have been performed in the electronic domain: converting the optical signal to electronic signal, electronic routing and switching, and converting back to an optical signal. The main drawback in this approach is that due to the inherent throughput limitation of signal processing in the electronic domain a serious bottleneck is created for the full exploitation of the tremendous bandwidth that is available on the WDM links. To date, the bit rate on each wavelength has reached up to 40 Gb/s and the number of WDM channels per fiber has reached above 80 over the common band (c-band). On the other hand, in electronic devices the amount of bandwidth that can be input or output from them is currently limited to 3.125 Gb/s per link [2]. Besides, the electronic switches can now scale only to 40 Gb/s per line card [3]. One promising approach to solve this problem is optical switching, without converting to electrical form, through the deployment of optical switches at the network nodes. The potential benefits of optical switching are increased switching capacity, flexibility to data rate, format, and protocol, and cost effective modular growth.

The emphasis on the current generation of networks is on maintaining the signal transparency at the network nodes to build all optical networks. With the advent of the optical add/drop multiplexers (OADMs), which can add, drop, and switch through wavelengths, the wavelength routed networks have become a reality and the deployment of such networks has been initiated in the metro region and long-haul [4], [5].

In wavelength switched networks, the finest granularity that can be used for handling traffic requests is wavelengths, so, the bandwidth is handled coarsely. Optical packet or burst switching has been proposed as the next step [6], [7]. However, realization of packet switching in the optical domain that is comparable to currently applied electronic packet switching is faced with many technical challenges, such as realization of optical buffers, clock recovery and synchronization, and optical header processing. As interim solutions towards all optical packet switched WDM networks, networking examples [8], [9] and packet switch node structures [10]-[13] with reduced complexities have been proposed.

In all optical networks, regardless of switching granularity level, the extent to which the optical transparency could be maintained is often influenced by the accumulations of physical layer impairments, which necessarily appear due to the non-ideal performance of the subsystems and devices that constitute the network. As the network scale, in terms of nodes and links supported, the signal quality gets severely affected due to the accumulation of certain impairments, including interference noise or crosstalk that comes from the switches and filters [14]-[16] and amplified spontaneous noise that come from the amplifiers [17]. Such impairments can not be entirely eliminated or compensated without the need for pure signal regeneration which, to date, can only be done maturely through optical-electrical-optical (O-E-O) conversion.

1.1 Objective and motivation

The foundation of any network is its physical layer, consisting of the necessary hardware such as transmission fiber, amplifiers, switches, and transceivers. The performance and the scalability of the physical layer with adequate performance expectations are essential for the successful operation, maintenance, and growth of the network.

Optical switches play a vital role in optical networks not only by performing the essential switching and routing but also by enabling network growth in terms of capacity and scale. To enable future developments in rapidly evolving optical networks, the study of the following aspects are of prime importance:

- a. Predicting the scalability of switches to maintain impairments induced penalty within a given system margin,

- b. Exploring various switch architectures and technology options to optimize optical performance and cost of the switch, and
- c. Understanding the switch interaction with other network elements and assessing the impact of combined impairments to network scaling.

Over the last few years, numerical studies on the scalability of optical switches has been reported widely, but many of them used closed-form models with limited insights and accuracy or used generalized models, not accommodating all possible impairments in the switch that is realized with any given technology. The study on the scalability of networks, has been mainly devoted to investigate the cascadability of switches in the absence of fiber dispersion, which is often compensated entirely (in experiments) or ignored (in theory) and the switch crosstalk being modeled with limited accuracy both in experiments and theory. Further, no work has been reported in studying the impact of combined impairments, dispersion, ASE, and crosstalk to scaling of metro networks, which is cost sensitive and do not employ expensive dispersion compensation modules in eliminating the dispersion entirely, at bit rates of 2.5 or 10 Gb/s.

The objective of thesis is to address the above mentioned aspects, **a** and **b** by conducting experiments and/or developing appropriate and more accurate theoretical models, and **c**, by using an experimental re-circulating model, backed by theory, while taking into account all dominant impairments. Moreover, to be lined up with the demand for improving the bandwidth utilization to meet the increasing diversified traffic requests, switch structures for multi-granularity switching are also looked at and their physical layer performance is investigated.

1.2 Thesis organization

Chapter 2 is devoted to provide some background information on optical switching along with the literature review on the state of the art on optical switching technologies, switches, and subsystems.

In Chapter 3, the core switch implementation options for an agile all photonic network (AAPN) are looked at. The scalability of these switch structures due to crosstalk is

investigated using analytical crosstalk models to meet the large switch port counts requirements.

Electro-optic directional coupler (DC) based switches have become an attractive technology option in realizing cost effective, compact, fast, and scalable switch fabrics. In Chapter 4, the state of the art on this technology and the architectural options are reviewed. The scalability of various switch structures is investigated in detail using a numerical model that takes into account all possible impairments in the switch.

Reconfigurable optical add/drop multiplexers (ROADMs) are the key elements in building the next-generation, dynamically reconfigurable optical networks. Wavelength selective switches (WSSs) are the latest generation of wavelength routing devices that promise to build flexible and degree upgradeable fully functional ROADMs. In Chapter 5, optical characterization of off-the-shelf WSS units is reported and various architectural options for the implementation of multi-degree ROADMs are explored and assessed in terms of performance and cost. Cost-optimal structures are proposed.

In Chapter 6, the physical layer performance of periodic optical ring networks constructed with WSS based ROADMs is studied both experimentally and numerically. A re-circulating loop test bed is constructed to experimentally investigate cascade effect of multiple nodes in optical ring networks. An experimentally verified model is then used to study the impact of combined impairments on the tolerance to switch crosstalk.

In Chapter 7, the physical layer performance of optical networks with heterogeneous switching nodes is investigated. The switch that can handle both wavelength and packet switching and is constructed using WSS based ROADM and Semiconductor Optical Amplifier gates, respectively.

Chapter 8 provides the conclusions and future directions.

2 Optical switching: background and state of the art

In this chapter, a review on material with regard to optical switching that is informative and beneficial to this thesis is presented. A generic network model and the key network elements and their functions are discussed in Sec. 2.1. Different classes of switching are identified in Sec. 2.2. The performance parameters of optical switches are discussed in Sec. 2.3. Currently available optical switching technologies are reviewed in Sec. 2.4. Finally, in Sec. 2.5, the issues related to scaling of the optical switches are discussed.

2.1 Elements of an optical network

The current generation of optical networks is evolving based on two main technical advancements, WDM transmission and optical switching. The key network elements that enable optical networking are optical line terminals (OLT), optical add/drop multiplexers (OADM) and optical cross connects (OXC) [18].

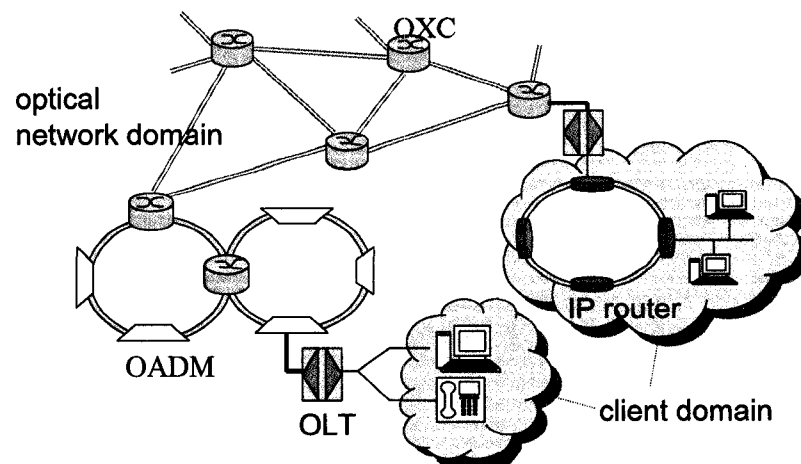


Fig. 2.1. Optical network: a generic example

A generic example of an optical network is shown in Fig. 2.1, where fiber links are used to interconnect the nodes. Each optical link typically constitutes other elements such as optical amplifiers and dispersion compensator to overcome the transmission impairments. Each link can support a certain number of wavelength channels, which are separated typically by 50 to 200 GHz, depending on the components' suitability and link characteristics. A wavelength window at 1550 nm is predominantly used to take advantage of the wide gain spectral bandwidth of the EDFAs that is centered around 1550 nm.

2.1.1 OLT

OLTs are used primarily as the interface between two domains for the purpose of signal format adaptation. OLTs consist of transponders, multiplexers, and de-multiplexers. A transponder adapts the signal coming in from one domain into a signal suitable for transmission over the other domain, for example, converting to the appropriate wavelength and adding/removing appropriate overheads for signal management. The adaptation is done through an O-E-O conversion. Multiplexer and de-multiplexers are passive optical devices. Multiplexers combine different wavelength channels at its input ports into a combined signal at its output port and demultiplexers separate the combined signal in its input port into separate wavelength channels at its output ports.

The secondary functionalities of OLTs include send and receive optical supervisory channel (OSC), which is carried in a separate wavelength, different from those carrying the actual traffic and monitoring the bit error rate of the channels at the ingress and egress points in the network.

2.1.2 OADM

OADMs, are mainly used in line or ring topology at locations where some fraction of the traffic is dropped or added locally, while the remaining traffic is passed through the node without the need for termination. Hence, a significant reduction in the network cost is achieved by eliminating the unnecessary O-E-O conversion at the bypassing nodes. The capability of OADMs is limited to handling the traffic at wavelength levels. The OADM takes in signals at multiple wavelengths and selectively drops or adds any fraction of these wavelengths while passing through the remaining wavelengths.

Various OADM architectures and technologies have been proposed, a few have matured enough and are available commercially [19]-[21]. Early generations of OADMs were static or not flexible (add/drop wavelengths to given ports are fixed) and the add/drop scheme had to be planned ahead. Today, the fourth generation of OADMs, called reconfigurable OADMs or ROADMs, enable flexible add/drop or express pass-through of individual or group of WDM channels at the network nodes to meet the changing traffic requirements.

2.1.3 OXC

OXC performs a similar function to what of a ROADM but at a larger scale in terms of number of ports and wavelengths. The OXC's functions may or may not include adding and dropping optical paths at the local node. In wavelength routed networks, optical paths, also called wavelength paths, are asynchronous to each other. Thus, it is easy to switch the incoming wavelengths independently between input-output fiber ports as the need for bit synchronization is not needed. This non-synchronous nature allows a crossconnect node with incremental throughput growth in terms of number wavelengths per fiber, fiber ports and bit rates. The high modular growth capability offers the economical introduction of optical crossconnects to transport nodes whose needed throughput range from small to large [22].

The applications of OXCs are mesh networks and ring-to-ring or multi-rings interconnects. Another important application is in short reach interconnects for high performance computing and storage area networking [23]. Compared to OLTs and ROADMs, which reached a certain stage of maturity with applications in operator networks, the developments of OXCs have been progressing with the appearance of prototypes and field trails [24].

In the literature, OXC (or crossconnect) is also represented as a core optical switch surrounded by transceivers at the input and output. In the context of this thesis proposal, OXC, represents a pure optical switch, also referred simply as a switch unless otherwise stated.

2.2 Optical switching: classification and applications

In optical transport networks, optical switches are employed for a variety of applications. Different application requires different switching capabilities (or granularity level). Optical switching capabilities can be classified as follows:

2.2.1 Fiber or space switching

In fiber switching all wavelengths of an input fiber are switched to an output fiber port. An important application of this switching is for protection where the whole traffic from the primary transmission fiber is switched onto another fiber in case of fiber failure such as fiber cuts.

Space switches have been reported using various technologies and the port count of these vary from the basic of 2×2 up to 230×230 [25].

2.2.2 Wavelength switching

In wavelength switching, individual wavelength channels of any input fiber are simultaneously switched to any output fiber. The main application of wavelength switches is providing a lightpath in optical ring and mesh networks. At the network nodes, these switches are reconfigured appropriately to setup new lightpaths and to re-route the existing lightpaths according to the traffic conditions. These switches are more complex and expensive compared to fiber switches and require large port counts.

There are few variations in wavelength switches as such as waveband switches and wavelength interchange switches. In waveband switching, the transmission spectrum is grouped into bands that are switched together. Thus, a reduced component count is achieved but at the expense of flexibility to support changing and unpredictable traffic demands. In wavelength interchange switching, in addition to wavelength switching the wavelength conversion capability is also added to the switch.

The feasibility of realizing wavelength switches have been reported by various research groups at various port counts, 16×16 [26] and others [27], [28]. Wavelength switches are also available commercially at ports counts of 1×5 and 1×9 supporting 42 wavelengths [19], [20] that are intended to build flexible ROADMs.

2.2.3 Packet switching

In packet switching, the signal is switched packet-by-packet basis (time domain switching). Hence, the bandwidth per wavelength can be shared among several users and the network usage can be greatly improved. The implementation of optical packet switching is still under study, since some relevant functionalities, such as optical buffers, clock recovery and synchronization, and header processing which are easy to implement with electronics, are technically challenging to realize with optics. The research on packet switching has been progressing and test beds demonstrating packet switching at various levels of complexities have been reported [10]-[13], [29].

2.2.4 Multi-granularity switching

Multi-granularity switching combines the switching capabilities waveband, wavelength and packet or any combination of these in an OXC. Network nodes employing switches that are capable of multiple switching granularities are attractive to handle traffic with diversified statistical characteristics.

Recently, demonstration of wavelength and packet switching node performance in a bus topology has been demonstrated [29].

2.3 Characteristics of OXCs

The characteristic classes that are used to determine the suitability of OXCs in optical networks are its blocking nature, optical performance, and scalability, which are discussed in detail below. Other issues that are taken into account are reliability, power consumption, size, and cost. The cost of the switch is often influenced by the technology used, level of complexity and functionality desired, port counts, and the level of optical performance required. In metro and access networks, low cost switches are desired at the expense of performance trade-offs. Whereas, in backbone long-haul networks high performance optical switches are required

2.3.1 Blocking characteristics

The blocking nature of a crossconnect is determined by the architecture or structural organization of switch elements. Crossconnect architectures, in general, can be identified as

blocking or nonblocking according to their blocking nature. A crossconnect is called blocking if some permutation of input/output combinations can not be realized. Nonblocking crossconnects allow any permutation of input/output combinations. The degree of nonblocking nature, however, may vary as *rearrangeably* nonblocking, *wide-sense* or *strict-sense* nonblocking. *Rearrangeably* nonblocking system requires interruption or rearrangement of existing connections in establishing new connections while the other two do not. The only difference between wide-sense and strict-sense is that a wide-sense nonblocking switch is algorithm-dependent while the other is algorithm-independent (permutations are never blocked even if some previous permutations are routed arbitrarily). Obviously, the last of these is the most desirable.

In context of WDM networks, a crossconnect can provide nonblocking in a limited sense, where an input signal on a given wavelength can be switched to any free output fiber on the same wavelength or enhanced nonblocking, where an input signal on a given wavelength can be switched to any free output fiber on any available wavelength.

2.3.2 Optical performance

The key parameters that are used to measure the optical performance of a switch are as follows:

Insertion loss (IL): The fraction of power in decibels (dB) that is lost due to the presence of the switch

Switching speed: Defined as the time period from the moment the command is given to the switch to change state to the moment the IL of the switch path achieves more than 90 % of its final value [25]

Loss uniformity: Maximum variation of IL among different combinations of input output ports

Extinction ratio: The ratio of output power in the on state to the output power in the off state at a given output port

Crosstalk: The ratio of power, in dB, that appears from the desired input to the power that appears (or leak) from the other (undesired) inputs

Polarization dependent loss (PDL): The maximum variation of IL for different polarization states of the input signal

Filtering characteristics: Filtering characteristics, which are relevant to wavelength switches, include channel pass band (typically expressed in Hz at 3 dB roll off), center channel spacing (expressed in Hz), and channel isolation within a specified pass band expressed in dB

Another essential feature of an optical switch is its scalability or the ability to build the large port count switches that can perform adequately. The issues related to switch scalability are discussed in detail in Sec. 2.7.

2.4 Switch architectures

In transport networks, the concept of path is of critical importance for effective traffic engineering. In WDM networks, the paths are identified by their wavelengths. For the realization of optical path networks, two types of optical paths, called wavelength paths (WPs) and virtual wavelength paths (VWPs) has been proposed [30]. In WP approach, one optical path is established between source and destination nodes by allocating one wavelength to the path and the intermediate nodes along the WP perform WP routing according to the wavelength. In VWP approach, VWP is allocated link by link, and thus the wavelength of each VWP on a link has local significance instead of global significance.

The routing and setting-up of paths at the nodes is achieved using the optical switches. The switch architectures that support WDM networking, are generally classified, according to the path scheme that they can support as WP architectures and VWP architectures. WP switch, is simple compared to the VWP switch, which requires transparent wavelength converters.

2.4.1 Wave path architectures

WP switches are simple and can be constructed using cost-effective components. However, in networks constructed using WP switching nodes the wavelength assignment problem must be solved by the time the network is reconfigured. WP architectures are mostly suitable where the traffic demands are relatively static as they are more likely to suffer from contention under dynamic traffic conditions compared to VWP architectures. There are two major WP architectures available, wavelength layered switch and broadcast and select switches.

2.4.1.1 Wavelength layered switch

Fig. 2.2 shows the architecture of a wavelength layered switch, which connects any wavelength coming in from any one of the F input fibers to any one of the F output fibers. The switch consists of W number of space switch fabrics, each with a dimension of $F \times F$. All the lightpaths with λ_i will be routed and switched through the switch i . This wavelength plane switching approach can carry a total capacity of FWB b/s, where B is the line rate per wavelength; W is the number of wavelengths per fiber; and F is number of fibers connected to the node. In principle, this modular architecture has the advantage of scaling the capacity as the number of wavelengths and fibers increase.

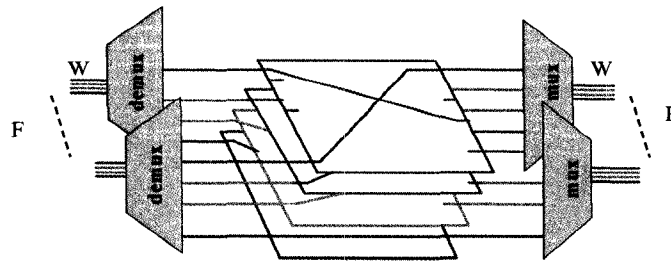


Fig. 2.2. Wavelength layered switch.

2.4.1.2 Broadcast and select switches

The Broadcast and Select (B&S) concept is based on space and wavelength selection using SOA gates. The architecture of a B&S switch is illustrated in Fig. 2.3. Each set of the F incoming WDM signals is amplified using an EDFA to compensate for subsequent power splitting and broadcasted using splitters to each one of the F selection stages. Each selection stage consists of F pairs of multiplexers and de-multiplexers and each pair is connected through W number of SOAs, where W is the number of wavelengths per fiber. The output of the multiplexers, in each stage, are combined and attached to an output fiber. Note that, only one out of F gates per wavelength channel from F input fibers destined to the same output fiber is activated at a given time.

The modular nature of this architecture allows scaling in terms of number of fiber ports and number of wavelengths per fiber.

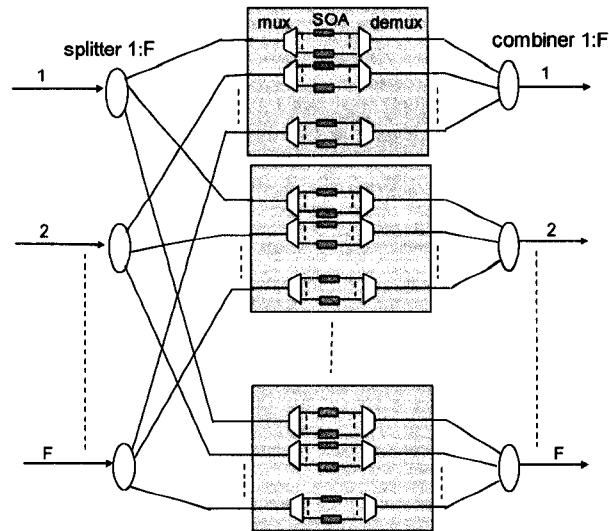


Fig. 2.3. B&S architecture.

2.4.2 Virtual wave path architectures

VWP switches compared provide more flexibility, better connectivity, and optimal blocking characteristics to a network with WP switches since the VWP switches support wavelength conversion capabilities. However, VWP switches are more complex and expensive to implement.

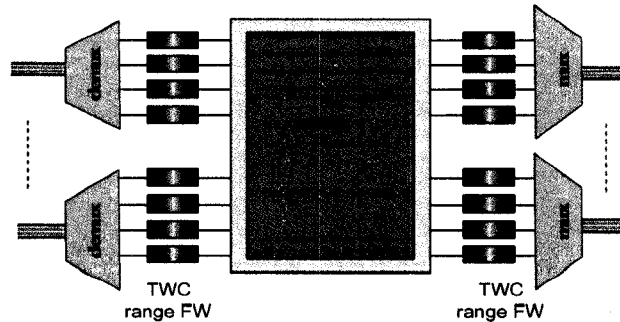


Fig. 2.4. VWP switch realized using AWG and TWC

Fig. 2.4 shows a VWP architecture constructed using a $FW \times FW$ arrayed waveguide grating (AWG) router and tunable wavelength converters (TWC). AWG routers are passive devices and very reliable. Their routing pattern (the input and output mapping) is fixed such that routing of a signal at any of its input port is decided according to its wavelength. To do dynamic switching from any input port to any output port, TWC can be integrated at the input ports of the AWG router such that the incoming wavelengths are

converted appropriately to achieve the required routing. A tuning range of FW , is need to overcome any internal blocking. At the AWG router output, a second set of wavelength converters is necessary to convert the wavelengths that are compatible to the multiplexer input.

The scaling of above architecture is limited to the number of ports available at the AWG router and tuning range on TWCs. A multistage, Clos structure, can be considered, where the switch blocks in each stage are realized with the structure shown in Fig. 2.4 [31], [32]. Another option is to use B&S architecture, similar to the one shown in Fig. 2.3, but with modified selector stage; the arrays of SOA gates are replaced with an AWG router and TWCs that are attached to the input and output ports of the AWG [33].

The implementation of VWP switches solely depends on the realization of optical wavelength conversion technology and the integration of TWCs with other functional devices such as AWG in chip-form for any practical application.

2.5 Switch technologies

The main optical switching technologies, that are currently available and matured enough, are as follows.

Micro Electro Mechanical switches (MEMS): MEMS uses a tiny reflective surface, typically silicon based, to redirect the beam to the desired port. The movement of the mirrors is activated electro-statically or electro-magnetically. There are two version of MEMS structures available, two-dimensional (2-D) digital or by-stable switch and three-dimensional (3-D) analog switch [34]. 3-D MEMS offer the best potential to realize very large port count switches with port counts above 1000.

MEMS is the most mature technology to date and are fabricated using batch processing techniques. These switches offer very good optical performance such as low loss, loss uniformity, and polarization and wavelength independent operation. Their slow switching time in the range of ms, however, limits their application to protection and wavelength switching. MEMS switches are available commercially from several vendors with port counts up to 32 x 32 [35].

Electro-optic switches: In an electro-optic switch, the refractive index is changed by applying an electric field. A basic 2×2 switch element is realized using a directional coupler, whose coupling ratio is varied by changing the refractive index to switch the signal between the two ports. The most popular material used is lithium niobate (LiNbO_3). Large port count switches can be realized by integrating 2×2 switches. Various switch structures have been reported with port counts up to 16×16 [36].

The main advantages of this switch are the fast switching time, in ns, and modest level of integration.

Thermo-optic switches: The basic switch element is a 2×2 directional coupler or a Mach-Zehnder interferometer, constructed in a waveguiding material whose refractive index is controlled by means of thermal effect. The most common material used is silica on silicon. Switch port counts up to 16×16 have been demonstrated [37].

The switching time in these devices is limited to ms since the thermo-optic effect is relatively slow. The other drawbacks are high power dissipation and issues related to optical performance such as crosstalk. On the positive side, the silica on silicon technology allows the integration of other devices such as arrayed waveguide gratings (AWG) and variable optical attenuators on the same chip.

Liquid crystal (LC) switches: LC switches are optically transparent and operate on controlling the polarization of the light by an electro-optic effect. The materials mainly explored are ferroelectric LC (FLC) and nematic LC (NLC). This technology is still at the laboratory stage and prototype of an 1D switch with port counts of 1×8 [38] and 2D switch with port counts of 64×64 [39] have been demonstrated.

Liquid crystal switches, though they are free space, are solid state devices with no moving parts. They are reliable and can be manufactured in volumes. Their switch time is in the order of micro seconds. Unlike in other switches, the switch loss does not scale with switch dimension and it is mainly limited by the diffraction efficiency of the liquid crystal cells.

Semiconductor optical amplifier (SOA) switches: SOA can be used as an ON/OFF switch (or gate switch) by varying the bias voltage applied to it. At a reduced or low bias voltage, no population inversion is reached and the SOA absorbs the signal. At a high voltage, SOA

can amplify the signal. Very large extinction ratios can be achieved in the switches, due to the combination of absorption in the OFF state and amplification in the ON state. Large switch fabrics are realized by integrating the SOA with passive splitter and combiners. Demonstration of SOA switches with port counts of 4×4 [40], [41] and 8×8 [42] have been reported.

The switching time of SOA is in the order of ns. Other attractive features of the SOA switches are optical gain, compact size, and the possibility of monolithic integration with other functional devices such as wavelength converters and signal regenerators.

2.6 Wavelength conversion technologies

Optical wavelength conversion is a very useful function for optical networking. A wavelength converter can convert the wavelength of the incoming data into a tuneable output wavelength on the fly without passing it to the electronic domain. Two main functional units needed to realize a TWC are fast tuneable CW laser element and wavelength converters. Fast tuneable lasers with wide tuning ranges are becoming commercially available. A combination of spectral sources and wavelength selection switches is an alternative solution for tuneable wavelength source. Different classes of wavelength converters have been proposed, including SOA electro absorption modulator [43], SOA-four wave mixing [44], [45], and SOA- cross-phase and cross-gain modulation [46]. Recent developments indicate a new class of wavelength converters that consists of the integrated version of TWC – monolithically integrated Sampled Grating Distributed Bragg Reflector (SGDBR) laser with SOA based Mach-Zehnder Interferometer (MZI) wavelength converter in InP [47].

Main requirements of the TWC are operating speed and ability to convert over a wide range of wavelengths including the same wavelength. Many of the TWC implementations reported have been shown to perform 2R signal regeneration through amplification and improvements in pulse shape due to their nonlinear transfer function.

2.7 Scalability

A major concern in choosing a switching technology and architectural option is its scalability to large port counts. Scalability is limited by two main performance

degradations, the insertion loss and the crosstalk. The insertion loss can be compensated all optically using EDFAs on a per fiber basis, but at the expense of ASE noise. However, preventing the accumulation of crosstalk, which degrades the BER performance, requires signal regeneration or O/E/O conversion.

2.7.1 Crosstalk or interferometric noise

Numerous studies indicate that the optical crosstalk is one of the key considerations in the design of an optical network supporting many switching nodes. The crosstalk contributions are unwanted power additions to the main signal of interest. Due to the nonideal performance of various components that constitute an optical switch, power leaks to the unselected ports and the leaked portion gets accumulated as it traverses through the network. These power additions have either the same wavelength as the main signal or different wavelengths, producing inband crosstalk and interband crosstalk, respectively. Interband crosstalk can mostly be removed with narrowband filters at the receiving end. Inband crosstalk that falls within the receiver bandwidth creates fluctuations (beating) in the signal power and degrades the system performance. Note that some inband crosstalk contributions may combine coherently if they are phase correlated with the signal, causing coherent crosstalk while the other crosstalk components that are not phase correlated with the signal give rise to incoherent crosstalk.

For networking applications, the optical switch is an essential element to switch and route signals to various destinations. While routing the channels from its input to output ports, it also produces some inband crosstalk to the main signal and degrades the quality of the signal. This noise is a serious impairment and needs attention in the design and scaling of the switch.

To accurately model the inband crosstalk, the interference of the underlying fields must be considered rather than the simple power addition. Various studies have been reported in modeling inband crosstalk in optical crossconnects [16], [48], [49], and in WDM networks [14]. The impact of crosstalk is quantified by considering the crosstalk power penalty (PP), which is defined as the additional power, in dB, required for the signal to achieve the same error rate as that without the crosstalk.

2.7.2 Insertion loss

The optical power budget is also a concern in scaling the switch size. The IL of a switch typically increases with increasing switch dimension. In addition to loss, loss uniformity among different wavelength channels at any output port is also a concern as these variations may lead to serious nonlinear impairments when a typical static EDFA is used to compensate the loss. The maximum loss incurred and any loss variations among all possible interconnection patterns varies depending on the structure of the switch architecture.

3 Core switch architectures for Agile All Photonic Network

The aim of this work is to analyze the technology and architectural options to implement the core switch for an agile all photonic network (AAPN). To design and implement the switch, the main issues to take into consideration are to understand the functions of the core switch, identify suitable technology options, and investigate the scalability of the switches in terms of physical impairments to meet large switch port counts requirements. This chapter is organized as follows: Sec. 3.1 introduces the AAPN network and Sec. 3.2 and 3.3 discuss the required functionality and the implementation options of the core switch, respectively. Scalability analysis of the switches is presented in Sec. 3.4 and the results are given in Sec. 3.5. Finally, a summary is given in Sec. 3.6.

3.1 Agile All Photonic Network

In all photonic networks, the signal is carried between the source and destination nodes in the optical domain without conversion to the electronic domain. An agile network has the capability of handling abruptly changing traffic demands through efficient bandwidth utilization schemes. An agile network example, called agile all photonic network (AAPN) was proposed with a goal of extending the photonic portion of the data path as close as possible to the end user to benefit high capacity transmission and switching [8]. To achieve this goal, the network deploys a time domain multiplexing scheme for agile bandwidth allocation and engages the necessary concentration of control and routing functionality at the ingress/egress electronic edge nodes - to avoid optical memory and optical header recognition which are believed impractical in the near future. The most popular network topology is a mesh topology, which distributes traffic over many network nodes/switches. The coordination and control of the switches in these networks to overcome contention for resources at the switches with no buffering, however, is a challenging issue. To simplify the

control problem, an overlaid star topology is adopted for the design of AAPN, as depicted in Fig. 3.1.

Each core node with a photonic switch fabric provides interconnection between any pair of ingress (input port) and egress nodes (output port). The overlay of several stars, connecting each edge node to every core node, provides robustness to link or core failures. Buffers at the core are avoided and any contention in time, wavelength, and space are taken care of at the scheduling stage such that no two input ports, carrying data on the same wavelength, are to be connected to the same output port at any given time.

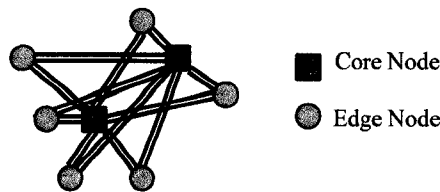


Fig. 3.1. AAPN topology: overlaid star.

3.2 Core node: functions and requirements

Functionally the core resembles the operation of a circuit/wavelength switched node in WDM networks except it transports data at packets/time slot level allowing bandwidth sharing on per wavelength basis. Such a packet switched node has to be reconfigured fast enough to support switching at timescales of duration of a packet length- which is in the range of ns. The constraints on switching speed, nevertheless, can be relaxed to some extent by gathering multiple variable sized packets, which are destined for a given output, to a fixed length envelope or time slot. Thus, the minimum time between changes in the switch configurations is determined by the duration of the time slot. The trade-off is any bandwidth loss due to the fragmentation of variable sized packets in to fixed length time slots. The main concern in deciding the size of the time slot would be maximizing the bandwidth utilization while minimizing the loss due to the time taken for switching. In regard to AAPN, the duration of 100 Kb time slot at a line rate of 10 Gb/s, is 10 μ s. If transmission efficiency of better than 90 % is to be achieved, switching speeds of at least 1 μ s have to be realized. Two mature technologies, Semiconductor Optical Amplifier (SOA) gates and electro-optic switches, both operating in the ns range, currently meet this speed requirement. Switches based on Arrayed Waveguide Grating router (AWG) with Tuneable

Wavelength Converters (TWC) have also been proposed as an enabling technology to realize fast switches at speeds in the nanosecond range [32].

From the AAPN network perspective, each edge node can be a member of every overlaid star. So, the port count or the dimension of the core switch should be scalable to at least the total number of edge nodes that are to be supported in the network. The maximum switch block size readily available now is 64×64 [50]. Recent developments in SOA gate arrays in integrated chip form promise various architectural design approaches by making use of the WDM dimension for fast gating [51].

A variant of the conventional packet switching, called burst switching, has also been considered for the operation of the AAPN network. Data bursts are typically long and variable in length. In packet/time slot switching, the switch is reconfigured at every time slot, called synchronous mode of operation. Thus, it is sufficient to have rearrangeable nonblocking core switch. But in burst switching, similar to that of wavelength switched networks, duration of connection among ports overlap in time due to variable burst sizes and a strictly nonblocking switch is needed to ensure no interruption among the existing connections when setting up a new connection. The total number of switch elements required in constructing a strictly nonblocking switch fabric is more than that needed for a rearrangeable nonblocking one and the additional elements needed increases rapidly as the switch dimension grows. A strictly nonblocking switch can obviously support synchronous mode switching but the rearrangeable nonblocking switch can not support asynchronous (burst) mode switching.

Numerical study comparing burst and slot-by-slot switching from the AAPN prospective revealed that slot-by-slot switching performs favourably in terms of robustness to variations in traffic and bandwidth efficiency [52]. Moreover, slot-by-slot switching provides cost benefits and it will be the most likely choice of operation for AAPN. Accordingly, rearrangeable optical switch architecture options are considered in this study for the core node implementation.

The initial step in AAPN network design is solving the topological design problem to determine the network parameters such as optimal number, size, and placement of edge nodes and core nodes based on the predicted traffic requirements. Analytical cost optimal solutions sought for the core node details for both Metro designs (MAN) and Wide Area

Designs (WAN) indicate [52] that the required switch ports counts vary from small (21) to large (748) and the number of wavelengths needed go as high as 124.

3.3 Switch architectures

Three different switch structures, a rearrangeably non-blocking directional coupler (DC) switch, broadcast and select switch based on SOA gate, and waveguide grating router with tunable wavelength converters are considered.

3.3.1 DC switch

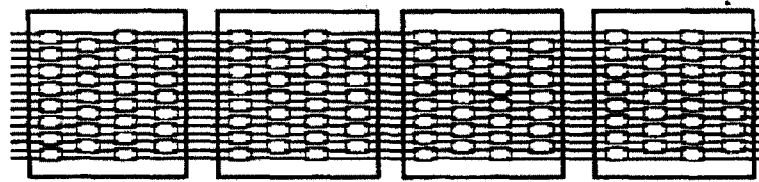


Fig. 3.2. Spanke-Benes structure: partitioned 16×16 rearrangeable nonblocking switch [53].

Fig. 3.2 shows the DC switch architecture, proposed by Spanke and Benes [53]. It can be realized with no crossovers, which relaxes the crosstalk impairment arising from interconnecting waveguide crossovers. Fig. 3.2 shows the structure of a 16×16 switch, which is partitioned into several identical subblocks. The subblocks can be fabricated on separate chips which are interconnected conveniently by using fiber-ribbons.

For an $N \times N$ switch, there are N stages of DC elements and the total number of DCs required is $N(N-1)/2$. In the worst case, the signal traverses through N DCs. The shortest path is through $N/2$ DCs.

3.3.2 Broadcast and select (B&S) switch

Fig. 3.3 shows the architecture of the B&S switch [26]. Each set of the F incoming WDM signals is amplified using an EDFA to compensate for subsequent power splitting and broadcasted using splitters in a tree structure to each one of the FW selection stages. In contrast to the selection scheme in the conventional switch, shown in Fig. 2.5, the space and wavelength selections in this switch are achieved using two successive SOA stages, which are connected with an AWG (the chosen spatial group containing W wavelengths is

demultiplexed as it passes through for subsequent wavelength selection stage). The main advantage of using an AWG is that it can offer superior performance by suppressing the crosstalk effect to second order.

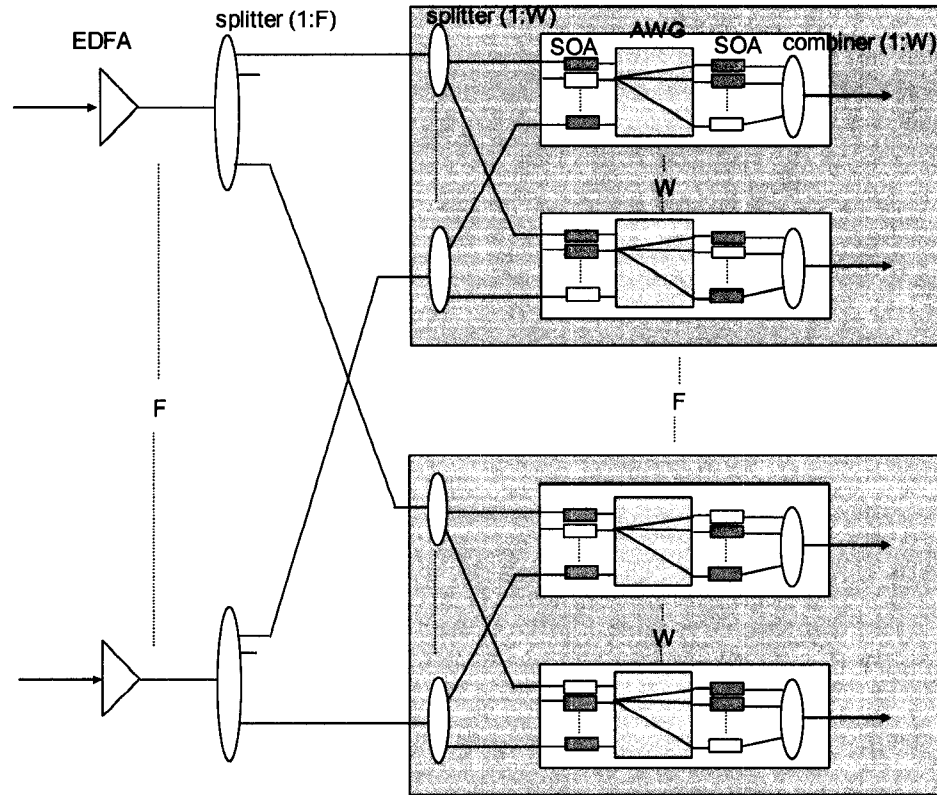


Fig. 3.3 The architecture of the B&S switch [26].

Implementation of power splitting can be done in single stage (with F number of $1:FW$ splitters) or in two stages with $F(1:F)$ and $W(1:W)$ splitters. There will be $FW(F+W)$ number of SOA gates, FW numbers of $1:W$ combiners, and F numbers of multiplexers. Since each selector independently selects the one out of FW channels, these architectures offer a strictly non-blocking switch.

Fig. 3.4 shows the architectural options of the SOA gates selection stage: (a) uses the conventional sequence of the combiner and the demultiplexer; (b) employs $F \times W$ Arrayed Waveguide Grating routers (AWGs) and makes use of the WDM dimension, such that the chosen spatial group containing W wavelengths is demultiplexed as it passes through the AWG for subsequent wavelength selection stage. AWGs offer two main

advantages: (1) the power budget is improved, and (2) coherent crosstalk effect is suppressed to second order.

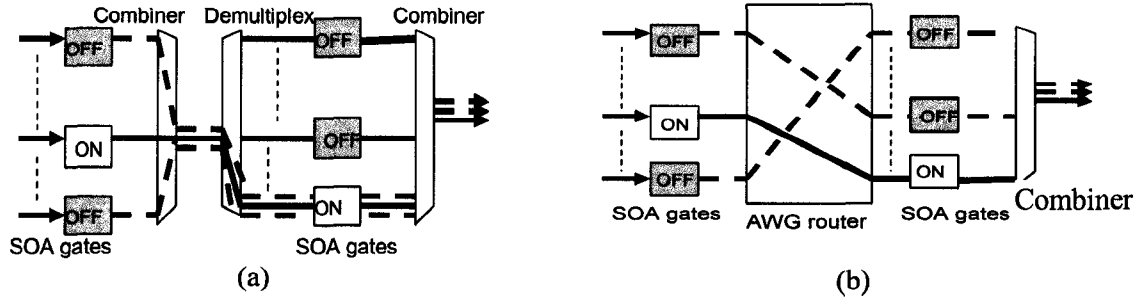


Fig. 3.4. Architectural options for the selection stage. (a) SOAs with combiner and demultiplexer; (b) SOAs with AWG

Fig. 3.5 shows three possible causes of coherent crosstalk effects: (a) Signals from the same wavelength channels that leak through SOA gates (extinction X_{SOA} dB) are spatially separated by the AWG and leak again through the non selected second SOA gates, suppressing the effective crosstalk level to $2 X_{SOA}$ dB; (b) The second contribution is where the same signal that leaks through the other ports of AWG (isolation X_{AWG} dB) get coupled back through the non selected second SOA gates array, improving the effective crosstalk to $(X_{SOA} + X_{AWG})$ dB; (c) The third effect is where signals from the same wavelength channels that leak through SOA gates leak again to the same AWG output port as with the main signal giving an effective crosstalk of $X_{SOA} + X_{AWG}$ dB.

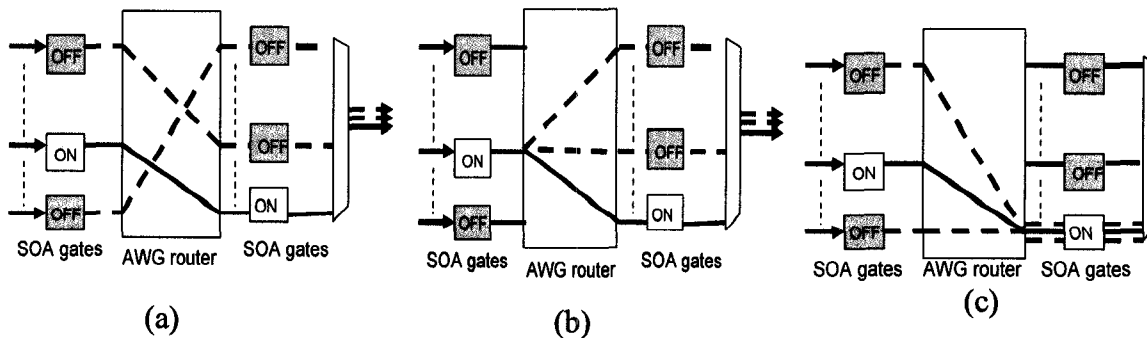


Fig. 3.5. Causes of coherent crosstalk (main signal- solid line, crosstalk- broken line).

The scalability (F, W) of these options is influenced by the available sizes of the components used. The conventional approach is limited to the implementable size of the demultiplexer. The highest reported dimension of wavelength (de)multiplexers is 1×1000 [54] at 6.25 GHz channel spacing and bit rates per channel of up to ~ 2.5 Gb/s. In the other approach, maximum (F, W) is limited to the size of the AWG router ports. To date, the highest reported number of AWG ports is 128×128 [55].

The number of SOA gates required and its integration level with the other components as a module is also a concern with respect to reducing the volume and complexity of the switch fabric. If multiple SOA gates become integrated as modules then the compactness of the switch fabric can be improved. Demonstrations of 32 channel hybrid optical wavelength selector (demux, SOA gates, and mux) [56] and 32 SOA gates module fully equipped with electronics [51] have been reported. The total number of SOA gates required increases with both F and W . When $F = W$, the number of SOA gates required is optimized to $2S^{3/2}$, where, $S(= FW)$, is the switch scale.

3.3.2.1 Multistage options

The complexity of splitting and shuffling is also a concern especially at large port counts. This problem can be reduced to some extent by breaking the switch into number of stages where each stage can be constructed with smaller switch blocks. Multistage Clos like architecture can be considered. For a strictly non-blocking switch, each block in the first stage (third stage) should have a dimension of $n \times k(k \times n)$, where $k \geq 2n - 1$ - asymmetrical requirement in the input/output port counts for the B&S switch block.

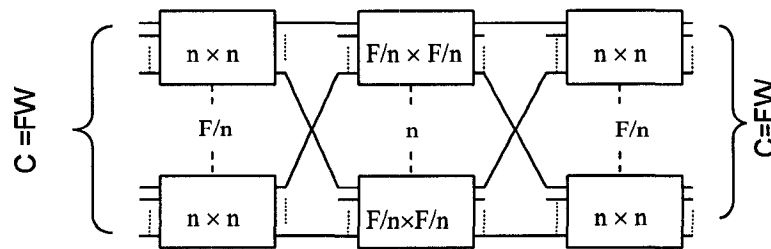


Fig. 3.6. Rearrangeable nonblocking three stage Clos architecture

However, Clos like architecture with B&S approach can still be used to realize a rearrangeable non-blocking switch, which requires smaller port counts in the switch blocks as $k = n$ [53]. Fig. 3.6 shows a three stage Clos architecture implemented with B&S switch blocks, where each block in the first and third stage are chosen to optimize the number of SOA gates in these switch blocks - the number of ports, n , is set to be equal to the number of wavelengths in each fiber, $n = W$ ($W < F$). The total number of SOA gates, C , in this three stage switch will be

$$C = \frac{2F}{n}(2n^3) + nF\left(\frac{F}{n} + n\right) = 5SW + S^2 / W^2, \quad (3.1)$$

where N , is the total number of DWDM fiber ports, and total switch scale, $S = FW$. The number of SOA gates are minimized when $W = (2S/5)^{1/3}$.

Fig. 3.7 shows the total number of SOAs versus the number of wavelengths, W per fiber, for different switch scales, S , for both single and three stage structures. For scales, S , below 64, single stage structure provides lowest number of SOA gates- the number of SOA gates are optimized when $W = \sqrt{S}(= F)$. At higher scales, for low number of wavelengths usage, the three stage structure is efficient requiring smaller number of SOA gates. But as the number of wavelengths supported increases, single stage requires less SOA gates.

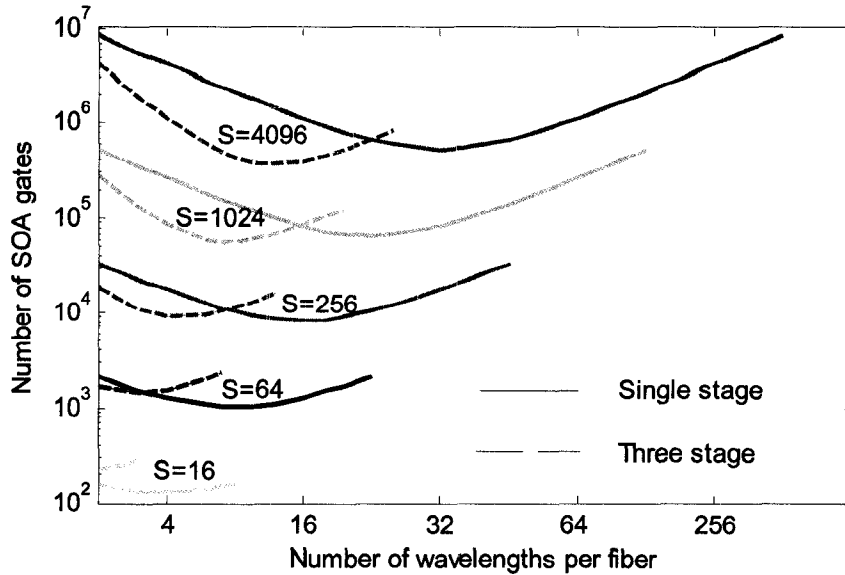


Fig. 3.7. Total number of SOAs required as a function of number of wavelengths per fiber.

If signal regenerators or wavelength converters are used surrounding the switch, the number of wavelengths internal to the B&S structure, W' , can be chosen different from W so as to optimize the SOA gates requirement. The optimal choice for single stage would be $W' = \sqrt{FW}$. In the three stage network, the overall number of SOA gates can be minimized by optimizing W' independently in each stage [57].

3.3.3 AWG and TWC

Another possible implementation option of the core switch is to use a static AWG router, integrated with TWCs at the input ports to dynamically switch any input port to any output port of the AWG router, as discussed in Sec. 2.4.2. For large scale switches, a multistage rearrangeably non-blocking Clos-like structure [32] is considered to increase the number of fiber ports and to relax the requirement on the tuning range, as shown in Fig. 3.8. If wavelength continuity for each packet is not a concern, the TWCs at the last stage can be replaced with Fixed Wavelength Converters (FWC).

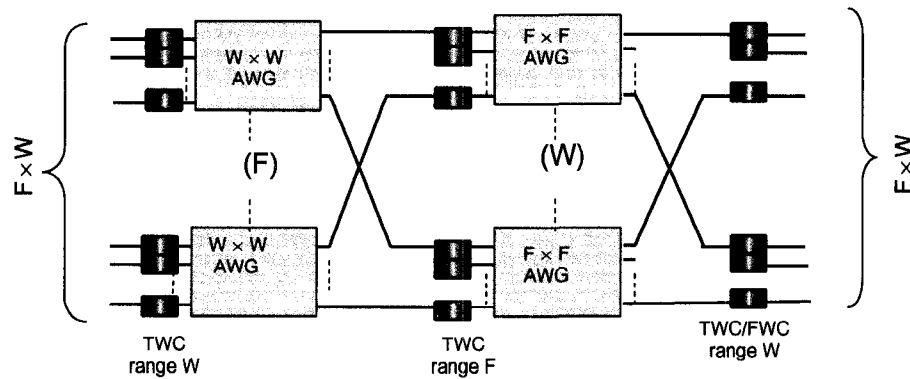


Fig. 3.8. Three stage Clos architecture by using AWGs and TWCs.

TWCs with tuning range of W (for the first and third stage) and F (for the second stage) are required in this configuration. A tuning range of $W (> F)$ is realistic as tuneable lasers which are the key component in TWC, closely follow the number of wavelengths used in fibers. A switch capacity of $128^2 B$ b/s, where B is the channel rate, can be achieved considering the current limit on AWG router ports of 128×128 .

3.4 Scalability of the switches

The major performance impairment in optical switches, the in-band crosstalk, is analyzed using a statistical model to evaluate and compare its impact on the scaling of the switch fabrics. The switch element crosstalk requirement is estimated as a function of switch dimension and a suitable technology option that is realistic for various switch capacities is presented.

3.4.1 Crosstalk model

In this study, the crosstalk model presented in [16] is used as a basis to evaluate the crosstalk performances of different architectures. The model fits systems with optical amplifiers in which the dominant noise at the receiver is the signal-spontaneous beat noise. The noise other than the crosstalk is signal-spontaneous beat noise and is assumed to be Gaussian. It has been verified that for large number of crosstalk contributions (16 or more), the crosstalk noise can also be modeled as Gaussian and the power penalty can be estimated by theory. The crosstalk power penalty, PP for a system, with intensity modulation/direct detection (IM/DD) and receiver using an integrate-and-dump filter, is given by

$$PP = -10 \log \left[1 - 4\sigma_{RIN}^2 Q^2 \left(\frac{r}{r-1} \right)^2 \right] \quad (3.2)$$

where σ_{RIN} is the crosstalk relative intensity noise (RIN), r is the extinction ratio, and Q , satisfies the given BER according to the formula $(1/4)erfc(Q/\sqrt{2}) = BER$. The assumptions made in deriving the above equation are: receiver noise is neglected; signal-crosstalk beat noise dominates; all interferers are in the ‘mark’ state; and a receiver with midway decision threshold is considered. The limitation of using this model is that it under estimates the BER (& PP) when ASE noise is high or the extinction ratio is poor (> 0.1) due to the fact that errors by detecting bit ‘zero’ as bit ‘one’ are neglected.

To model the crosstalk in optical switches, the causes of crosstalk, which are OXC structure dependent, need to be identified. The value σ_{RIN} depends on the coherence relations among various components such as propagation phase delay which is OXC hardware dependent, transmission laser coherence time, and the duration of the bit period.

For a 10 Gb/s system, a bit period of 0.1 ns is generally less than the laser coherence time, which can vary from 0.5 ns for a simple laser to 1 μ s for a high quality narrow-linewidth laser. The OXCs are generally not integrated as one but consist of individual components, such as mux/demux and the switch. The individual components are interconnected via fibers and the delay is often more than the bit period; For example, a fiber path length difference of approximately 20 mm exceeds the length of a bit period at 10 Gb/s. Thus, two situations to be considered are,

Case 1: delay > laser coherence time > bit period;

Case 2: laser coherence time > delay > bit period.

In both cases, crosstalk contributions are uncorrelated with each other and with the main signal - the delays experienced exceed the bit period and eventually produce the same noise effect for all the architectures considered in this study.

3.4.2 Wavelength layered switch

For a fully loaded OXC (Fig. 2.2.), there will be $F + W - 2$ cross-talk contributions, $F - 1$ of which are leaked from the optical switch, and $W - 1$ are leaked from the demultiplexer. The signal of interest, at a wavelength λ_i , will be interlaced with $F - 1$ crosstalk contributions leaked from the other $F - 1$ signals with wavelength λ_i coming in from the other $F - 1$ input fibers. Similarly, there can be $W - 1$ cross-talk contributions, which leaked with other wavelengths at the demultiplexer, passed through the switches and arrived with the signal of interest wavelength λ_i at the multiplexer. These $W - 1$ contributions can be leaked from any signal with wavelength λ_i , including those from the signal of interest itself. However, these will be filtered at the multiplexer- noise is suppressed twice and it is negligible compared to those come that directly from the switch. Considering an intensity modulated signal, the electric field of the main signal with the summation of the crosstalk terms can be expressed as

$$\vec{E}(t) = Eb_s(t) \cos[\omega t + \phi_s(t)] \vec{P}_s + \sum_{i=2}^F \sqrt{\epsilon} Eb_i(t - \tau_{ix}) \cos[\omega (t - \tau_{ix}) + \phi_i(t - \tau_{ix})] \vec{P}_{ix} \quad (3.3)$$

where $\bar{E}_{(t)}$ is the signal field amplitude and is assumed to be unchanged as the power leaked is low; $b_s(t)$ and $b_i(t)$ are binary data sequences with values 0 or 1 of the main signal and the noise contributions ($i=[2,F]$) coming from the other signals, respectively; $\phi_s(t)$ and $\phi_i(t)$ are phase noises of the lasers; \bar{P}_s and \bar{P}_{ix} are the unit magnitude polarization vector of the signal and noise contributions; ε is the crosstalk power leaked relative to the actual signal; τ_{ix} propagation delay differences of the contributions.

At the destination node, the photo current of the detector will be the addition of that from the signal, signal-crosstalk beat noise, and crosstalk-crosstalk beat noise. Other noise additions such as shot and thermal noise components are negligible in systems where amplifier gain is large (> 10 dB) and the dominant noise at the receiver is the signal-spontaneous beat noise. In the presence of crosstalk, the dominant source of noise is signal-crosstalk beat noise. The crosstalk-crosstalk beat noise is negligible compared to that of the signal-crosstalk beat noise.

The total number of first order crosstalk contributions is $(F - 1)$ for a fully loaded single switch block with a size of F . The maximum value of RIN, $\max(\sigma_{RIN}^2)$ can be derived as $\frac{2}{3}(F - 1)\varepsilon$ [16]. For a three stage switch, constructed with switch blocks dimension of $(n \times n)$ for the first and third stage and $(\frac{F}{n} \times \frac{F}{n})$ for the middle stage, $\max(\sigma_{RIN}^2)$ is obtained as $\frac{2}{3}(2n + \frac{F}{n} - 3)\varepsilon$. Power penalties in each case can be calculated by substituting $\max(\sigma_{RIN})^2$ in Equation 3.2.

3.4.3 B&S switch

Assuming the splitting and shuffling is achieved without any crossovers (i.e. by using fibers), the main factors that cause crosstalk are the extinction ratio of the SOA gates and the interchannel isolation of AWG. The three sources of crosstalk contributions are as discussed in Section 2.2. $\max(\sigma_{ss}^2)$ for a single stage switch block is obtained as

$$\max(\sigma_{ss}^2) = \frac{2}{3} \left\{ (F-1)\epsilon_{SOA}^2 + (W-1)\epsilon_{SOA}\epsilon_{AWG} + (F-1)\epsilon_{SOA}\epsilon_{AWG} \right\}. \quad (3.4)$$

Assuming $\epsilon_{SOA} = \epsilon_{AWG} = \epsilon$ to simplify the calculation, $\max(\sigma_{ss}^2)$ gives

$$\max(\sigma_{ss}^2) = \frac{2}{3} (2F + W - 3)\epsilon^2. \quad (3.5)$$

For a three stage switch, constructed with switch blocks scale of $n \times W$, $\max(\sigma_{ms}^2)$ is given by

$$\max(\sigma_{ms}^2) = \frac{2 * 3}{3} (2n + W - 3)\epsilon^2. \quad (3.6)$$

3.4.4 AWG and TWC

This technology is very attractive for achieving the best crosstalk efficient switch. The wavelength converted signal is free from the interband crosstalk carried with it before the conversion. No two same wavelengths will pass through the last stage of WCs set that is connected through a MUX to each output fiber. Any inband crosstalk contribution will be suppressed twice to $\epsilon_{TWC} + \epsilon_{MUX}$ dB, where $\epsilon_{TWC}, \epsilon_{MUX}$ are the input signal suppression ratio of the TWC and crosstalk of the MUX respectively. In the worst case, the number of crosstalk contributions would be $(W - 1)$, where W is the number of wavelength channels per fiber. $\max(\sigma^2)$ is given by

$$\max(\sigma^2) = \frac{2}{3} (W - 3)\epsilon^2 \quad (3.7)$$

where, it is assumed that $\epsilon_{TWC} = \epsilon_{MUX} = \epsilon$.

3.5 Performance evaluation and comparison

3.5.1 Wavelength layered switch

Fig. 3.9 shows the power penalty, calculated for a BER of 10^{-12} , as a function of element crosstalk for the wavelength layered switch constructed with single switch blocks with

various port counts. For element crosstalk of less than -40 dB, switch ports above 64 are impossible to be realized even at high power penalties.

For large scale switches, multistage options can be considered to reduce the number of elements that the signal has to traverse in the worst case. Fig. 3.10 shows the element crosstalk requirement as a function of switch port counts for single and three stage structures for a given power penalty of 1 dB, which is generally the allowed power margin for crosstalk impairment in transmission networks [18]. The target BER is set to 10^{-12} . Switch block sizes, $n \times n$, for $n=8, 16$, and 32 are considered for the first and the third stages. The middle stage block size is N/n , where N is the total number of input/output ports. Also shown is for the single stage switch block in which the element crosstalk increases rapidly with switch dimension. For ports counts up to around 250, three stage switches with $n=8$ and 16 , relaxes the element crosstalk requirement to not less than -45 dB. Port counts above 250 and to up to 1000, can be constructed with $n=16$ if the element crosstalk of -48 dB is achieved. Switches with $n=32$ don't improve the element crosstalk requirement considerably because block size of 32 is already large to reduce the overall crosstalk effect.

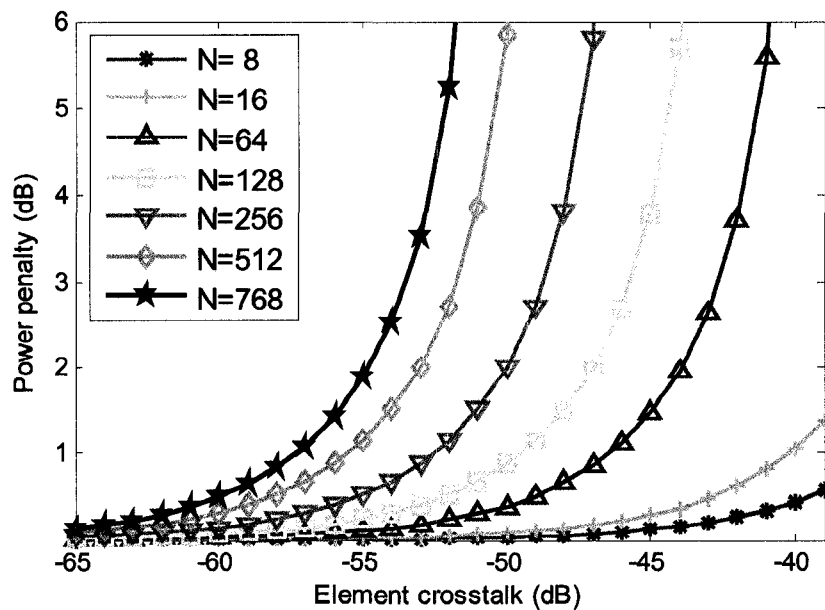


Fig. 3.9. Power penalty vs element crosstalk for $Q=7$ ($BER = 10^{-12}$) and extinction ratio, $r=20$.

Today, 4×4 switch blocks are readily available. Ports counts can be improved by interconnecting these switch blocks in multistage structures. Element crosstalk requirement for multistage switches constructed using these 4×4 blocks are also shown. Element crosstalk requirement of -42 dB has to be reached in order to construct a 64×64 switch form these 4×4 switch blocks. Meanwhile if the switch is constructed as a single stage/block with a size of 64×64 , an element crosstalk of -46 dB would be required to meet the performance requirement of BER of 10^{-12} at a power penalty of 1 dB.

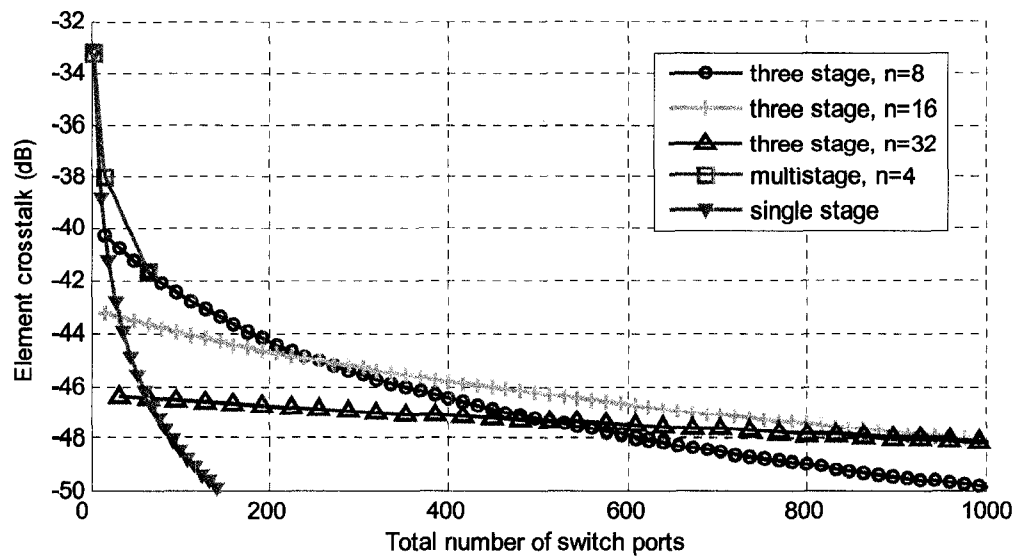


Fig. 3.10. Element crosstalk vs switch port counts for single stage and multistage switches.

3.5.2 Broadcast and select switch

Unlike in the layered switch approach where each layer represents a switching plane for a specific wavelength, the B&S switch does the interconnection all in one layer. Each switch port will represent a multicoloured or a DWDM signal. Fig. 3.11 (solid line) shows the component crosstalk requirement as a function of number of DWDM fiber port counts. Single stage switch is considered and the number of wavelengths, W , is assumed to be equal to that of number of DWDM fibers, F , such that the total number of SOA gates is optimized in each case. Fiber counts up to 150 with switch scale of 500^2 can be achieved for component crosstalk of -30 dB. Developments on integrated SOAG arrays indicate an extinction ratio of -40 dB [51]. The crosstalk values reported for AWG range from -15 dB

for 128×128 ports [55] to -30 dB for 16×16 ports [58]. The required interchannel crosstalk of the AWG, assuming an extinction ratio of -40 dB for the SOA, is also shown in Fig. 3.11 (dash-and-dot line). Interchannel crosstalk of -20 dB is sufficient to achieve switch scales up to 250^2 .

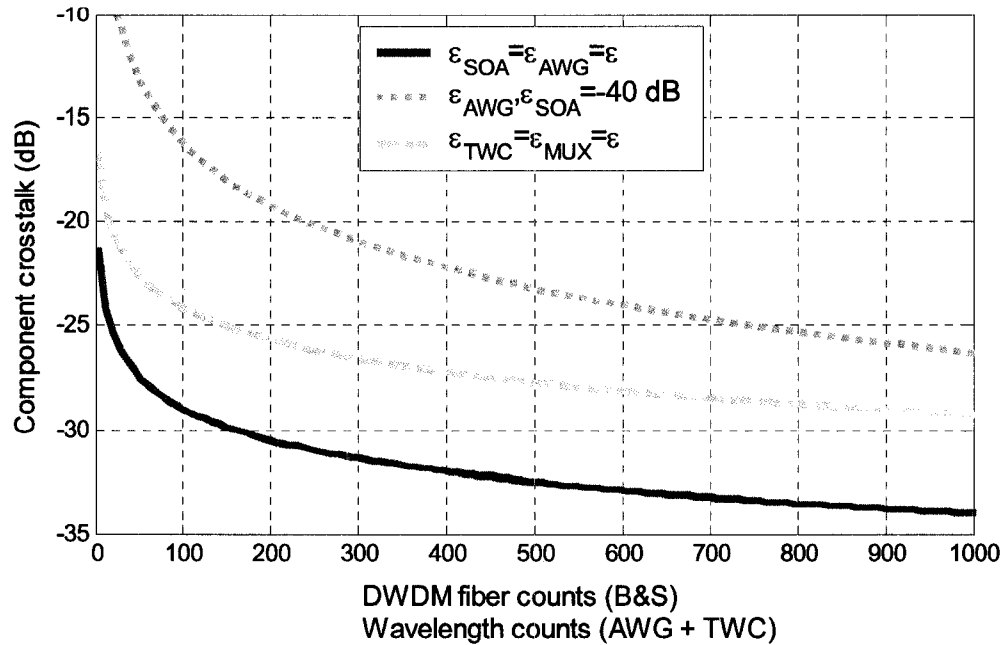


Fig. 3.11. Component crosstalk requirement as function of fiber port counts.

In situations, when F is more than W , three stage switches can be implemented with channel counts of $n \times W$ ($n = W$) for each switch blocks in the first and the third stage. Not only the number of SOA gates is minimized, this way, but the splitting complexity in each block is relaxed as it can be done equally in two stages to improve modularity.

3.5.3 AWG and TWC

As seen in Section 3.3, the lowest order crosstalk contributions in this switch are of order 2. The effective crosstalk is independent of the number of fibers by neglecting the other higher order contributions. The TWC crosstalk requirement as a function of number of wavelengths transmitted in each fiber is also shown in Fig. 3.11 (broken line). 100 wavelengths can be used at a crosstalk level of -24 dB. An input signal suppression ratio (ISSR) of best as -25 dB has been reported to date [59].

3.5.4 Architectural choices for different switch scales

Table 3.1 presents core node details, taken from [52], together with the technology choices to implement the switch. For port counts ~ 50 with small number of wavelengths (~ 10), single stage/block or three stage DC coupler switches in the wavelength layered structure would be the most least cost option among all. As the number of wavelengths and fiber counts increase, the wavelength layered approach becomes cumbersome and the wavelength dimensional switches, B&S and AWG+TWC, become efficient. Though these options are costly, they offer better power budget and crosstalk characteristics- relaxed and realistic component crosstalk requirements. Single stage and three stage B&S are appropriate when F (number of fibers) $\approx W$ (number of wavelengths) and $F \gg W$, respectively. For $W > F$, AWG + TWC structure is appropriate. For single coloured networks, the choices are DC switches and the AWG + TWC. For large port counts (~ 800), however, three stage DC switches can be implemented cost effectively if the DC element crosstalk can be improved to ~ -45 dB.

Table 3.1. Core node details and switch technologies.

| | WAN (Total traffic 307.2 Tb/s) | | MAN (Total traffic =3.6 Tb/s) | | |
|------------------------------------|--------------------------------------|-----------------|----------------------------------|------------------------|-----------------------|
| | | | | | |
| Number of overlaid core nodes | 3 | 5 | 3 | 3 | 3 |
| single colored port counts | - | - | - | - | 748 |
| DWDM port counts | 83 | 179 | 40 | 21 | - |
| Number of wavelengths at 10 Gb/s | 124 | 35 | 3 | 6 | 1 |
| Switch architecture and technology | AWG +TWC | Three stage B&S | Single block DC switch | Single block DC switch | Three stage DC switch |

3.6 Summary

Three suitable architectural and technological options were analyzed for the implementation of a AAPN core switch. The major performance impairment in optical switches, the inband optical crosstalk which deteriorates the BER performance of the system, was studied using

a statistical crosstalk model. Its impact on switch fabric scaling was evaluated by estimating the crosstalk level to be achieved at the switch element level in order to meet specific performance requirements.

Best choices in terms of crosstalk are B&S and AWG with TWC switches though they are costly. In these switch structures, the crosstalk contributions are suppressed to second order and as a result the requirements on element crosstalk levels are well relaxed to realistic values. DC switch structures, on the other hand, are the most cost effective amongst the options considered and are suitable for single coloured networks and WDM networks with fiber counts up to ~ 50 and with small number of wavelengths, ~ 15 . As the number of wavelengths and fiber counts increase, the DC wavelength layered approach becomes cumbersome and the other two wavelength dimensional switches, B&S and AWG+TWC, become efficient.

4 Performance analysis and scalability of directional coupler switches

Integrated optics device technology solutions is promising for realizing cost effective, compact, and scalable switch fabrics. Electro-optic directional coupler (DC) based switches are an attractive option when switching speeds in the range of ns are desired (e.g. packet switched networks). The basic building element in these switches is a 2×2 DC switch which can be cascaded using interconnecting waveguides in numerous structures to realize large port counts switch fabrics. The accumulation of insertion loss (IL) and crosstalk from the switch element, however, limits the size of the switch.

Dilated switch structures using 1×2 switches instead of 2×2 have been demonstrated to reduce the switch element crosstalk. However, these utilize increased number of DCs and create a larger number of interconnecting waveguide crossovers which also introduce loss and crosstalk and these can not be ignored. It is open whether a low crosstalk deployment of switching elements can be combined with minimization of cross-points. There have been various studies which report the impact of crosstalk (or interfering noise) in optical switch architectures. The power penalty is estimated using statistical models. Closed-form expressions are often derived for convenience assuming the worst case scenario for the interferers. The IL has been ignored or treated separately. Unlike in most of the switches, the IL increases with the switch size in DC switches and signal amplification is unavoidable. The aim of this work is to review various DC switch architectures and their characteristics and to study the scalability of those architectures while taking into consideration: (1) the crosstalk from waveguide crossovers in addition to the crosstalk from DC; (2) the noise from the loss-compensating amplifier. A numerical model is developed for more accurate representation and the switch performance is investigated as a function of various parameters.

The organization of this chapter is as follows: the state of the art on DC switches is given, initially, in Sec. 4.1, followed by the details of the architectural options in Sec. 4.2. A performance comparison among the structures is given in Sec. 4.4. Details on the numerical model and penalty calculations are presented in Sec. 4.3 and 4.4, respectively. In Sec. 4.6 a DC switch design example is given. Finally, a summary of this work is given in Sec. 4.7.

4.1 Directional coupler switches: state of the art

There have been a variety of reports demonstrating the realization of Electro-optic DC switch fabrics [36], [60]-[63]. All these switches are implemented using Lithium Niobate (LiNbO_3) technology. The large electro-optic coefficient of LiNbO_3 enables low voltage operation. The strength of this technology is its fast switching time, around a few tens of ns. The limitations of this technology are mainly polarization sensitivity, loss and crosstalk accumulation in cascaded switches, and the long length of the DC, which prevents building large port counts switches on single substrates. Port counts as large as 16×16 on a single substrate [62] and 128×128 with multiple substrates fiber interconnected with inter stage amplifiers [61], have been demonstrated. The polarization sensitivity can be overcome at the expense of large driving voltages [64] but the loss and crosstalk accumulations remain the major limiting factors in scaling the switch dimension.

In integrated optical switch solutions, interconnecting waveguide crossovers is unavoidable and they too introduce loss and crosstalk in addition to those from the switch elements. While loss can be compensated with the integration of amplifiers, DC crosstalk can be minimized by using only one port of the DC element active because the most severe crosstalk arises when both inputs are active. Methods based on bipartite graph design principle with 1:1 DC switches have been described for constructing strictly non-blocking low crosstalk switches [65]. The networks (architectures) suggested, however, require a large number of directional couplers due to the unused DC port and create more crossovers due to the dilation of the network. Yet, it can not be concluded that these networks are crosstalk efficient unless the crosstalk effect from the crossovers are considered and combined with low crosstalk deployment of DC elements. Further, the reduced integration level subsequently lowers the number of switch ports per wafer.

4.1.1 DC element

A directional coupler is an electro-optic device that can be used as an optical switch, as shown in Fig. 4.1. It is composed of two optical waveguides, which are titanium diffused into a LiNbO₃ substrate. These two waveguides are brought close to each other for some distance such that the optical energy can couple to each other. Electrodes are also placed over the waveguides in this region. An electric field applied to these electrodes can alter the refractive index in the waveguides in this coupling region and hence create a change in the optical path length. Thus, for an appropriate design length and the applied field, the device can either be switched to the bar state, in which the upper (lower) optical inputs are directed to the upper (lower) outputs; or to the cross state, in which the upper (lower) optical inputs are directed to the lower (upper) outputs. When designing DCs, the device is often set in a cross state with zero voltage applied and to switch to the bar state a voltage in the range of 5-20 V (varying with the electrode design and device coupling length L), is applied. However, if a polarization independent device operation is required, voltages as high as 100 V are needed [64].

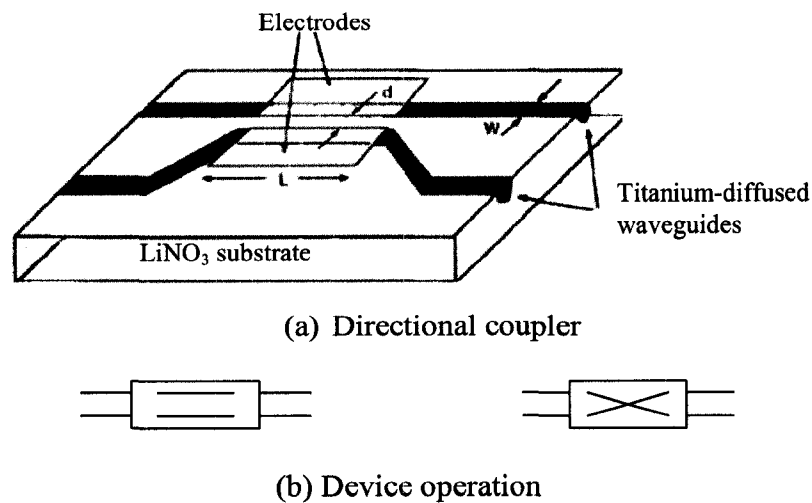


Fig. 4.1. Directional coupler

4.1.2 Sources of loss and crosstalk in DC based switches

Fig. 4.2 shows the DCs in a switch with some other elements, such as passive splitters and combiners that are typically integrated along with DCs in various switch architectures.

The sources of insertion loss (ratio of output power to the input power) and crosstalk (the unwanted power leakage to an unselected port) in DC based switches are also shown. DC insertion loss, which arises from incomplete coupling within the DC and the propagation and radiation losses in the waveguide arms, is typically in the range of 0.5 -1.0 dB. Passive 1:2 splitters introduce a loss of 3 dB (due to 50 % split) which does not include any extra losses in the waveguides. It should be noted that the passive combiners also introduce an insertion loss of 3 dB. According to the *Constant radiation theorem*, unless the product of the total cross-sectional area and the square of the numerical aperture is maintained between the N fan-in beams and the resultant beam, the power transferred to the resultant beam can not exceed $1/N^{th}$ of the total incident power carried by all fan-in beams [66]. Coupling loss (~ 1 dB) is incurred to get the signal on and off the LiNbO₃ substrate. This waveguide-to-fiber loss arises due to the mode mismatch loss and any reflection loss at the interface.

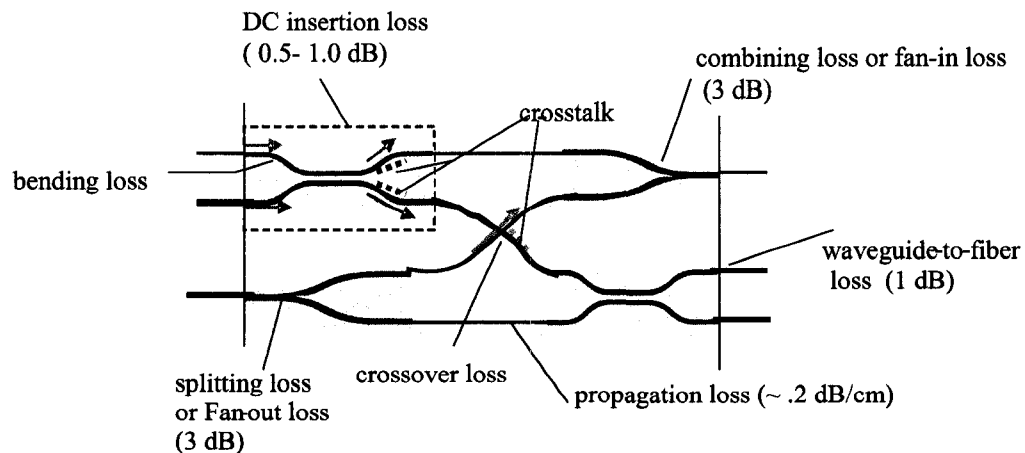


Fig. 4.2. Sources of insertion loss and crosstalk in a DC based optical switch.

Additional loss also occurs in waveguide based planar switches from the waveguide crossovers where two interconnecting waveguides cross each other. This crossover loss is dependent on the intersection angle. A loss of less than 0.2 dB is expected for angles above 7° and the loss is negligible for angles above 11° [67]. The allowable angle is determined by the required packing density of the elements in the available chip area. Another layout parameter that affects the packing density is the bend radius of the waveguide curves. To

prevent the radiation loss at the bends, a minimum bend radius of 40-50 mm has to be maintained for the connecting waveguides and the DC waveguide arms [68].

The sources for the crosstalk are the DC crosstalk, which is given by the extinction ratio of the DC element and the crossover crosstalk, which again depend on the intersection angle. Typical values for DC crosstalk range from -35 to -40 dB for single polarization device and -20 to -25 dB for double polarization device [64]. Crossover crosstalk is below -35 dB for angles above 5° [67].

4.2 Switch architectures for DC based switches

In building large switches, the switch characteristics such as number of switch elements, foot print of the switch layout, loss, and crosstalk are mainly influenced by the choice of switch architecture. In this study, only wide-sense or strict sense non-blocking architecture options are considered such that a complete point-to-point connectivity can be obtained between all the input and output terminals without any need for interruption or rearrangement of existing connections. The architectures studied are crossbar, double crossbar, Clos, Spanke, and modified Spanke [69]-[71].

It is assumed that the switches are formed on a single chip using the integrated planar lightwave technology (iPLC). The performance of these architectures, such as switch elements, number of crossovers, IL, and IL uniformity are compared as a function of switch dimension. The power penalty due to the in-band crosstalk and ASE is estimated using numerical calculations.

4.2.1 Crossbar and Double cross bar

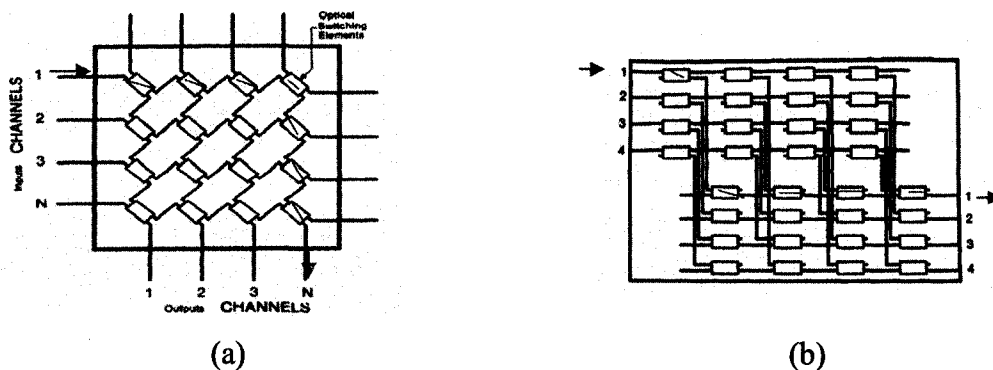


Fig. 4.3. Switch architectures (a) Crossbar (b) Double crossbar

Crossbar (x-bar) architecture is a square or a rectangular switch as shown in Fig. 4.3(a). It has no waveguide crossovers and is well suited to waveguide switches. Setting all switch elements to the cross state disables all outputs and switching the element E_{ij} to the bar state and establishes an optical path between the i^{th} input and j^{th} output. Insertion loss varies with the path through the matrix because the number of elements the signal goes through depends on the path. The shortest path encounters 1 element and the longest, the worst case, is $(2N - 1)$.

The double crossbar is constructed using two cross connected cross bars as shown in Fig. 4.3(b). It is designed to improve the crosstalk performance by switching at two stages. However, it requires twice the number of switching elements and many waveguide crossovers. Although the number of switch elements the signal goes through is the same for all interconnection patterns, the total loss varies due to crossovers, in the worst case $N(N - 1)$ crossovers. As can be seen from the geometry, both crossbar and double crossbar are wide-sense non-blocking architectures.

4.2.2 Clos

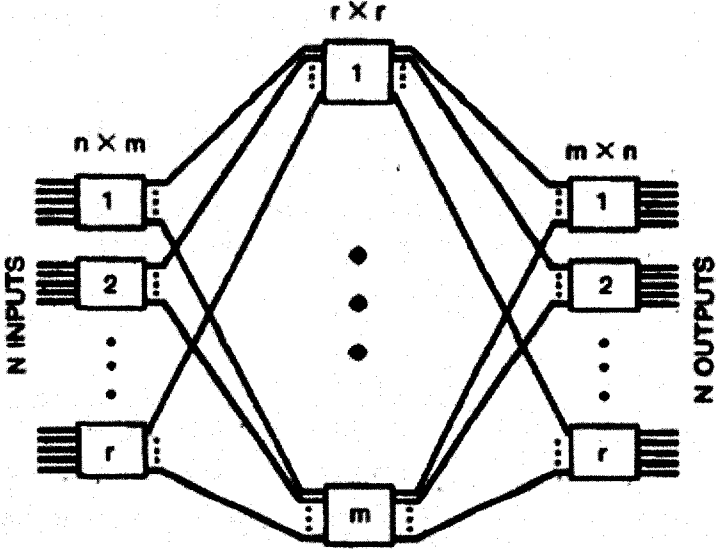


Fig. 4.4. Clos architecture

Clos demonstrated that the total number of cross points in an $N \times N$ switch matrix could be reduced if the switch is implemented by breaking it down into an odd number of stages

where each stage is implemented by several smaller rectangular matrices. Fig. 4.4 shows a three stage $N \times N$ port Clos network. The first and third stages consist of r number of $n \times m$ switch matrices, where $N = rn$. The middle stage consists of m number of $r \times r$ switch matrices (each output from the first stage and each input from the third stage are connected to all the inputs and outputs of the middle stage respectively, as shown). The Clos switch is strictly non-blocking if $m \geq 2n - 1$. The number of stages of the Clos network can be increased by replacing each middle stage switch by a three stage network. Each of the sub-switch blocks can be implemented using any non-blocking switch architectures including a sub-Clos. In this study, a three stage Clos with crossbar switches as the building blocks will be used for comparison.

To obtain the minimum number of switch elements, a relationship between N and n has to be found. The total number of switch elements, C , is

$$\begin{aligned} C &= 2rmn + mr^2 \\ &= (2n - 1)(2N + N^2/n^2) \end{aligned} \quad (4.1)$$

where $m = 2n - 1$. For a given number of N , the minimum number of elements occurs when $dC/dn = 0$, which gives:

$$2n^3 + N - Nn = 0 \quad (4.2)$$

This equation does not solve for an integer value of n for all values of N . Two of the integer pair solutions are $n=2, N=16$ and $n=3, N=27$. However, for a given value of N , the nearest integer value for n can be sought (e.g. $N=40, n=4$ and $N=60, n=5$). In situations where N is a prime number or is not divisible by a given n , the switch may be constructed as:

$$N = kn + r \quad (4.3)$$

where remainder, r , is an integer greater than zero and less than n . The first and third stage will have k input and k output switches of size $n \times (2n - 1)$ and one input and output switch of size $r \times (n + r - 1)$. It can be seen that the Clos architecture still offers savings of switch elements compared to that from an equivalent $N \times N$ crossbar for values of $N > 23$.

As N approaches large values, equation 4.2 can be approximated as $N \cong 2n^2$ and a relationship of $n = \sqrt{N/2}$ will be used in this study to evaluate the switch performance.

4.2.3 Spanke

The Spanke architecture is constructed using two stages of binary tree arrays and there are two basic types available, Spanke I and Spanke II. Spanke I uses cross connected arrays of active binary splitter and combiner trees, as shown in Fig. 5(a). Spanke II uses active binary splitters or combiners at one end with their passive counterparts at the other end, as shown in Fig. 4.5(b). Both types are strictly non-blocking and Spanke II can perform broadcast and multicast operation in addition to point-to-point networking.

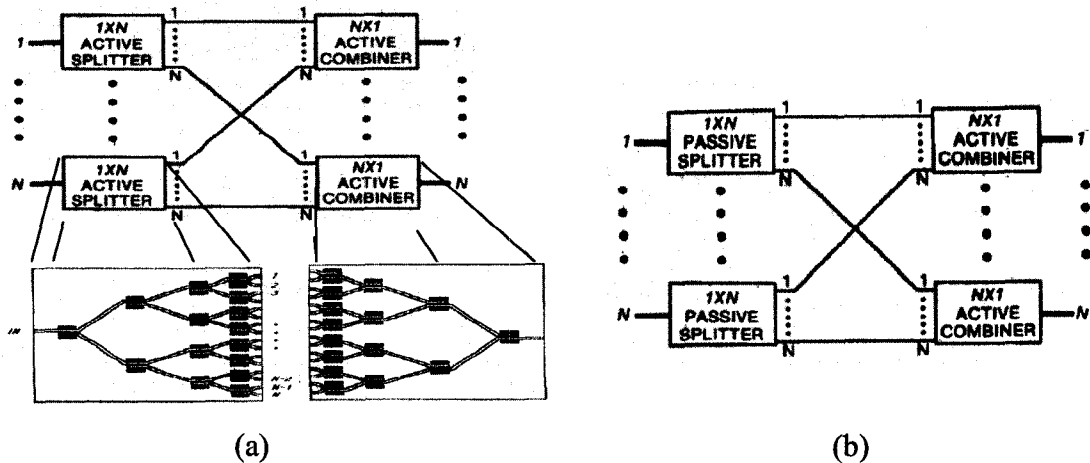


Fig. 4.5. Spanke architecture (a) type I (b) type II

An $N \times N$ switch requires $2N$ binary trees and each tree will have $\log_2 N$ stages and $2N-1$ switch elements. The signal will pass through $2\log_2 N$ switches independent of the input-output combination. However, there will be still insertion loss variations due to many crossovers in the middle and in the worst case the signal has to cross $(N-1)^2$ waveguide crossovers. There will be only $(N-1)$ crossovers active contributing to the crosstalk. Spanke I shows a good crosstalk performance at the expense of more switch elements, because all the DC elements are three port 1×2 switches and only one output port is active at a time – the worst case is a second order effect, which occurs when $\log_2 N$ number of the highest $P_{in} X_c$ noise powers from the active splitters passing through an active combiner branches with only one additional extinction, X_c (Table 4.1). Spanke II has higher insertion loss due to extra fan-in/fan-out loss of $3\log_2 N$ dB.

4.2.4 Modified binary tree or Omega

It has been proposed that the total number of elements in the binary tree architecture can be reduced by condensing the structure [70]. For example, the layout of a binary tree structure of a 4×4 switch, shown in Fig. 4.6(a), is rearranged to form groups of four switch elements with their four connecting waveguides in the center (b). Since only one output port in these elements is active at a time, these four DCs can be replaced by single 2×2 DC switches to yield a layout as shown in (c). The extension to the $N \times N$ matrix, where $N = 2^j$, is obtained as shown in (d). $2^{j-1} \times 2^{j-1}$ matrices also consist of four $2^{j-2} \times 2^{j-2}$ matrices and this procedure is repeated until the smallest matrices become 2×2 . This modified binary saves the number of switch elements from N^2 at the center to $N^2/4$ without changing the non-blocking nature of the switch. Omega will have a first order crosstalk term from the central 2×2 switch elements. The number of crossovers in the worst case is estimated based on the recursive procedure adopted in building the switch architecture.

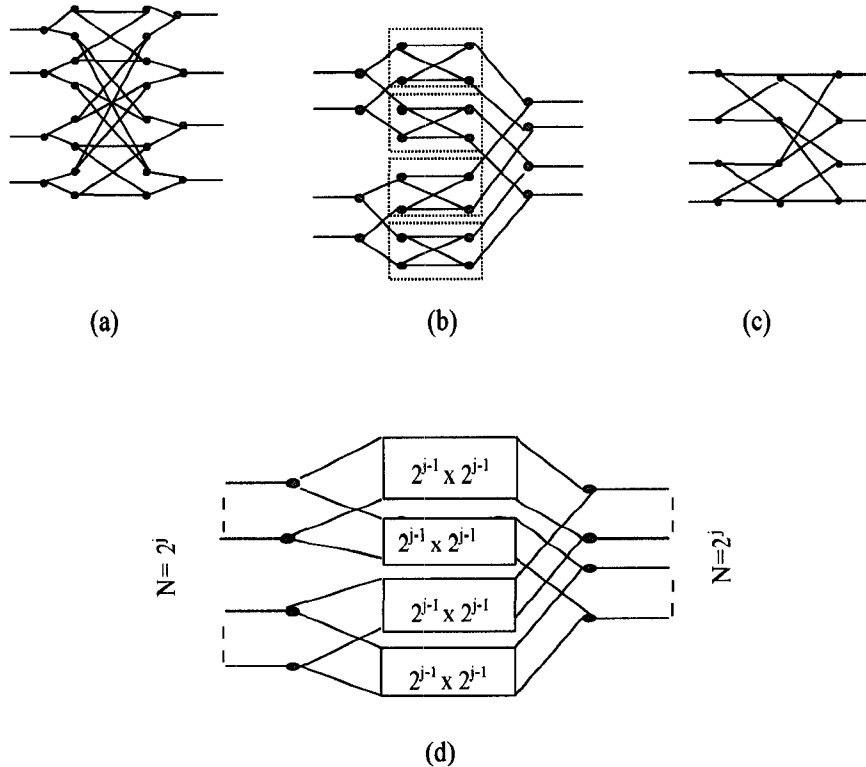


Fig. 4.6. Construction of Omega architecture from binary tree. (a) 4×4 binary tree (b) Rearranged layout of 4×4 binary tree (c) 4×4 Omega architecture (d) Configuration of an $N \times N$ Omega architecture.

4.3 Performance comparison of DC switch architectures

Table 4.1 summarizes the expressions for the number of switch elements and the worst case insertion loss, crosstalk, and differential loss as a function of switch dimension, N , for the architecture types discussed above. The crosstalk expressions are approximated to the first and second order crosstalk terms.

Table 4.1. Expressions of switch characteristics for the architecture types discussed in Sec. 4.2. N is the switch dimension, l_c DC IL, l_x the waveguide crossover loss, l_{w-f} fiber-to-waveguide loss, x_c DC crosstalk, and x_x is crossover crosstalk.

| Switch | Blocking nature | Switch elements | Worst case IL (dB) | Differential loss (dB) | Crosstalk (dB) |
|-------------------|--|------------------------|---|---|---|
| Crossbar | wide-sense (point-to-point) | N^2 | $(2N-1)l_c + 2l_{w-f}$ | $2(N-1)l_c$ | $10\log_{10}[(N-1)x_c]$ |
| Double crossbar | wide-sense (point-to-point) | $2N^2$ | $(N+1)l_c + N(N-1)l_c + 2l_{w-f}$ | $(N-1)^2l_x$ | $10\log_{10}[(N-1)x_c^2 + (N-1)x_x]$ |
| Clos | strict-sense (point-to-point) | $(2n-1)(N^2/n^2 + 2N)$ | $(6n+2N/n-5)l_c + \{4n(2n-3)+4\}l_x + 2l_{w-f}$ | $(6n+2N/n-8)l_c$ | $10\log_{10}[(2n+N/n-2)x_c + n(\sqrt{2N}-1)x_x]$ |
| Spanke-I | strict-sense (point-to-point) | $2N(N-1)$ | $2(\log_2 N)l_c + (N-1)2l_x + 2l_{w-f}$ | $(N-1)2l_x$ | $10\log_{10}[(\log_2 N)x_c^2 + (N-1)x_x]$ |
| Spanke-II | strict-sense (point-to-point,) multicast, and broadcast) | $N(N-1)$ | $(\log_2 N)(l_c + lp+3) + (N-1)2l_x + 2l_{w-f}$ | $(N-1)2l_x$ | $10\log_{10}[(\log_2 N)x_c + (N-1)x_x]$ |
| Modified Spanke-I | strict-sense (point-to-point) | $5N^2/4 - 2N$ | $(2\log_2 N - 1)l_c + \left(\sum_{i=1}^{\log_2 N - 1} \frac{N}{2^i} + \frac{N}{2^{i-1}} - 2\right)l_x + 2l_{w-f}$ | $\left(\sum_{i=1}^{\log_2 N - 1} \frac{N}{2^i} + \frac{N}{2^{i-1}} - 2\right)l_x$ | $10\log_{10}[x_c + (\log_2 N - 1)x_c^2 + (N-1)x_x]$ |

4.3.1 Switch elements

Fig. 4.7 shows the total number of elements required as a function of switch dimension, N . Among all, Clos requires the lowest number of switching elements for N above 25. Crossbar and Omega are good for dimensions less than 20. However, for waveguide optics device solution, the layout area or footprint is the one that mostly influences the device cost.

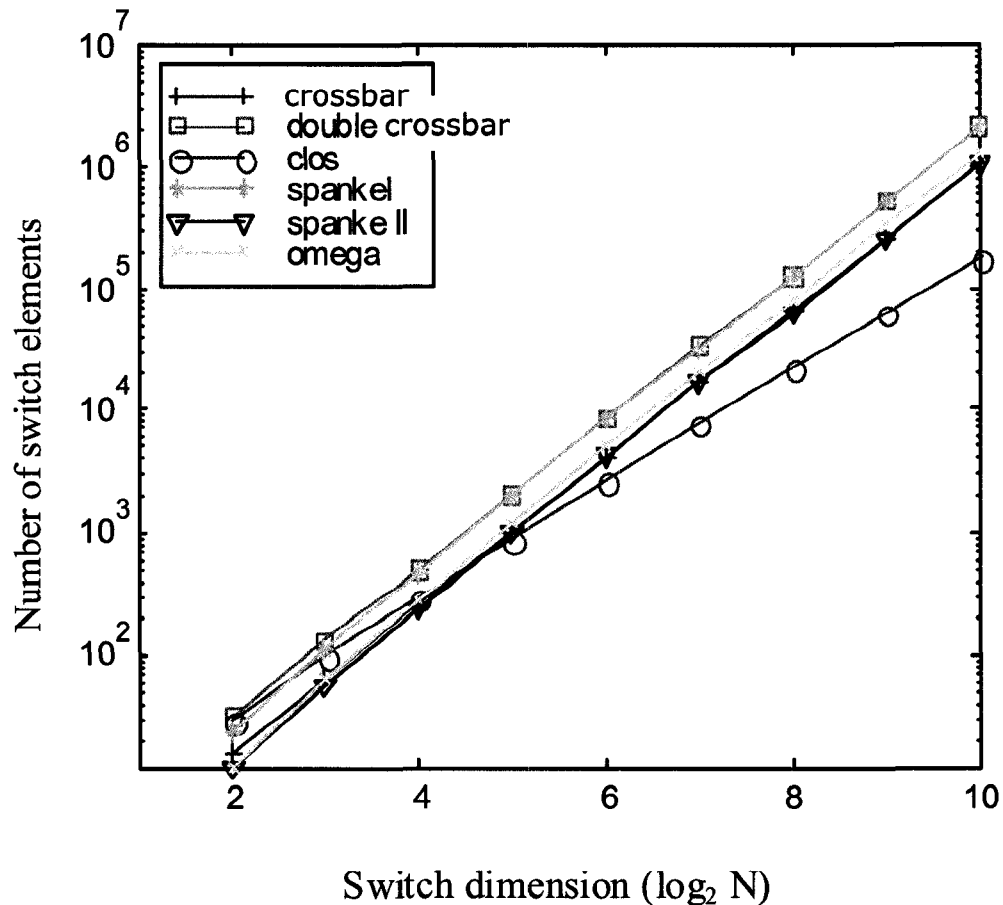


Fig. 4.7. Total number of switching elements required versus switch dimension

4.3.2 Switch insertion loss

The device insertion loss is one of the main parameters that determines the achievable matrix size. As discussed in Section 4.1.2, there are various sources that contribute to the total insertion loss. DC element loss and the fiber-to-waveguide coupling loss are taken to an achievable minimum loss of -0.5 dB and -1dB respectively. Fig. 4.8 shows the worst

case insertion loss as a function of switch dimension obtained for two values of waveguide crossover loss, -0.2 dB (a) and negligible or 0 dB crossover loss (b). In case (a), for a total IL limit of -30 dB, the maximum switch dimension that can be achieved is ~ 50 using Omega and next to that, 32 using Clos or Crossbar networks. For negligible crossover loss the best choices are Spanke I and Omega because the total number of switch elements that the signal goes through is less even though both require higher number of elements per switch. It can be seen from (a) and (b) that Omega performs much better than Spanke I in situations of losses from crossovers due to the reduction of many waveguide crossovers in the rearranged layout.

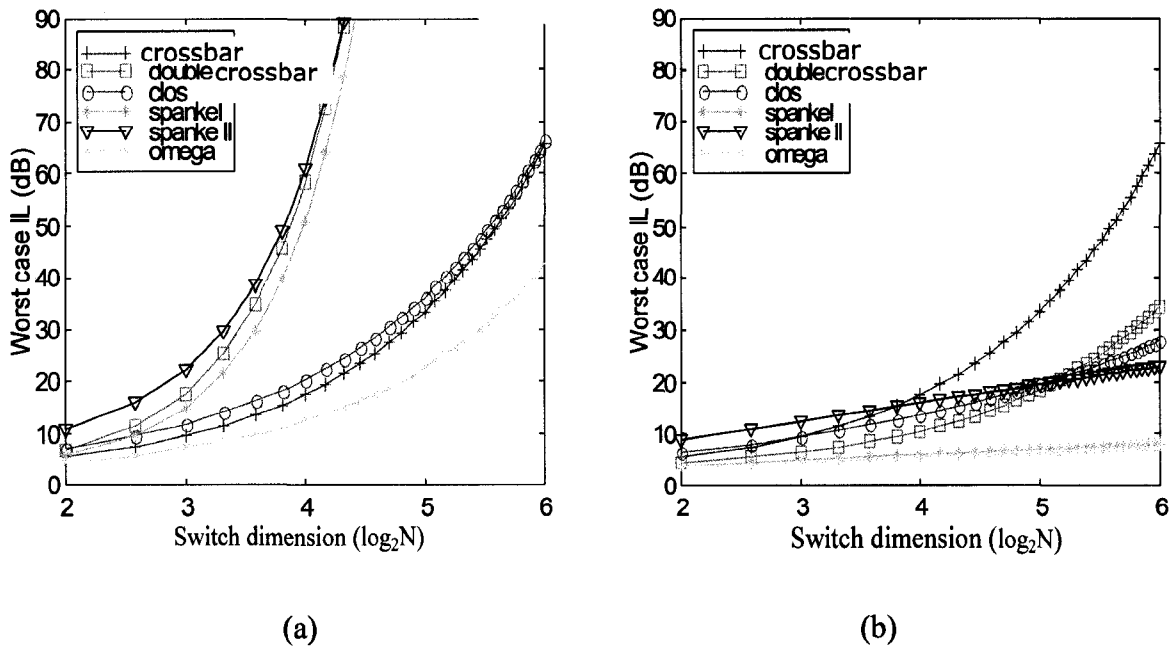


Fig. 4.8. Worst case IL versus switch dimension. DC IL = 0.5 dB, and fiber-to-waveguide loss = 1 dB (a) Crossover loss = 0.2 dB (b) Crossover loss = 0 dB

The crossover loss is the main parameter that plays an important role in the layout design because to achieve a higher level of integration in one chip the intersection angle has to be minimized to the acceptable limit of the crossover loss. Fig. 4.9 shows the single crossover loss requirement as a function of the switch dimension for a total IL limit of -30 dB. Switch dimensions of more than 60 can be achieved using Clos and Omega networks if the crossover loss is maintained below -0.01 dB.

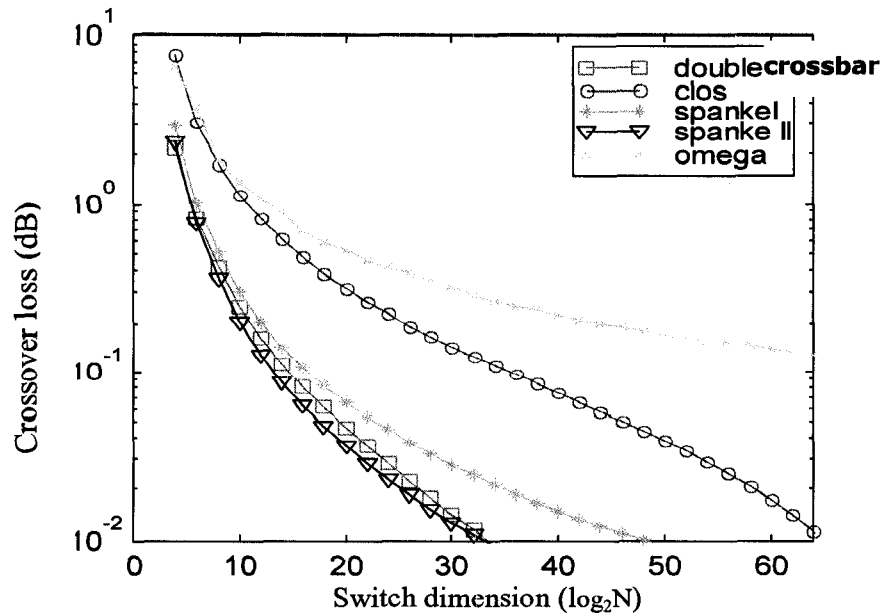


Fig. 4.9. Single crossover loss needed versus switch dimension for a given total IL of -30 dB, DC IL = -0.5 dB, and fiber- to-waveguide loss = -1 dB

4.4 Noise analysis

For a signal corrupted by in-band crosstalk channels, the primary noise source at the receiver is signal-crosstalk beat noise. The secondary noise is crosstalk-crosstalk beat noise, which can be neglected for Bit Error Rate (BER) degradation at practical crosstalk levels [48]. Experimental as well as theoretical studies on in-band crosstalk effect have been widely reported assuming thermal noise limited detection [14], [15], [48].

The signal loss in optical switches also affects the quality of the signal. Optical amplifiers are often placed at the input and/or output of the switches to compensate the loss and to extend the reach of the signal. However, the ASE noise power that falls within the receiver optical bandwidth creates additional noise at the receiver. In an optical amplified system the main sources of noise contributors are signal-spontaneous and spontaneous-spontaneous beat noises. Analytical models in estimating penalties due to in-band crosstalk in the presence of ASE have been reported [73]-[75] with the assumption of fixed ASE noise at the receiver regardless to scaling of the switch and/or networks. Closed-form expressions are often derived with these models, which are only good for midway or optimized decision thresholds.

In this work, the penalty due to in-band crosstalk is numerically evaluated as a function of ASE noise, crosstalk, extinction ratio, and decision threshold levels.

4.4.1 In-band crosstalk

The in-band crosstalk generates the worst-case noise performance when the polarizations states of the main signal and crosstalk channels are matched, while it vanishes for orthogonal polarization states. It has been shown experimentally that systems with randomly polarized fields display near worst-case operation and the systems must be designed to face for the worst case [76].

The signal-crosstalk beat noise current at the receiver, due to $(N-1)$ number of interferes with aligned polarization states, can be given as

$$i_{s-IN} = \Re P 2 \sum_{i=2}^N \sqrt{\varepsilon_i} \cos[(\omega_1 - \omega_i)t + \phi_1(t) - \phi_i(t)], \quad (4.4)$$

where \Re is the receiver responsivity; P is the power of the main signal; ε_i is the power of the i^{th} crosstalk channel relative to the main signal; ω and ϕ are the optical frequency and the independent phase fluctuation of the signal and the interferers with the subscripts, 1 to denote the signal and i ($= 2$ to N) denote the interferers. In the case of, $\omega_1 = \omega_i$ and $\varepsilon = \varepsilon_i$, for $i = 2$ to N , i.e. interferers with equal power and aligned frequencies, the variance of beat noise current is obtained as $2\varepsilon NP^2$. It is assumed that laser phase noises are distributed uniformly over the range from 0 to 2π .

4.4.2 ASE noise

4.4.2.1 Amplifier model

Amplifier gain is taken as unchanged between data ‘one’ and ‘zero’ transmission. At high bit rates (≥ 10 Gb/s), the bit period is much less than the carrier life time of both Erbium-doped fiber amplifier (~ 10 ms) and Semiconductor Optical Amplifiers (~ 0.5 ns). The gain, G , is calculated [77] at average signal power, P_{av} , as

$$P_{av} = \frac{P_{sat}}{G-1} \ln\left(\frac{G_0}{G}\right), \quad (4.5)$$

where P_{sat} is the saturation power; and G_0 is the maximum amplifier gain; P_{av} is $P(1+r)/2$, where P is the signal power when data ‘one’ is transmitted and r is the signal extinction ratio.

4.4.2.2 Beat noise variances due to ASE

In an optical amplified system the main sources of noise contributors are signal-spontaneous and spontaneous-spontaneous beat noises, which are given [77], respectively, as

$$\sigma_{s-spont}^2 = 4\Re^2 P P_n (B_e / B_0) \quad (4.6)$$

$$\sigma_{spont-spont}^2 = \Re^2 P_n^2 \left(\frac{2B_e}{B_0} - \frac{B_e^2}{B_0^2} \right), \quad (4.7)$$

where B_0 and B_e are the optical and electrical bandwidth of the detector, respectively; $P_n = (G-1)h\nu n_{sp} B_0$ is the ASE noise power, n_{sp} is the spontaneous emission factor, h is the Planck’s constant, and ν is the frequency of the signal. Noise power in single polarization is considered. The amplifier noise is assumed to be Gaussian and the noise spectrum is white over the optical filter bandwidth, B_o . A p-i-n receiver is considered.

4.5 BER and power penalty calculations

BER calculations are performed with p-i-n receivers. It is assumed that there are N number of interfering signals, each at a crosstalk level of ε and with aligned polarizations and bit-boundaries with that of the main signal, to represent the worst-case scenario. The impact of beat noise is quantified by numerically calculating the PP, which is defined in dB as the additional signal power required at the receiver in order to maintain the same BER as without the interferers (or noise). Every noise source is considered as independent and Gaussian statistics are invoked in calculating the total noise variance.

In this study, the PP values are evaluated at a BER of 10^{-9} with the following values assumed for the variables; $B_0=12.5$ GHz, $B_e=5$ GHz, $\Re=1$, $n_{sp}=1.4$, $P_{sat}=-3.6$ dB, and i_{th} (thermal noise current) $=3$ pA / $\sqrt{\text{Hz}}$.

4.5.1 BER by weighted averaging

The widely used assumption for interfering bits is ‘mark’ for all interferers to represent the worst case. In this study, by considering all possible combinations between the signal and the interferers, the mean BER is evaluated by statistically weighted averaging the conditional probability density functions (PDFs). Assuming equal probability for receiving a ‘one’ or ‘zero’, the probability that k number of interfering bits are ‘ones’ is given by a binomial distribution,

$$P_{(k)} = \frac{1}{2^N} \frac{N!}{(N-k)!k!}. \quad (4.5)$$

Considering all possible combinations between the signal and the interferers, the mean BER can be evaluated by statistically weighted averaging of the conditional probability density functions (PDFs) as:

$$BER = \frac{1}{4} \left\{ \sum_{k=0}^N P_{(k)} \left(\operatorname{erfc} \frac{I_1 - I_d}{\sqrt{2(\sigma_1^2 + \sigma_{INk}^2)}} + \operatorname{erfc} \frac{I_d - I_0}{\sqrt{2(\sigma_0^2 + \sigma_{INk}^2)}} \right) \right\}, \quad (4.6)$$

where $\sigma_{INk}^2 = 2\mathcal{E}P^2(k+(N-k)r)$ and $\sigma_{INk}^2 = 2r\mathcal{E}P^2(k+(N-k)r)$ are the noise power variance when k number of data ‘ones’ and ‘zeros’ are transmitted, respectively; I_1 and I_0 represent the received current levels for data ‘one’ and ‘zero’ respectively. I_d is the decision threshold setting; σ_1^2 and σ_0^2 represent the additional noise powers for data ‘one’ and ‘zero’, respectively (Sec. 4.4.2.2).

4.5.2 Thermal and shot noise detection

In p-i-n receivers, thermal and shot noise are present and are given as $\sigma_{th}^2 = i_{th}^2 B_e$ and $\sigma_{shot}^2 = 2qPB_e$, respectively. i_{th} is the thermal noise current and q is the electron charge.

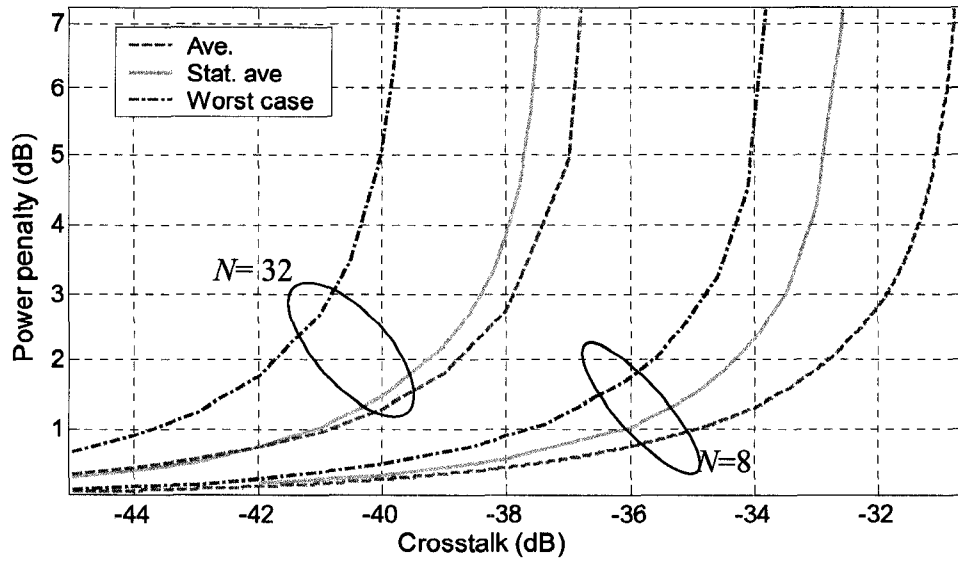


Fig. 4.10. PP versus element crosstalk.

Fig. 4.10 shows the PP calculated (from the BER versus received power curves) as a function of element crosstalk for total number of interferers of 8 and 32 (solid lines), at a BER of 10^{-9} . Also shown are the PP calculated using the widely quoted equation [48] [76] ,

$$PP(dB) = -5 \log_{10} \left(1 - 4\sigma^2 Q^2 \frac{(1+r)}{(1-r)^2} \right), \quad (4.7)$$

at a BER of 10^{-9} ($Q=5.9$): for average total noise power assuming the density of ‘ones’ as 0.5 (dashed lines), $\sigma^2 = \sigma_{av}^2 = N\epsilon$; and for total noise power (upper limit), assuming all interferers in ‘mark’ state, $\sigma^2 = 2N\epsilon$ (dash and dot lines). All the penalties are calculated with mid-way decision threshold and $r=0.01$.

Calculations based on average powers underestimate the PP compared to that of weighted average calculations. This effect is significant for low number of interferes. At 1 dB of power penalty, the element crosstalk is underestimated by 1dB for 8 interferers. A comparison of experimental penalties measured (for aligned polarizations) with that of theoretical calculation based on total average powers also showed that the measured penalties for various number of interferes up to 32 are higher than that of calculations [76]. BER floors or infinite PP are also reached at lower element crosstalk with symbol conditioning. However, for large number of interferes, the predictions with statistical averaging tend to merge with that of the sample average.

4.5.3 ASE noise limited detection

Consider a scheme where the signal loss through the switch is compensated by placing an amplifier at the output of the switch. The amplifier maximum gain G_0 , is set to be equal to the inverse of the worst case signal loss through the switch. The signal power at the receiver is $(P_{in} + \sum 2\varepsilon_i P_{in}^2)G / G_0 + P_n$, where P_{in} is the input signal power to the switch. BER calculations, given in equation (4.6) will now include two other noise beat terms, signal-spontaneous and spontaneous-spontaneous noise, as given in Sec. 4.4.2.2.

4.5.3.1 Impact of decision threshold on ASE induced penalty

In a ASE noise limited system, the dominant source of noise at the receiver is the signal-spontaneous beat noise, which is signal dependent. Thus, for a fixed midway threshold, it creates more error when data ‘one’ is transmitted compared to that of ‘zero’. Further, the noise increases with increasing loss compensation as it depends on the amplifier gain as well. Fig. 4.11 (a) shows the ASE induced PP (the main signal with zero interferers), at a BER of 10^{-9} , as a function of normalized decision threshold, I_d / I_1 for switch losses of 10 dB (solid line) and 17 dB (dashed line). The extinction ratios are 0.02 (‘+’), and 0.1 (‘□’). The optimum threshold for lowest PP is shifted more towards ‘zero’ as the loss increases. For the same loss, increase in extinction ratio, however, pushes the optimum threshold more towards midway. This is because more error is created with lower threshold settings when data ‘zero’ is transmitted at high extinction ratios. The optical signal to noise ratio (OSNR) at the receiver with the optimum PP is 22.6 dB (10 dB loss) and 19.5 dB (17 dB loss) for the extinction ratio of 0.02; and is 23.3 dB (10 dB loss) and 21.2 dB (17 dB loss) for the extinction ratio 0.1. This shows that at a given loss, increase in the extinction ratio requires higher OSNR at the optimum threshold.

The effective ASE noise or the OSNR, for a given loss, can be improved with distributed amplification. It is a costly option for DC switches while it is a viable solution for SOA based switches. PP calculated with two amplifiers, each placed at the input and output of the switch with maximum gain set to the inverse of one half switch loss is also shown in Fig. 4.11 (a), plotted as dash-dot line. Switch loss of 17 dB and extinction ratio of 0.1 are assumed. As seen, the ASE induced PP can be greatly improved at higher losses

with distributed amplification. An OSNR of 24 dB can be obtained at the optimum threshold level of 0.37. The optimum threshold setting at a given BER is thus determined by both ASE noise level and the signal extinction ratio.

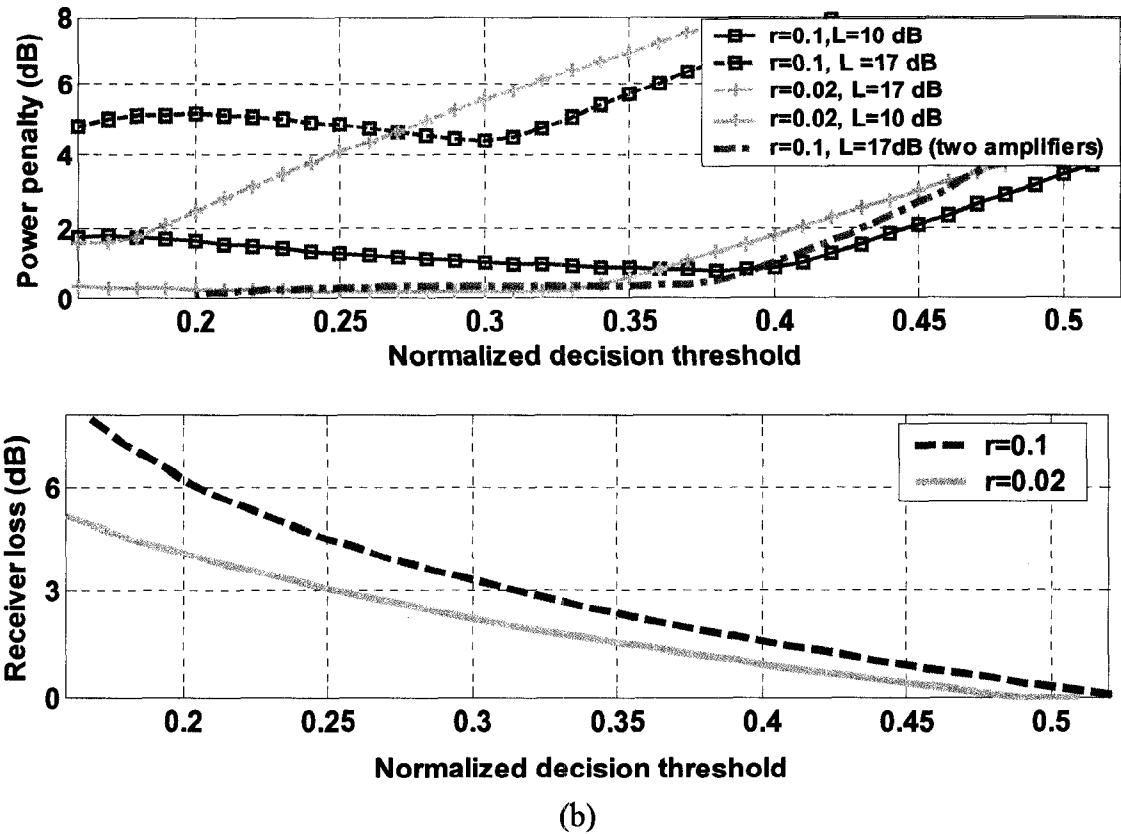


Fig. 4.11. (a) PP versus normalized decision threshold: single amplifier-IL=10 dB (solid lines) and 17dB (dashed lines) for $r=0.02$ ('+') and $r=0.1$ ('□'); two amplifiers for IL=17 dB and $r=0.1$ (dash-dot line). (b) Receiver loss versus normalized decision threshold.

Setting the initial threshold away from midway, however, increases the loss in the receiver sensitivity and it has to be minimized as possible. In the absence of ASE, the dominant source of noise at the receiver is thermal noise, which is independent of the signal level and a midway decision threshold would optimize the power required for a given BER. Fig. 4.11 (b) shows the receiver loss as a function of normalized decision threshold for the extinction ratios of 0.02 (solid line) and 0.1 (dashed line).

4.5.3.2 Impact of decision threshold on the tolerance to crosstalk in the presence of ASE.

In the presence of interferers, it was observed that the optimum thresholds for minimum total PP, due to ASE and crosstalk, shift slightly towards zero with increasing crosstalk as compared to those of ASE alone. Fig. 4.12 shows the crosstalk induced power penalty as a

function of element crosstalk for 16 number of interferers at a 10 dB loss level. Signal extinction is 0.1. The normalized decision threshold settings were, for a single amplifier 0.55 (midway), 0.38 (ASE optimum), and 0.35, which are plotted as ‘o’, ‘□’, and ‘*’, respectively; for two amplifiers, 0.41, plotted as ‘+’. As seen, mid-way decision threshold shows a very steep slope to element crosstalk levels. However, a well relaxed tolerance, up to -36 dB at 1 dB, is achieved when the initial decision threshold level is set a little below the ASE optimized settings. Higher OSNR obtained with distributed amplification provide better tolerance to crosstalk at low element at crosstalk levels (<-38 dB). A similar trend was shown experimentally for a single interferer [85].

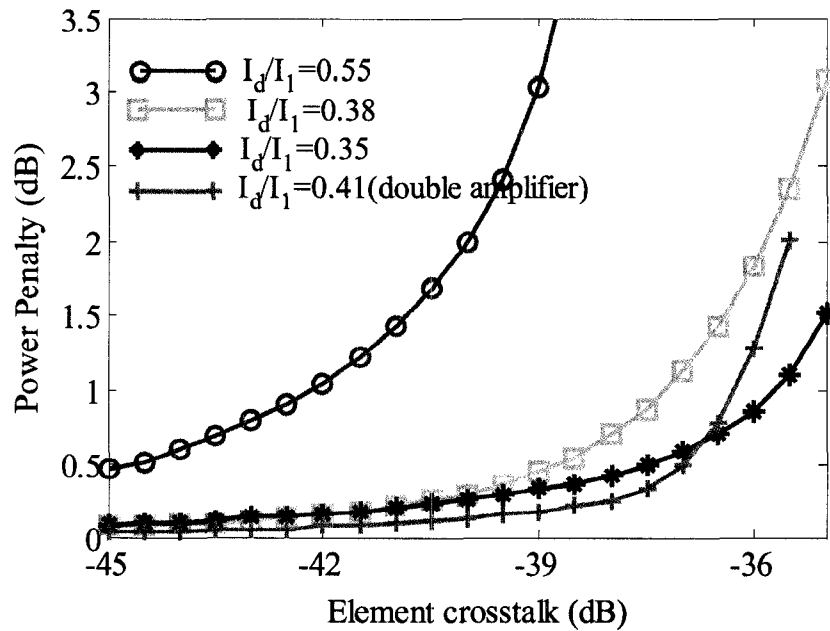


Fig. 4.12. PP versus element crosstalk.

4.6 DC switch design: an example

The model presented above was used to study design requirements on DC switches. Three different strictly non-blocking single chip DC switch architectures were considered, crossbar, Spanke, and modified Spanke. In a given switch structure, the worst-case signal loss is fixed for a given switch dimension. However, the interference noise added to the main signal is determined by how many ports are activated and the path taken by the main signal through the switch. The worst case insertion loss and crosstalk for the above structures are given in Table 4.2, as a function of number of inputs, N , DC element

crosstalk (X_c), waveguide crossover crosstalk (X_x), DC loss (l_c), and waveguide crossover loss (l_x). For crosstalk, the first order contributions are considered. Unlike in Spanke and modified Spanke, in crossbar the worst case signal loss path will not be the path for worst case noise addition. Further, it has no waveguide crossovers and has the first order crosstalk contributions that come from the 2×2 switch elements. The other two structures use binary tree structures with 1×2 switch elements which are interconnected through waveguide crossovers, except in modified Spanke, the elements are rearranged with a single column of 2×2 switches in the middle to minimize the total number of crossovers and switch elements. In these structures, major source of crosstalk is from the crossovers while the DC crosstalk is reduced to second order.

Table 4.2. Worst case IL and crosstalk. l_c and X_c are the losses of DC and crossover, respectively, in dB; l_x and X_x are the crosstalk of DC and crossover, respectively, in dB.

| Switch | Worst case IL (dB) | Crosstalk |
|-----------------|--|---|
| Crossbar | $(2N-1)l_c$ | $2P^2 \sum_{k=0}^N (k-1)10^{-X_c/10}$ |
| Spanke | $2(\log_2 N)l_c + (N-1)^2 l_x$ | $2P^2 \sum_{k=0}^N (k-1)10^{-X_x/10}$ |
| Modified Spanke | $(2 \log_2 N - 1)l_c + \sum_{i=1}^{\log_2 N - 1} (N/2^i + N/2^{i-1} - 2)l_x$ | $2P^2(10^{-X_c/10} + \sum_{k=0}^N (k-1)10^{-X_x/10})$ |

Fig. 4.13 shows the component crosstalk requirement (X_c for crossbar, and X_x for Spanke and modified Spanke, with X_c of -35 dB for the single 2×2 DC in the middle) as a function of crosstalk induced PP, calculated at a loss of 12 dB and $r = 0.1$. Single amplifier configuration with a decision threshold setting at 3dB of receiver loss is considered. The approximate switch dimensions for $l_c = 0.3$ dB and $l_x = 0.05$ dB are 20, 16, and 64 for crossbar, Spanke, and modified Spanke, respectively. For small switch sizes (< 20), component crosstalks up to -36 dB can be tolerated at 1 dB of PP while higher switch dimensions (64) is possible with X_x up to -42 dB. These results are shown as an example.

Higher switch dimensions can be achieved by optimizing the noise levels with efficient amplification scheme and corresponding optimal thresholds, as described in Sec. 4.5.3.1.

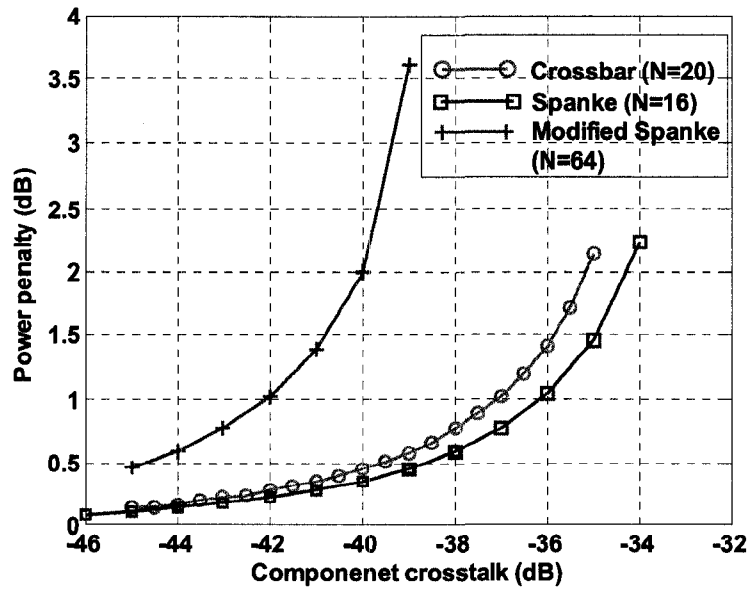


Fig. 4.13. PP versus element crosstalk.

4.7 Summary

In this chapter, the architectural options for DC coupler based switches were reviewed and the performance characteristics of these structures to switch scaling were studied and compared. A numerical model that takes into consideration every source of noise and loss in the switch and also the additional noise, ASE that come from loss-compensating amplifier, was presented. Numerical results indicated that the receiver threshold setting has an impact on crosstalk and ASE induced power penalties and it can be optimized for improved switch performance.

Initially, the influence of loss from waveguide crossovers to the switch performance was investigated. To study the impact of crossover loss on the total IL, the worst case insertion loss as a function of switch dimension was obtained for a waveguide crossover loss, -0.2 dB and compared with the one with negligible or 0 dB crossover loss. Except crossbar, which doesn't have crossovers, the total IL of the switches rapidly increases with increasing dimension due to the increasing number of crossovers created and the loss

incurred; for a total IL limit of -15 dB, the maximum switch dimension is limited to ~ 32 , thus demanding signal amplification in the switch to realize large port count switches.

Secondly, for a more accurate representation, a numerical model was next developed, taking into account all possible impairments combinedly with aim of optimizing the switch performance (or power penalty) in terms various parameters. BER was evaluated by weighted averaging of all possible combinations among signal and interfering bit streams, rather than adopting the well-known worst case approach, to represent a practical scenario.

Thirdly, the impact of decision threshold setting on the ASE and crosstalk was investigated. It was shown that, by choosing an optimal decision threshold for a given ASE noise level or optical signal to noise ratio (OSNR) and extinction ratio, the tolerance to switch element crosstalk levels can be greatly improved (relaxed by ~ 6 dB). Noise level improvement through distributed amplification for a given loss, further enhances the tolerance to element crosstalk levels at reduced receiver loss.

Finally, a tutorial on a design example was presented. The element crosstalk requirements were estimated for three different DC switch architectures at a given loss limit such that suitable architectural options can be sorted out for the required switch dimensions at realistic element crosstalk levels. At practical crosstalk and loss levels for both DC and crossovers, switch dimension of 64 can be realized at a switch loss of 12 dB.

5 ROADMs based on wavelength selective switches: architectures for multi-degree ROADMs and performance characterization in terms of crosstalk

Reconfigurable optical add/drop multiplexers (ROADMs) are the key elements in building the next-generation, dynamically reconfigurable optical networks. ROADMs enable dynamic add/drop or express pass-through of individual wavelength division multiplexed (WDM) channels or group of channels at network nodes without the need for costly optical-electrical-optical (O-E-O) conversions. While the first generation ROADMs were of degree two and supported ring or line architectures, new ROADMs are expected to support high-degree nodes which are essential for the design and deployment of future optical transport networks [78]-[82]. Over time, to accommodate large topologies the networks will evolve from several interconnected rings to large meshes, hence requiring the intersecting node degree to increase.

For a given network, the choice of ROADM architecture and underlying technology depends on how effectively one can address present network needs and manage unforeseen changes. Wavelength selective switches (WSSs) are the latest generation of wavelength routing devices that promise to build flexible and degree upgradeable fully functional ROADMs. ROADM architecture and technology influence cost, optical performance, and configuration flexibility. Rational design of add/drop nodes would attempt to arrive at cost-reducing solutions without compromising optical performance and flexibility.

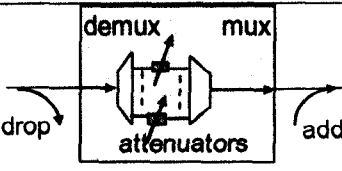
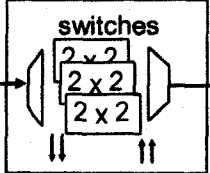
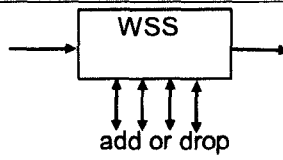
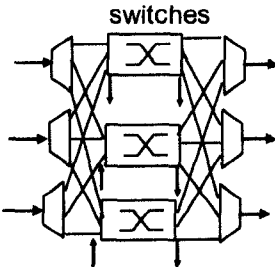
The aim of this work is to analyze multi-degree node implementation options of WSS-based ROADMs in terms of in-band crosstalk, the main performance impairment in switches, with an emphasis on the reduction in the number of wavelength selective switches used in the module.

5.1 Introduction

5.1.1 ROADM architectures and technologies

The main architectural options that have been used in ROADM developments are wavelength blocker (WB), small switch arrays (SSA), WSS, and optical crossconnects (OXC). Table 5.1 lists these ROADM configurations and their pros and cons.

Table 5.1 ROADM configurations and their features

| ROADM | Configuration | Pros | Cons |
|-------|---|---|--|
| WB |  | Add/drop all λ 's | Not degree upgradeable Filters for drop and combiners for add |
| SSA |  | Low-cost (iPLC) Small size Add/drop all λ 's | Non-degree upgradeable Fixed λ /port |
| WSS |  | Any multiple λ 's to any port Degree upgradeable | Two-units/ROADM Costly |
| OXC |  | Any multiple λ 's to any port Degree upgradeable | Next generation Costly if not iPLC |

In WB, there is no switching. The blockers are commonly implemented using MEMS or liquid crystals. WB is a matured technology but it is limited to integration flexibility and node upgradeability. SSAs are realized using integrated planar lightwave circuits (iPLC)- combination of AWGs and thermally driven directional coupler switches. Though integration reduces the cost, SSAs are not degree upgradeable. In term of upgradeability, node degree and multiple wavelengths (λ 's) to any port, the choices are

WSS and OXC. The approach sought in OXC is similar to that in SSAs, but OXC can support many ports by employing a large port count switches.

Among all, WSS technology has been a success and it has found many application in metro and long-haul networks. High level of integration, excellent spectral filtering properties and the ability to support node degree upgrades have favored the WSSs over other ROADM technologies [81], [82]. Nonetheless, in cost-sensitive network deployments and where node upgrades are not needed, WB and SSAs are still preferred because of lower cost.

5.1.2 ROADM performance in terms of crosstalk

ROADMs introduce network design constraints due to the accumulation of physical impairments while providing optical transparency at network nodes. One of the critical physical impairments is in-band crosstalk. In-band crosstalk added to wavelength channels at any node should be reduced in order to allow cascadability of nodes which is an important requirement in optical transport networks based on ring and mesh topologies. A study on in-band crosstalk applied to a single WSS in the drop configuration has been reported recently [83], but there have been no published reports on crosstalk in WSS-based multi-degree ROADMs. This work examines implementations of multi-degree WSS-based ROADMs, provides their crosstalk analysis, and assesses node and network scalability.

5.1.3 Organization of this work

WSS-based ROADM implementation options are discussed in Sec. 5.2. In Sec. 5.3, a description of WSS crosstalk mechanism is provided and it is argued that its magnitude can vary depending on how the WSS is configured in the ROADM. In Sec. 5.3, experimental results quantify the crosstalk-induced power penalties of an eight-degree ROADM node. Upgradeability to node degree eight is demonstrated with state of the art optical wavelength switching technology. In Sec. 5.4, a modular architecture of a large degree ROADM node implemented using WSSs as building blocks is proposed. Sec. 5.5 provides the summary of this work.

5.2 WSS-based ROADM configurations

The WSS under consideration is a path reversible $1 \times N$ wavelength routing module constructed by integrating demultiplexers (DeMUXs), optical switches based on micro-electro-mechanical systems (MEMS), and multiplexers (MUXs) [19]. The switch provides wavelength independent (colorless) ports, i.e., any incoming wavelength or set of wavelengths from the incoming ports can be switched to any of the outgoing ports. Incoming wavelengths can also be blocked or attenuated individually. A fully functional ROADM module is constructed by using a pair of WSSs, one for the add function and one for the drop function, as illustrated in Fig. 5.1. A one-directional signal flow is considered here. The ports can support any number of wavelengths, therefore a two degree ROADM can be upgraded up to a $N-1$ degree ROADM, or to a WXC with add and drop functionality. As shown in Fig. 5.2(a), among the N service ports of the WSS, one is dedicated to local add/drop and the remaining $(N-1)$ are used as crossconnecting ports to $(N-1)$ ROADM modules in the node. As an alternative solution, Figs. 5.2(b) and 5.2(c) show ways of implementing ROADM modules with a reduced number of switches, where instead of a pair of WSSs for each add and drop, one uses a combination of a WSS and an optical splitter or combiner. Both (b) and (c) simplify the design while maintaining the same level of flexibility in upgrading nodes of degree up to $N-1$ with the property of colorless add/drop at the local node. However, splitters and combiners introduce additional node loss, which can be compensated by fiber amplifiers. The advantage of the configuration in (a) is that cascaded WSSs provide very good overall (port-to-port) isolation, thus potentially leading to a very low signal crosstalk. Note, however, that option (b) has the advantage of supporting broadcasting functionality while the options (a) and (c) cannot.

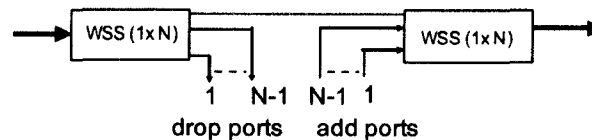


Fig. 5.1. Two degree ROADM module constructed using two WSS, each for add and drop.

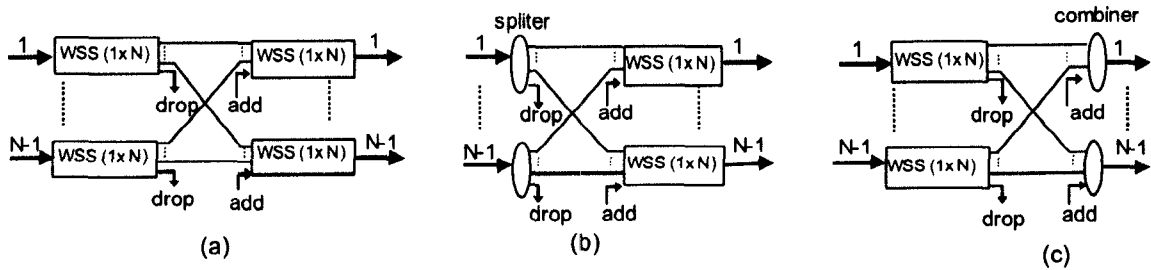


Fig. 5.2. Multiple-degree ROADM architectures: (a) WSSs for add and drop; (b) Splitters for drop and WSSs for add; (c) WSSs for drop and combiners for add.

5.3 Crosstalk analysis applied to different WSS-based ROADM configurations

The WSS architecture considered here incorporates MUX/DeMUX functionality by using a two-layer stack of Arrayed Waveguide Gratings (AWGs) that are interconnected through a free-space mirror array based on MEMS [19], as illustrated in Fig. 5.3.

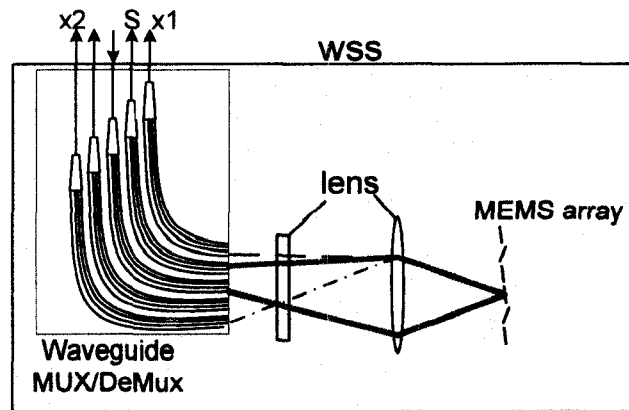


Fig. 5.3. The functional diagram of the WSS [19], consisting of a 2-layer stack of arrays of waveguide gratings, lenses and MEMS array. Thick gray line indicates the main signal, switched to the selected port, 'S', and the broken and dash and dot lines indicate crosstalk to non-selected ports, 'x1' and 'x2', respectively.

Switching of the WSS exhibits various isolation values among its ports. In channel dropping configuration, the de-multiplexer at the input port sends each channel to a dedicated mirror, which is capable of tilting in two dimensions and steers the channel towards any of the MUXs connected to each of the output ports. When a channel is dropped at selected port, 'S' (shown in gray line), there exists a possibility that - due to misalignment of mirrors, non-ideal filtering, or both - a small part of that channel leaks to an adjacent MUX (shown in broken line) and is present at a non-selected port, 'x1' or to a

non-adjacent MUX (shown in dash and dot line) and is present at an other non-selected port, 'x2'. The isolation on any channel in non-selected ports thus depends on the relative positioning of that port to the selected port; e.g. the power leakage to port 'x1' is higher than that to port 'x2'. In channel adding configuration, the light propagation direction is reversed. In add functioning there could be as many as N-1 in-band crosstalk contributions at the output port of a 1×N WSS. However, the crosstalk from non-adjacent ports is negligible.

The total in-band crosstalk of a WSS-based ROADM depends on how adding and dropping of channels is implemented and specifically, whether the WSS is used in dropping, adding, or both (Fig. 5.4). In option 5.4(c), WSSs are used for drop and combiners for add. The total added crosstalk scales with the node degree. This is because, when a WSS drops a channel, the leaked signals from the WSS (shown in broken lines) are mixed at the combiner with the locally added signal. In option 5.4(b), splitters are used for drop and WSSs for add. The WSS switches one channel at any given wavelength from any of the input ports while blocking all other same-wavelength channels at the remaining input ports. That is, the WSS functions as both the wavelength blocker and the switch. In option 5.4(a), WSSs are used for drop and add. The WSS on the add side will have a single channel at any given wavelength among its input ports since the WSS on the drop side selectively routes the wavelengths to its drop ports. Thus, the WSS functions solely as a switch. The crosstalk in options (a) and (b) is due to the accumulated isolations of input ports to the output (WSS in add) at given switch settings. However, in option (a), any in-band crosstalk is reduced to second order by the WSS on the drop side compared to that of a first order crosstalk in option (b).

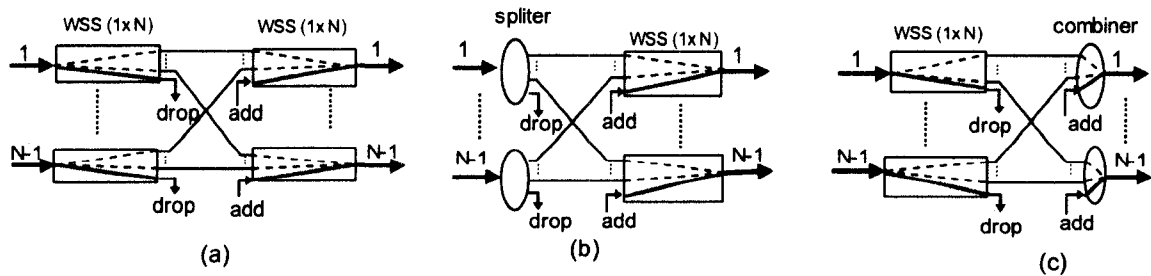


Fig. 5.4. Crosstalk in WSS-based ROADM: (a) WSSs for add and drop; (b) Splitters for drop and WSS for add; (c) WSS for drop and combiners for add. Thick gray lines indicate the main signal and the broken lines indicate the interfering signals or crosstalk.

5.4 Experiments

The loss characteristics and the crosstalk levels of WSS units in add/drop configurations are measured. The crosstalk induced power penalties in WSS-based add/drop ROADM node is investigated. In the experiments, three WSS units were used: an engineering prototype (WSS1) and two commercial units (WSS2, and WSS3). The units are 1×9 switches operating in the C-band wavelength window on the 100 GHz ITU-grid. A functional diagram and possible mechanisms of crosstalk in these WSS are discussed above in Sec. 5.2. A 1×9 WSS has the flexibility to support add/drop node degrees as many as eight with possible node configurations shown in Fig. 5.4.

5.4.1 Crosstalk measurements

Initially, the port and MEMS mirror settings that give the worst leakage powers were identified, for both add and drop functions of the WSS. For the add function, the measurement set up is shown Fig. 5.5(a). The power from the transmitter, TX, is split equally (1:9) to get equal signal powers at the WSS input ports. The power at the output port is then split equally to an optical spectrum analyzer (OSA1) for peak crosstalk and power measurements and via erbium-doped fiber amplifier (EDFA) to the receiver, RX, for BER analysis, which is discussed in Sec. 3.2. The observed port, marked as 'x', is kept open (not connected to the splitter) while the rest of the 8 ports are connected to splitter outputs. The mirror assigned to the transmission wavelength 1550.12 nm is set to port "x" and the total leakage power emerging from the output port is noted. The pass-through power of the observed port, 'x', is also noted by connecting the port 'x' to the splitter while keeping the rest of the ports open. For the drop function, the set up is shown as in Fig. 5(b). The coupler arm to the variable optical attenuator (VOA3) was kept open and the leak power at the observed port, 'x', was measured using OSA1 when the incoming signal was dropped at each and every other port. The pass through power of the observed port, 'x', is also noted by dropping the signal at port 'x'.

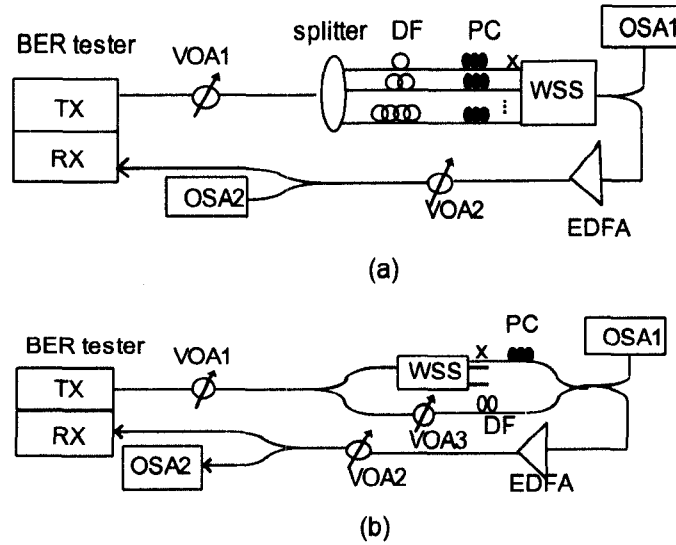


Fig. 5.5. Experimental setups for measuring crosstalk powers and BER of a WSS: (a) passive split and WSS add; (b) WSS drop and passive combine.

The attenuation levels on all channels within the WSSs were set at 0 dB. Crosstalk is derived as the ratio of leakage power to the pass through power of port, 'x'. To identify the worst case in both add and drop functioning, the measurement of leakage power was repeated by changing the observed port, 'x', from one through nine. It is to be noted that in network systems the internal attenuation of WSSs can be used to balance any power variations among channels. This functionality can influence the crosstalk levels. The purpose of this study is to compare the architectural options in terms of in-band crosstalk, provided that a given set of input power levels and WSS attenuation settings for the channels are maintained in all cases. Thus, for simplicity, equal channel powers with 0 dB internal WSS attenuation are considered.

Table 5.2 lists the measured worst case crosstalk values for all three units. The combined in-band crosstalk measured in the add function are below -40 dB in all three units. In the drop function, WSS1, the prototype, shows a high single in-band crosstalk of -25.1 dB while the other two commercial units show better in-band crosstalk of less than -42 dB. When two WSS units were used (configuration in (a)), one for add and one for drop, in-band crosstalk power was below -65 dB as expected, even in the worst case of using WSS1 for drop and WSS3 for add.

Table 5.2. Total in-band crosstalk in an eight degree ROADM.

| Unit | WSS in add function | WSS in drop function | |
|------|-------------------------------------|--------------------------------------|--------------------------------------|
| | Worst total crosstalk measured (dB) | Worst single crosstalk measured (dB) | Worst total crosstalk estimated (dB) |
| WSS1 | -41 | -25.1 | -16.1 |
| WSS2 | -48.8 | -42.5 | -33.3 |
| WSS3 | -40.8 | -42.2 | -33.1 |

5.4.2 Measurements of BER and power penalty estimation.

The experimental setup for quantifying the crosstalk-induced penalties is as shown, in Fig. 5.5. The BER tester transmits non-return-to-zero (NRZ), $2^{23}-1$ pseudorandom bit stream (PRBS) at 2.5 Gb/s, at a wavelength of 1550.12 nm. In each set of measurements, the variable optical attenuator (VOA1) and the gain of the EDFA are set appropriately to maintain a given optical signal to noise ratio (OSNR) at the receiver. This allows comparing the crosstalk-induced penalties among different WSS units and configurations. VOA2 is used to vary the received power levels. De-correlating fibers (DF) of different lengths are used to de-correlate the bit streams. OSA2 is used to measure the peak signal power. Polarization controllers (PC) are used to align the polarization states of the crosstalk channels with that of the main signal to create the worst signal-crosstalk beat noise.

The impact of in-band crosstalk in optical systems is conveniently represented by the power penalty incurred at the receiver to maintain a given bit error rate. Fig. 5.6 shows BER curves in log scale as a function of received power measured with and without crosstalk at the OSNR of 35 dB (0.1 nm resolution) at the receiver for the units WSS1 and WSS2. The port settings and the switching configurations were set to the worst case crosstalk values listed in Table 5.2. For the setup in Fig. 5.5(a), the power penalties due to the combined crosstalk- representing the configuration splitters for drop and WSSs for add of an eight degree ROADM node in Fig. 5.4(b)- are 0.9 dB (WSS 1) and 0.17 dB (WSS 2) at a BER of 10^{-9} . For the setup in Fig. 5.5(b), the main signal power to the combiner was set to be equal to the through power of the drop port, which carries the crosstalk. The power

penalties due to single crosstalk in the drop function are 2.1 dB (WSS 1) and 0.3 dB (WSS 2) at a BER of 10^{-9} .

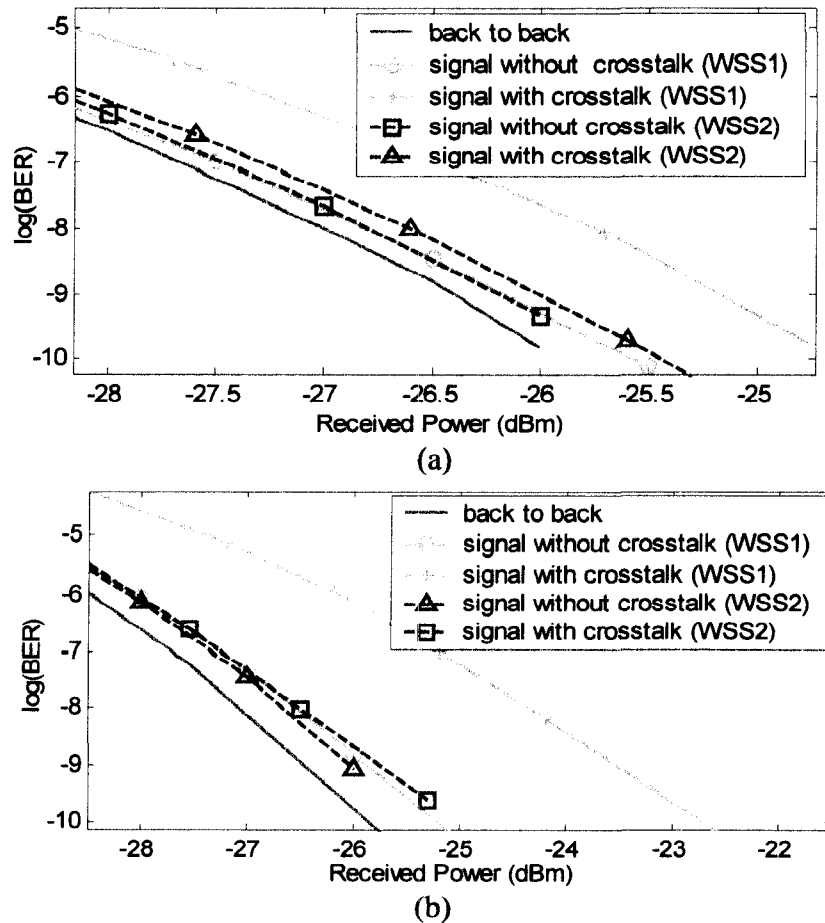


Fig. 5.6. BER measurements: (a) WSS add, set up as in Fig. 5.5(a); (b) WSS drop, set up as in Fig. 5.5(b).

Due to the limited availability of splitters/combiners, the impact of eight crosstalk terms - representing the configuration of WSS for drop and combiners for add of an eight degree ROADM node in Fig. 5.4(c) - was not measured. The power penalty increases with the number of interferers. When eight such equal interferers are combined, a higher penalty will result compared to that measured with a single interferer. No in-band crosstalk-induced penalty was observed when a pair of WSSs were used, as expected from the measured in-band crosstalk power level of < -65 dB.

Based on the above measurements on crosstalk induced penalties, an eight degree ROADM node can be implemented with passive splitters for the drop and WSSs for the add with a very low in-band crosstalk-induced penalty of 0.17 dB (commercial unit, WSS2). In

terms of in-band crosstalk effect, such a ROADM shows performance that is close to the one based on pairs of WSSs.

5.5 Large degree ROADM or WXC

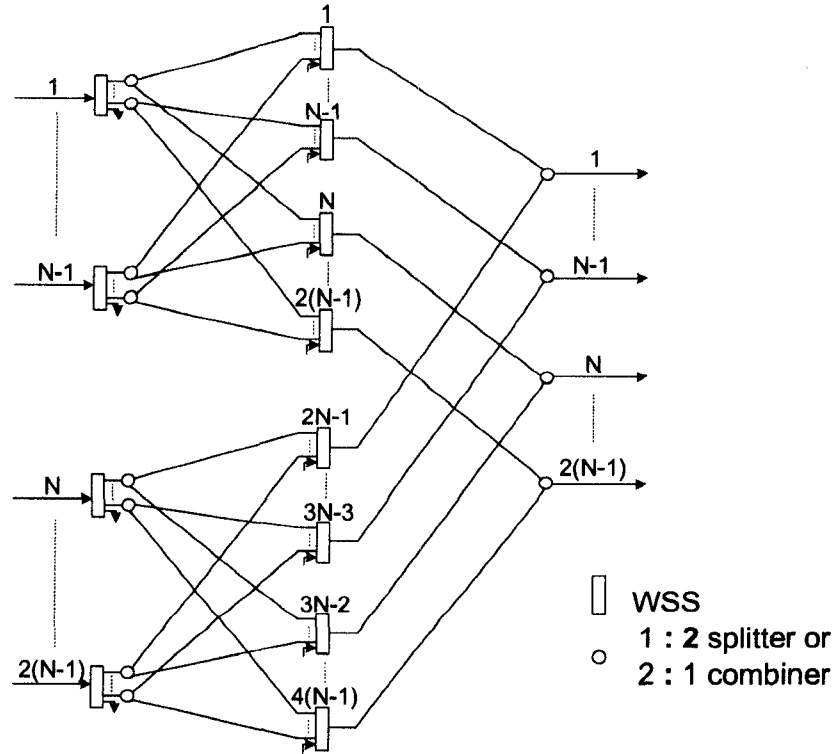


Fig. 5.7. Large degree WXC architecture.

The port counts in currently available WSSs are either 1×5 or 1×9 , limiting the node degrees to four or eight, if using the configurations in Fig. 5.2. Large degree WXC nodes are inevitable in future networks to support the connectivity of many rings via a central hub or WXC node or a large degree mesh node [79]. Since the networks will be constructed incrementally, a modular growth of the node degree is preferred. Such an approach offers several benefits: (1) one does not need to wait for large port count switches to become available; (2) node degrees can be upgraded by adding new identical switches without replacing the existing switches, thus enabling a demand-driven growth approach; (3) the startup cost can be kept low with the flexibility in choosing the low port count switches in the initial deployment.

Fig. 5.7 shows a modular architecture of a large degree WXC node with add/drop functionality. A node degree of $m(N-1)$ is constructed using $1 \times N$ WSSs, splitters(1:m), and combiners(m:1), where m is an integer greater than 1. As an example, $m = 2$ is illustrated. The total number of WSSs required in this architecture, referred to as option (A), is $(m + m^2)(N-1)$. The other options to reduce the number of WSSs are: (B) each of the WSSs in the drop side can be replaced by $m(N-1)$ splitters(1:m(N-1)); (C) the mirror image of (B), each input is split (1:m) and routed to $m^2(N-1)$ WSSs for the drop side and $m(N-1)$ combiners (m(N-1):1) for the add side. Options (A) and (B) provide $m(N-1)$ additional WSS ports for local add and option (C) provides $m(N-1)$ additional WSS ports for local drop.

Table 5.3. Equations for the number of WSSs required, insertion loss, and in-band crosstalk of a WXC node.

| Architectural choice | Number of WSSs required | Insertion loss | Sum of in-band crosstalk |
|---|-------------------------|---------------------------|---|
| (A) WSSs for add and drop | $m + m^2(N-1)$ | $\frac{10^{-2l/10}}{m^2}$ | $\left(10^{-(x+X)/10}\right); m = 1$ $\left(10^{-X/10}\right); m \geq 8$ |
| (B) Splitters for drop and WSSs for add | $m^2(N-1)$ | $\frac{10^{-l/10}}{Nm^2}$ | $\left(10^{-X/10}\right)m$ |
| (C) WSSs for drop and combiners for add | $m^2(N-1)$ | $\frac{10^{-l/10}}{Nm^2}$ | $\left(10^{-x/10}\right)8m$ |

Table 5.3 lists the number of WSSs required, insertion loss, and the in-band crosstalk calculated for all three options discussed above. Options (B) and (C) reduce the total number of WSSs required by $m(N-1)$ with an additional node loss of ~ 6.0 dB (taking the loss of WSS, l , as ~ 3.5 dB on average, as measured) regardless of the node size. It should be noted that, in terms of crosstalk, options (A) and (B), show equal effect for $m \geq 8$; the total crosstalk depends on the combined crosstalk of the WSS in the add side, represented by X . In option (A), for $m < 8$, there will only be $(m-1)$ crosstalk sources at the input of the WSS in the add side. The total crosstalk in option (A), however, can be reduced to second order by replacing the splitter in each output port of WSS in drop side

with WSSs (cascades of WSSs). But, this would be a costly option due to the increased number of WSSs required. In option (C), the total crosstalk depends on the crosstalk of the WSS on the drop side, represented by x , and scales rapidly as $(N-1)m$ due to passive combining in the add side.

5.5.1 Crosstalk performance

Fig. 5.8 shows the in-band crosstalk-induced penalty as a function of size of the WXC node for the three architectural choices listed in Table 5.3. For a signal with an ideal extinction ratio the power penalty, pp , is calculated using Gaussian statistics as [48][73][74]:

$$pp(dB) = -10 \log(1 - \sigma^2 Q^2) \quad (5.1)$$

$$pp(dB) = -5 \log_{10} \left(1 - 4\sigma^2 Q^2 \frac{(1+r)}{(1-r)^2} \right) \quad (5.2)$$

where σ^2 , the relative intensity noise, is equal to the sum of relative crosstalk contributions, r is the extinction ratio, and $Q=6$ for a BER of 10^{-9} . Two different receiver threshold settings are considered, an optimized decision threshold (Equation 5.1) and a midway threshold (Equation 5.2). These calculations are based on the following assumptions: the number of interferers is more than eight; interferers are polarization matched with the signal; interfering source powers are equal to that of the main signal, bits are intensity modulated with a mark/space density of 0.5; the signal and the interfering bits are aligned at the receiver.

A 1×9 WSS is considered as the building block. The values used for x , single crosstalk in drop, and X , combined crosstalk in add, are the measured values in dB for WSS2 and WSS3, as listed in Table 5.2.

Fig. 5.8 illustrates that optimum threshold settings offer better penalties with increasing node degree compared to that with midway threshold. Further, option (C), WSSs for drop and combiners for add, is not a good choice for large degree nodes since the power penalty due to in-band crosstalk increases rapidly with the increase of the node degree, thus limiting the maximum node size to 100 at 1 dB of penalty. Option (A), WSSs for drop and add, and option (B), splitters for drop and WSSs for add, perform equally well with respect

to scaling, indicating that node degrees up to 256 can be realized with penalties less than 0.5 dB. Indeed, the data for options (A) and (B), fall on the same curves, as seen in Fig. 5.8.

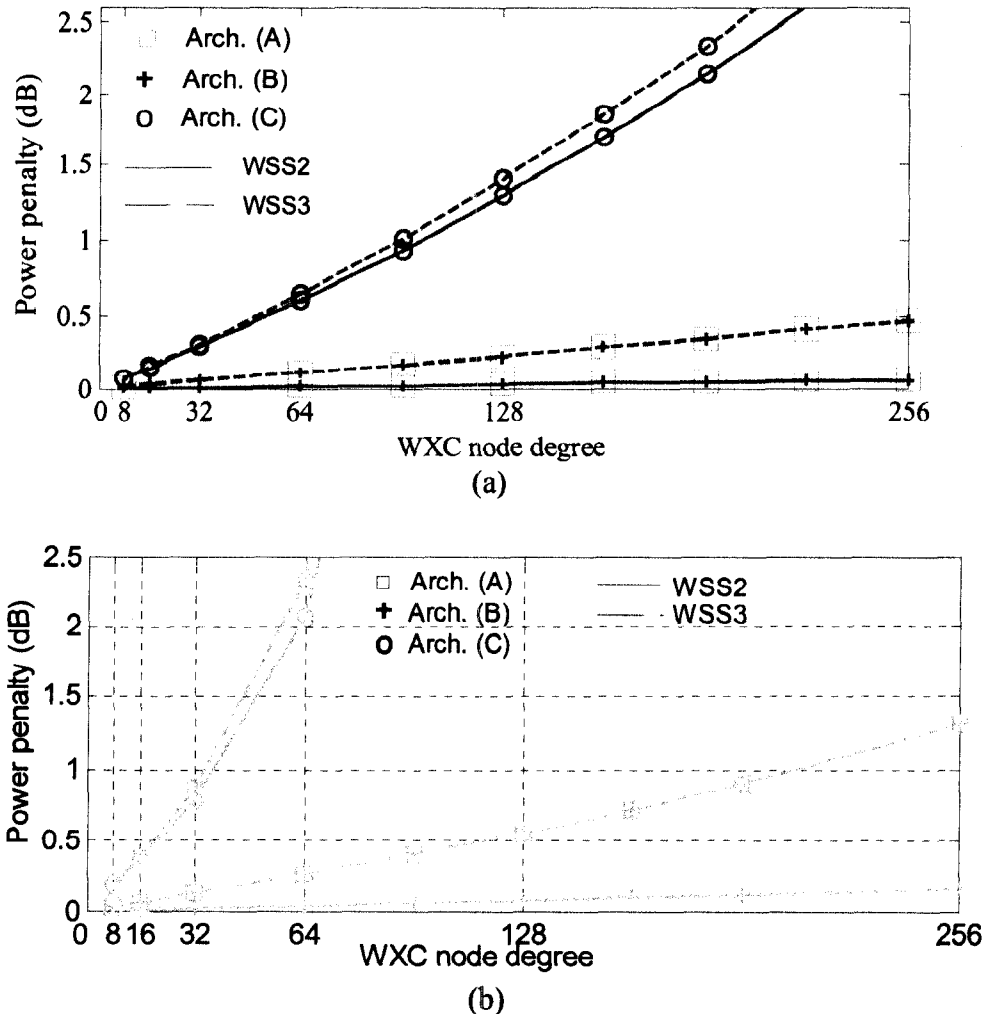


Fig. 5.8. Power penalty as function of WXC node degree. (a) Optimum decision threshold; (b) Midway decision threshold

Unlike in long-haul networks, in metropolitan applications such as dynamic wavelength routing star or multi-ring interconnects, cost effective options are preferred since the cost is shared by a small number of users. It would be interesting to see the tolerable crosstalk on WSS for a given network performance since a relaxed crosstalk requirement would reduce the overall cost of the WSS. Fig. 5.9 shows the maximum tolerable crosstalk of a WSS as a function of the size of the WXC node for the three architecture options. The crosstalk was evaluated at 1 dB of penalty using Eq. (5.1). When WSSs are used in the add side with either option A or B, the crosstalk requirement is

relaxed by ~ 10 dB compared to that of option (C), WSSs for drop and combiners for add, regardless of the node size. A 32-degree ROADMs node can be realized with splitters for drop and WSSs for add with a WSS crosstalk as high as -26 dB while for a 8-degree node, the highest likely in the present metro networks, WSS crosstalk required is only -23 dB.

If the signal traverses more than one node there will be more crosstalk contributions, which are added in each node of the network traversed. For a signal traversing S number of nodes, the worst case total crosstalk is listed in Table 5.4, for all three node implementation choices of (A), (B), and (C). The penalties due to in-band crosstalk to any given network model can thus be estimated in a straight forward manner using the Eq. (5.1).

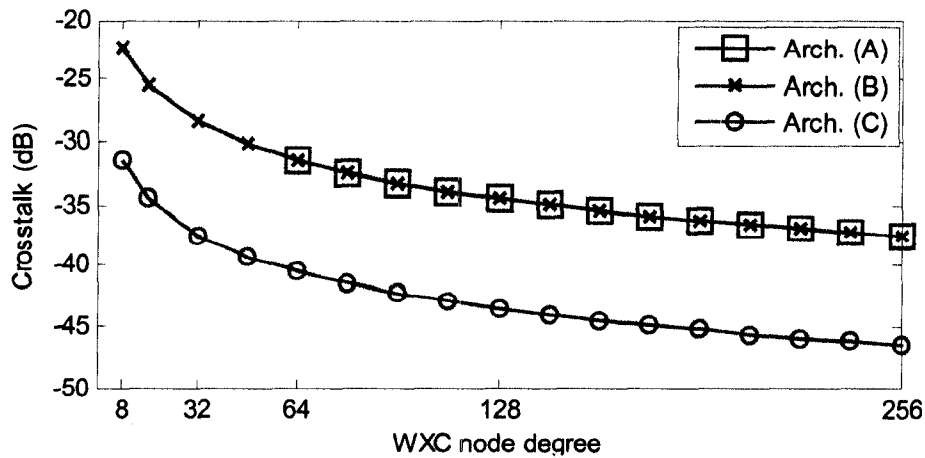


Fig. 5.9. WSS crosstalk as function of node degree at 1 dB of penalty.

Table 5.4. Total crosstalk of a signal traversing S number of nodes

| Architectural choice | Total crosstalk (worst case) |
|---|---------------------------------|
| (A) WSSs for add and drop | $\sum_i^S (10^{-X/10}) m_i$ |
| (B) Splitters for drop and WSSs for add | $\sum_i^S (10^{-X/10}) m_i$ |
| (C) WSSs for drop and combiners for add | $\sum_i^S (10^{-x/10}) n_i m_i$ |

subscript i denotes the i^{th} node. For node degrees $\leq N - 1$, n_i is the node degree and $m_i = 1$.

For large nodes, constructed with $1 \times N$ WSSs (Fig.5.7), $n_i = (N - 1)$ and $m_i > 1$ is the node degree scaling factor.

5.6 Summary

In this work, the implementation options of multi-degree WSS-based ROADMs were studied. In particular, the ROADM performance in terms of in-band crosstalk was investigated. It was shown through experimental investigation that for a given node degree and functionality, the reasonable approach is to reduce the number of WSSs in the node.

Initially, the switching functionality of a WSS and the possible mechanisms for the appearance of crosstalk in a WSS were described. Further, in studying the crosstalk of WSS-based ROADMs, it was noted that the impact of in-band crosstalk in the ROADM varies considerably depending on how the WSS is configured in the ROADM. It was then experimentally verified by examining the crosstalk in an 8×8 degree WSS-based ROADM.

Commercially available WSS units (1×9) were acquired and the crosstalk levels were measured both in add and drop configurations. The impact due to crosstalk in different ROADM architectures was investigated by performing BER measurements. The results indicated that when the 9×1 WSSs were used in the add side with passive splitters in the drop side, a very low penalty of 0.17 dB was shown for the eight degree ROADM. To achieve a good crosstalk performance, one takes advantage of the inherent nature of the WSS that could serve both as a wavelength blocker and a switch in adding.

To address the pay-as-you grow approach, a modular architecture to implement a large degree WXC node using currently available WSSs has also been proposed. The scalability of the proposed architectures with respect to in-band crosstalk was carried out analytically making use of crosstalk measurements carried out with the eight degree WSS-based ROADM node. Results show that the architecture constructed with the cost effective configuration consisting of splitters and WSSs has the potential to scale to very large degrees due to good WSS crosstalk performance, measured to be below -40 dB. Moreover, it is shown that the WSS crosstalk requirement can be relaxed to as high as -23 dB at 1 dB of penalty for node degrees up to eight. One concludes that design constraints on WSS itself could then be relaxed, thus reducing the overall device cost, which should benefit the cost-sensitive metropolitan networks.

6 Scaling limitations of NZ-DSF ring networks constructed with WSS-based ROADMs

So far, the work discussed in this thesis, has focused on the scalability of switches in a single stage/node set up and the main impairments taken into consideration are crosstalk and loss that are associated with the switching node. A study on the overall performance and scalability of networks, in terms of number of nodes, node degrees, and links that can be cascaded is also important. This work focuses on experimental and theoretical investigation of the physical layer scalability of optical networks in the presence of the impairments. A re-circulating fiber loop is constructed to experimentally emulate the effect of cascading certain number of nodes and links.

6.1 Introduction

Scaling of optical fiber networks is also limited by fiber impairments, loss and dispersion. At a wavelength of 1550 nm, the standard single mode fiber (SMF) shows a loss of 0.2 dB/km and a dispersion of 17 ps/nm-km. These two impairments must be compensated periodically to avoid the transmission penalty in long distance transmissions. EDFAs are often used to compensate the fiber loss, however, the ASE noise accumulations reduces the power budget improvements actually obtained. Unlike in the case of fiber loss, the dispersion induced penalty varies significantly as a function of wavelength and bit rate inclusively. In WDM networks, compensating the fiber dispersion, completely over the entire transmission band is complex and very expensive. The introduction of non-zero dispersion shifted fiber (NZ-DSF), designed with low dispersion (< 6 ps/nm-km over the C-band) and low dispersion slope (< 0.05 ps/nm²-km) enabled to lower the system cost by eliminating in-line and post compensation expenses, particularly in metro and regional

systems operating at 2.5 and 10 Gb/s. Any fiber dispersion left uncompensated, nevertheless, imposes limitations on the tolerance levels to other impairments such as ASE noise and crosstalk in maintaining a given system performance.

There have been many publications reporting the impact of in-band crosstalk in optical transmission systems. A single stage configuration is often considered, experimentally [15], [48] as well as theoretically [16], [84] assuming a fixed ASE noise at the receiver. However, in practice, the signal travels through many nodes that are connected with fiber links which could differ in length, loss and dispersion profiles. Consequently, the penalty calculations due to crosstalk using a single stage while ignoring the other impairments, the accumulation of ASE noise and any uncompensated dispersion does not accurately represent the real systems. In [85], the influence on the signal quality due to ASE to the tolerance to crosstalk has been reported. There has been at least one experimental work measuring the crosstalk influence due to the cascaded optical switches on the transparency length by using a re-circulating loop [86]; the fiber links were fully compensated for dispersion and the switch was modeled as a black box with attenuators for the transmission and crosstalk paths.

In this work, the combined effect of all possible impairments on the cascadability of add/drop nodes is investigated experimentally using a re-circulating loop (RCL). The RCL is constructed using a WSS-based ROADMs, NZ-DSF and EDFAs. Further, the tolerance to dispersion on the cascadability limit of the ROADMs due to in-band crosstalk is investigated using an experimentally verified re-circulating loop (RCL). The organization of this chapter is as follows. The implementation details of the re-circulating test bed and the loop operation are given in Sec. 6.2. The results on the RCL measurements are also discussed along with the simulation results obtained using the numerical model. In Sec. 6.3, periodic add/drop systems in fiber ring networks is investigated for crosstalk induced effects in the presence of dispersion by using a RCL model. Finally, a summary of this work is provided in Sec. 6.4.

6.2 Re-circulating loop

The experimental investigation of physical layer characteristics of optical networks requires certain number of switching nodes, fiber links, and other functional devices such as EDFAs

and dispersion compensators. Depending on the network size that is under study, the research facilities are often limited by the resources and space required. Also, studying the optimal configuration by reconfiguring the network is difficult and expensive. To overcome these problems, the idea of a re-circulating loop was introduced in the early nineties [87] and since then it has been extensively used as a powerful experimental model to study straight-line large-scale networks.

6.2.1 Experimental set up

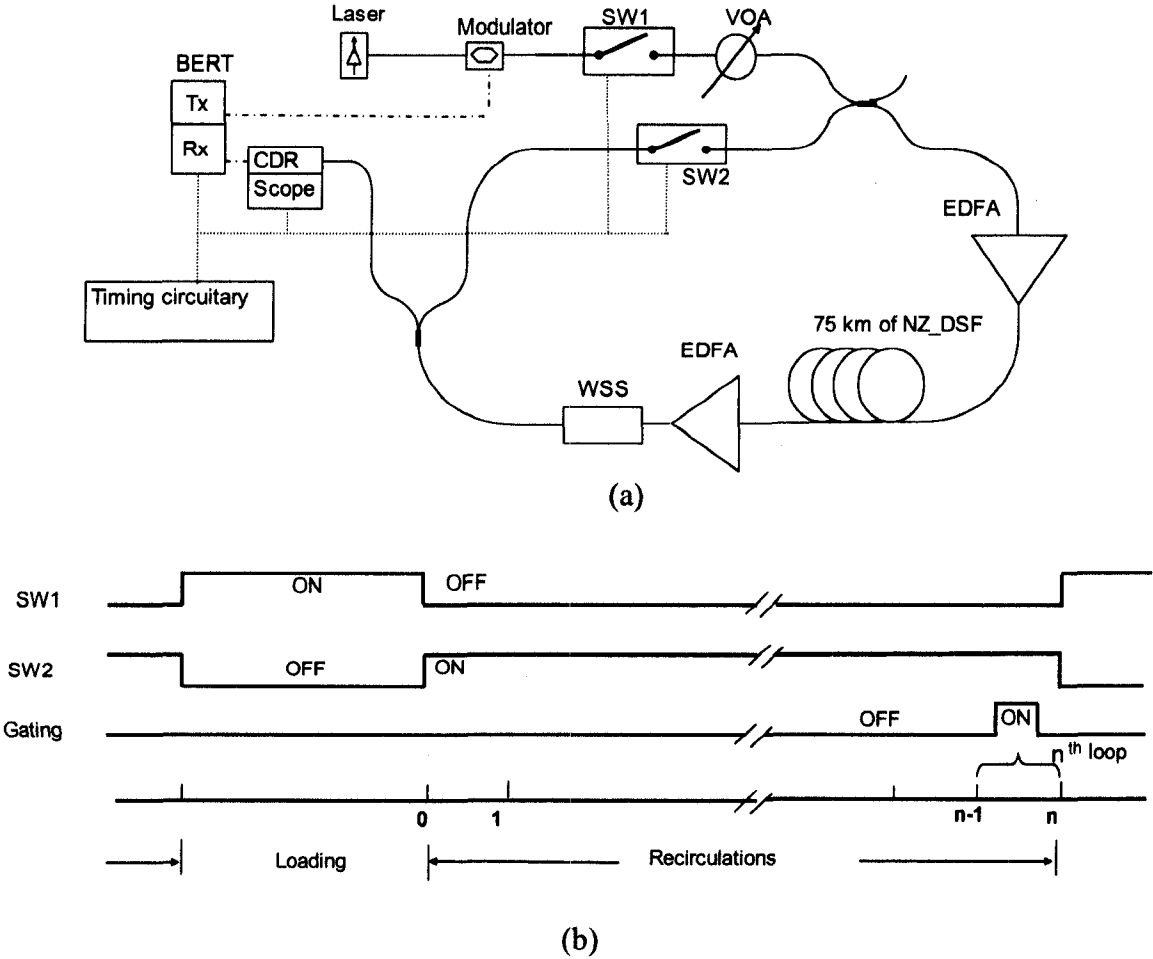


Fig. 6.1 (a) Experimental set up (b) The timing diagram

Fig. 6.1(a) shows the re-circulating loop (RCL) set up used in this work in studying the cascability of WSSs. The distributed feedback laser transmits a fixed power CW signal at a wavelength of 1561.4 nm. The signal is externally modulated using a Mach-Zhender modulator by a Non-Return-to-Zero (NRZ), $2^{23}-1$ pseudorandom bit stream (PRBS) at 2.5

Gb/s produced by the transmitter, Tx. A variable optical attenuator (VOA) is used to control the input power entering the loop. Two high speed 2×2 switches (Civcom), SW1 and SW2, are used to control the loop. The switching time of the switches is 250 ns, fast enough to control the loop length of 364 μ s in this work. The re-circulating loop contains, a reduced dispersion slope NZ_DSF (TrueWave RS fiber) at a length of 75.5 km, two EDFAs which are placed before and after the transmission of the fiber, and a 1×9 WSS following the second EDFA. Two 50:50 couplers are used to couple light into the loop and to couple light out to the measuring equipment. The received signal is fed via the Clock and Data Recovery (CDR) unit to the receiver, Rx, for the Bit Error Rate (BER) analysis. A pulse generating circuitry, based on Altera stratix II GX Field Programmable Gate Array (FPGA) development board, is used to generate pulses to turn ON/OFF the switches and to trigger the measuring equipment at the right timing [88].

Since the focus of this work is to study the cascadability of the WSS due to in-band crosstalk a single wavelength system is investigated.

6.2.2 Loop Operation

The timing diagram for the loop operation and measurement is shown in Fig. 6.1(b). At the loop length of 75.5 km, the time required for the signal to complete one loop is 364 μ s, called the loop time. Initially, at the loading stage, the SW1 is kept open to feed the loop with the signal while SW2 is kept closed. The duration of loading is set to more than one loop time (five loops/1800 μ s) to ensure any ASE noise accumulations from previous re-circulations are flushed out. Next, the transmission or the looping stage is initiated by reversing the stages of the two switches. This allows the signal to circulate inside the loop while the transmitter is blocked by closing SW1. Alternative switching operation of the switches for signal transmission allows avoiding any EDFA transients by maintaining the presence of the signal in the loop during the loop operation.

After the signal is transmitted for a desired number of re-circulations, gating pulse is sent to the measuring equipment to do the analysis on the received bits for a specified duration, little less than a loop time. As seen in Fig. 6.1(b), the gating signal for the measuring equipment starts and ends leaving some guard time after previous re-circulation and before the next re-circulation, respectively, in order to avoid registering head/tail bits

corrupted during the operation of the switches and to take into account any adjustment to loop timing calculations.

The number of bits collected for analysis in the above mentioned duration is < 0.9 Mb. To measure a BER of 10^{-10} , at least 10^{10} number of bits must be analyzed. To collect sufficient number of bits the looping cycle is repeated over a period of time using software.

6.2.3 Simulation Model/Numerical modeling

The RCL described above is also modeled numerically and simulated using VPI transmission maker™. The key parameters of all the components in the loop are measured and modeled accordingly. Fig. 6.2 shows the components arrangements the RCL model implemented with VPI. Table 6.1 summarizes the main parameters used in modeling.

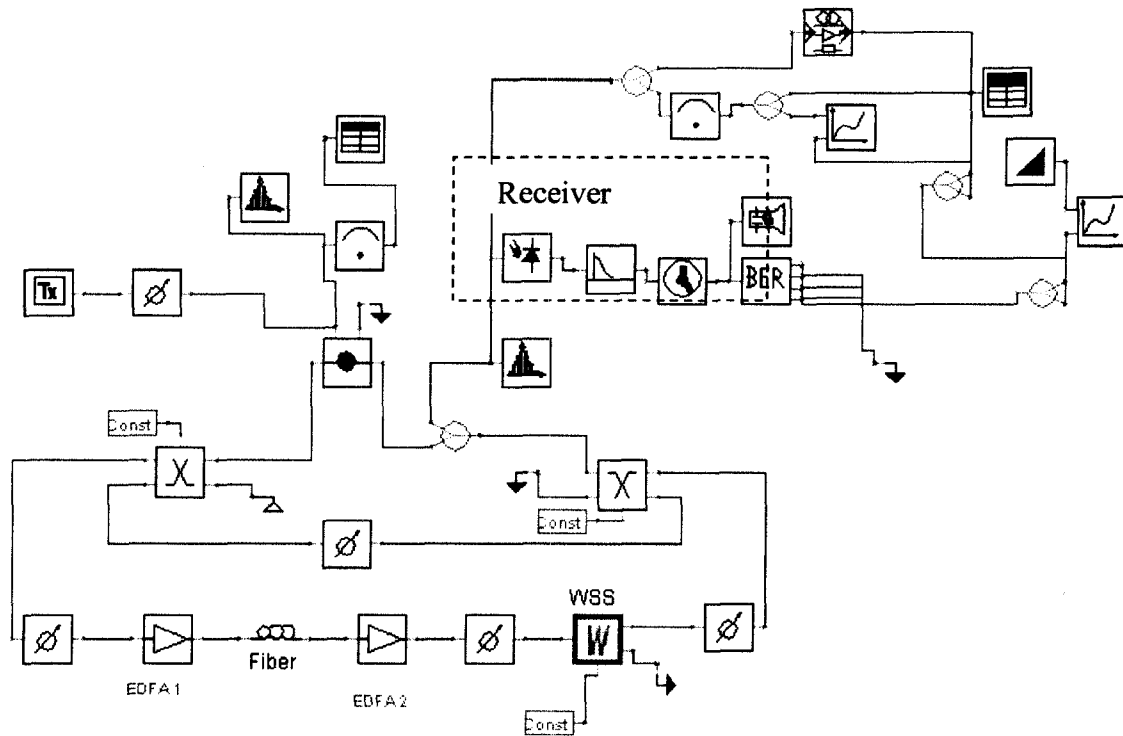


Fig. 6.2. RCL model implemented with VPI.

Fiber

The fiber is modeled as a dispersive module that solves the wave equation describing the propagation of two orthogonal polarization components of optical signals in the fiber. Any non-linear effects are set to zero. A single channel system with maximum power limited to

10 dBm at the input of the fiber ensures negligible non-linear effects in the fiber. Due to the unavailability of a sample fiber the values for dispersion and the dispersion slope of the fiber are used as specified by the manufacturer.

Table 6.1. The components and their key parameters that are used for the numerical model.

| Component | Key parameters | Value |
|----------------|------------------------|-------------------------------|
| Laser | wavelength | 1561.4 nm |
| | linewidth | 10 MHz |
| Transmitter | data stream | NRZ, PRBS $2^{23} - 1$ |
| | bit rate | 2.5 Gb/s |
| | extinction ratio | 12.5 dB |
| Fiber (NZ-DSF) | length | 75 km |
| | loss | 0.208 dB/km |
| | dispersion | 4.56 ps/nm-km |
| | dispersion slope | 0.0465 ps/nm ² -km |
| | zero dispersion | |
| EDFA | wavelength | 1466 nm |
| | unsaturated gain | 22 dB |
| | noise figure (NF) | 7.8 dB |
| | saturation input power | -10 dBm |
| WSS | amplitude | Fig. 6.4 |
| | group delay | Fig. 6.4 |
| Receiver | detector | PIN |
| | sensitivity | -19.1 dBm |

EDFAs

The two EDFAs, which are identical, are set to operate in saturation mode obeying the saturation curve specified by the parameters as listed. The saturation characteristics and NF measurements are as shown in Fig. 6.3. For ASE noise generation in the EDFAs, different seeds are used.

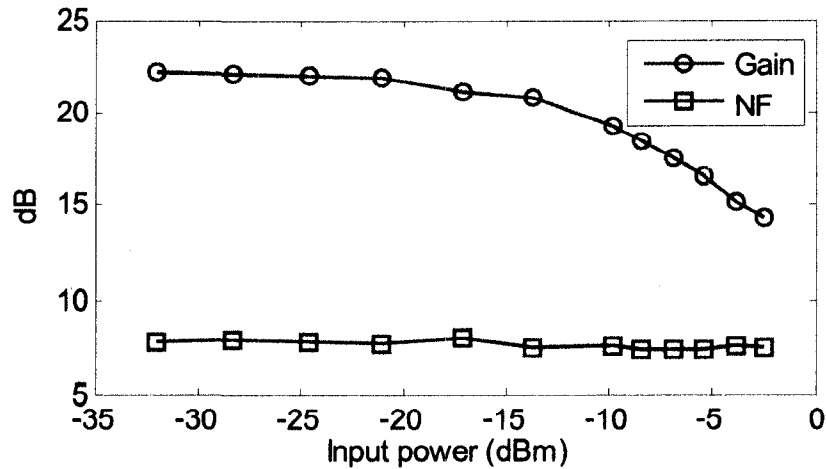


Fig. 6.3. EDFA gain and NF vs input power.

WSS

The WSS is a 1×9 port device supporting C-band operation at 100 GHz channel spacing. The filtering response of the WSS was obtained by using a vector analyzer for both the express port and a service port. Fig. 6.4 shows the IL and group delay as function of frequency at an ITU grid frequency of 192 THz (1561.4 nm) obtained when the signal is dropped at the express port. Insertion loss of 3.2 dB at the center and a group delay ripple of 0.8 ps over the 3 dB bandwidth are measured. The channel passband at 3 dB roll off is 76.7 GHz.

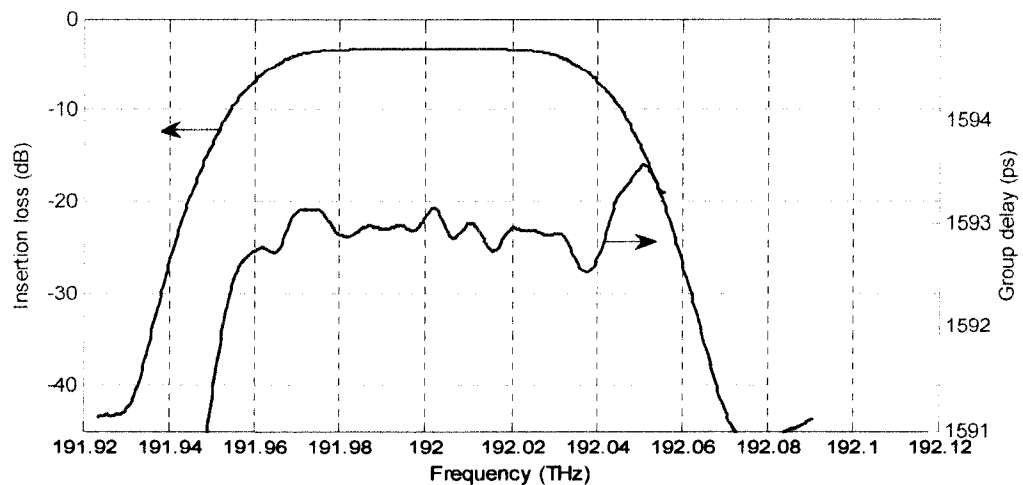


Fig. 6.4. WSS filtering characteristics; amplitude and group delay as a function of frequency.

Attenuators/Power budget

For the connector and splitter losses, extra attenuators are used and their values are adjusted accordingly to match with experimental power levels at various points along the loop. The power was balanced at the loop to ensure the same power is launched for each recirculation. This allows investigating the BER degradation at the receiver due to dispersion and any noise accumulations as a function of loops.

Receiver sensitivity

For the receiver sensitivity adjustment, a back-to-back BER vs received power measurement was obtained, showing a receiver sensitivity of -19.1 dBm at a BER of 10^{-9} . The receiver parameters such as thermal and shot noises, responsivity, and electrical bandwidth are set appropriately to match with the back-to-back BER vs received power measurements.

6.2.4 Results and discussion

Fig. 6.5 shows BER as a function of number of loops for a loop input power of -9 dBm and 0 dB loop loss, from both experiments (closed symbol) and modeling (open symbols, each indicating different sets of random seeds that were used for ASE noise sources). A good agreement between the experiment and modeling can be seen, with an error in theoretical prediction of $< 7.2\%$.

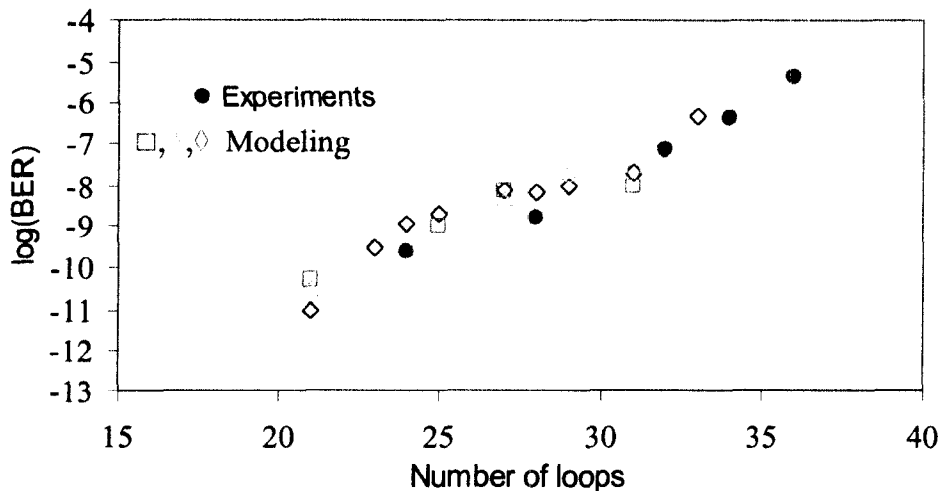
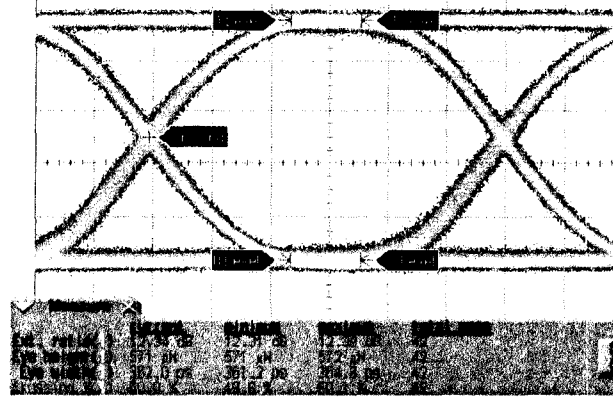
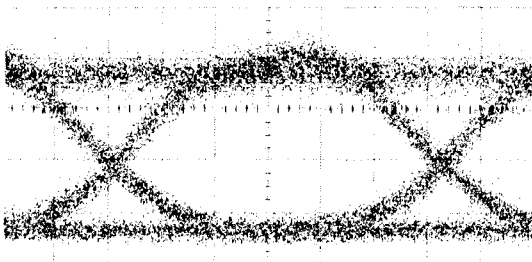


Fig. 6.5. Experimental (closed symbol) Vs theoretical results (open symbols) of the re-circulating loop.

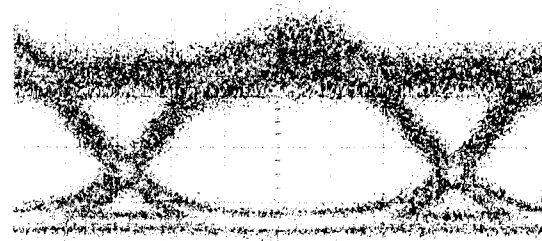
At a BER of 10^{-9} , the signal can re-circulate 24 loops traveling a distance of 1800 km. Since the out of band ASE from the EDFAs are filtered by the WSS in each round trip, the amplifier saturation due to accumulated ASE noise powers are avoided. The accumulation of in-band ASE noise powers and fiber dispersion ultimately limits the maximum distance.



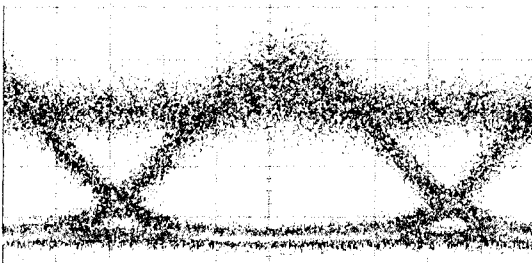
At the transmitter



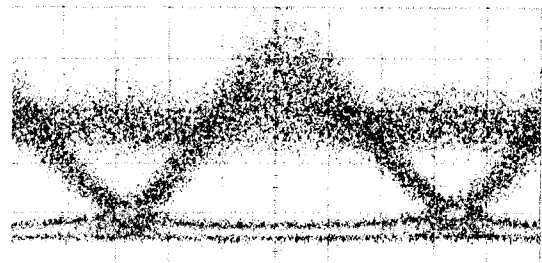
At 12 loops



At 18 loops



At 22 loops



At 28 loops

Fig. 6.6. The measured eye diagrams of the signal at various distances: At transmitter, 12, 18, 22, and 28 loops.

The measured eye diagrams at the transmitter and the received signal after 12, 17, 22, and 28 loops are shown in Fig. 6.6. The transmitted eye showed an extinction ratio of 12.5 dB and an eye crossing amplitude at 50%, with no overshoot in the 'one' level. As the signals reaches 12 number of loops, the measured eye diagrams start showing noticeable

peaking in the ‘one’ level due to the accumulated dispersion. The relative shifts in ‘one’ also increases with increasing number of loops due to the increase in signal-ASE beating noise at the receiver. The higher the accumulation of ASE, the more the eye closure between ‘one’ and ‘zero’ levels.

To find out the most severe factor, ASE accumulation or dispersion, that limits the number of loops, the experiment was repeated under same conditions but at a lower bit rate of 622 Mb/s. At this rate, the dispersion induced effect is less than that at 2.5Gb/s while the ASE accumulations are equal at both bit rates. At a BER of 10^{-9} , the number of loops was limited to 24 again, same as that of the 2.5 Gb/s. The eye diagram at 22 loops is shown in Fig. 6.7.

In this experiment, it can be concluded that the in-band ASE noise accumulation and the resulting signal-ASE noise beating at the receiver is the most limiting factor for the number of re-circulations or the total distance traveled.

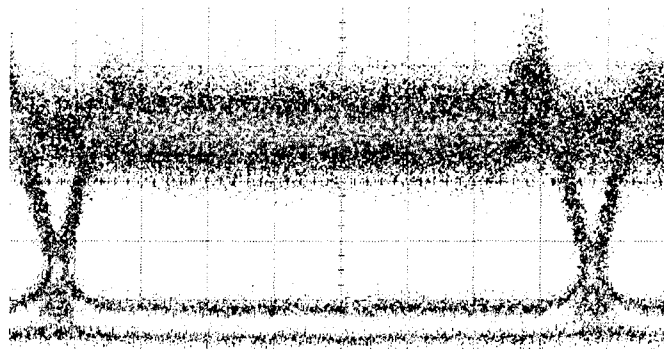


Fig. 6.7. The eye diagram at 22 loops at 622 Mb/s.

6.2.5 Analytical modeling

In order to estimate the limits on the transmission distance due to dispersion and ASE, each in isolation, analytical methods were used.

For an externally modulated laser with a very narrow line width the distance, l , due to fiber dispersion can be roughly estimated using [102].

$$l < \left[16(D\lambda^2 / 2\pi C) B^2 \right], \quad (6.1)$$

where D is the dispersion of the fiber; λ is the wavelength of the signal; C is the speed of light, and B is the bit rate. At bit rates of 2.5 Gb/s and 622 Mb/s, l is calculated as 1950 km

(25 loops) and 27200 km (360 loops), respectively, for the fiber dispersion of 4.5 ps/nm-km.

The power budget diagram of the RCL is shown in Fig. 6.8. The OSNR due to the ASE accumulation after N number of cascades is given as,

$$OSNR^N = \frac{P_{in}}{P_{ASE}^N}; \quad (6.2)$$

where P_{in} is the power at the input of the node in each cascade and P_{ASE}^N is the total ASE noise power at the input of N^{th} node, given as

$$P_{ASE}^N = Nh\nu B_o ((G_1 - 1)F_1 + (G_2 - 1)F_2); \quad (6.3)$$

where G_1, F_1 and G_2, F_2 are the gain and NF of the amplifiers EDFA₁, and EDFA₂ respectively, $h\nu$ is the photon energy, and B_o is the optical bandwidth for OSNR measurement. L_1 and L_2 are the loss of the fiber link and the node loss, respectively. In the re-circulating loop $L_1 = 17.5$ dB (fiber and connector losses) and $L_2 = 16$ dB (consisting the losses from WSS, switch, two of 50:50 power splitters, and taps).

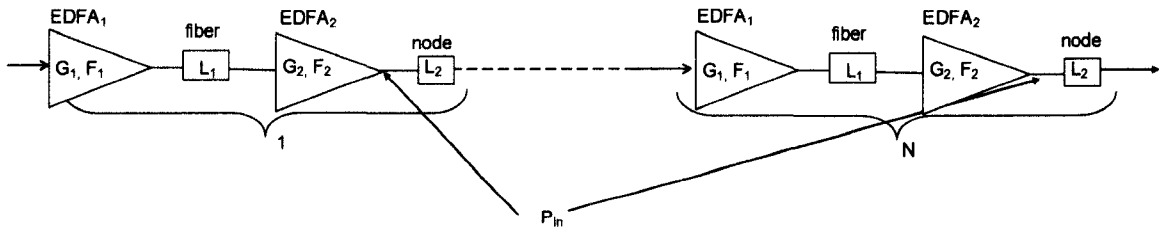


Fig. 6.8. Power budget diagram of the RCL.

The OSNR degradation as a function of number of loops is plotted in Fig. 6.9, at 0.1 nm optical resolution bandwidth, at a BER of 10^{-9} . Theory and simulations equally predict the OSNR degradation as function of number of loops. The OSNR drops by 14 dB at 26 loops.

The measurement of OSNR using the OSA was not possible within the short trigger-ON time due to the limitation on the scanning speed of the OSA. Under static transmission conditions with no impairments other than ASE in the link between the Tx and Rx, the OSNR limit for the receiver, at a BER of 10^{-9} , was measured as 23.5 dB (at sensitivity setting of OSA at -40 dB). After one loop, the OSNR measured, at the same sensitivity, is 36 dB. This represents an OSNR degradation of 12.5 dB. The difference in OSNR

degradation between theory (and modeling) and experiments can be attributed to the additional penalty incurred due to the dispersion, simultaneously with the ASE in the experiments. As a result, lesser OSNR degradation can be tolerated with ASE in the experiments at the given BER.

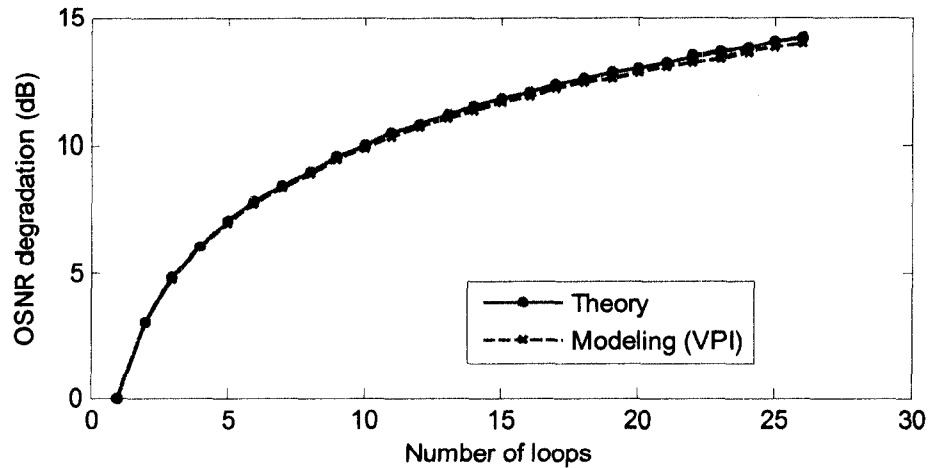


Fig. 6.9. OSNR degradation as function of number of loops, theory ('+') and modeling ('o').

6.3 Numerical study on the cascability of WSS by using the RCL

As discussed above, the cascability of the WSS was studied using a RCL where the signal was passing through WSS in each round trip experiencing no dropping and adding. However, in optical networks, at each node the signals are dropped and new copies of the dropped signals are added dynamically according to the traffic conditions. Consequently, the signal suffers from optical crosstalk that are added at every passing node.

6.3.1 Network model

In this work, we consider a generic network model consisting of metro and interconnecting rings and long haul, as shown in Fig. 6.10. ROADM nodes are created with varying node degrees. Metro rings are constructed with ROADM degree 2 (considering a bidirectional flow of signal, e.g. East to West and West to East) while the interconnecting ring that connects several metro rings requires ROADM with degree 4. A mesh node supporting $N/2$ fiber links thus requires an N degree ROADM.

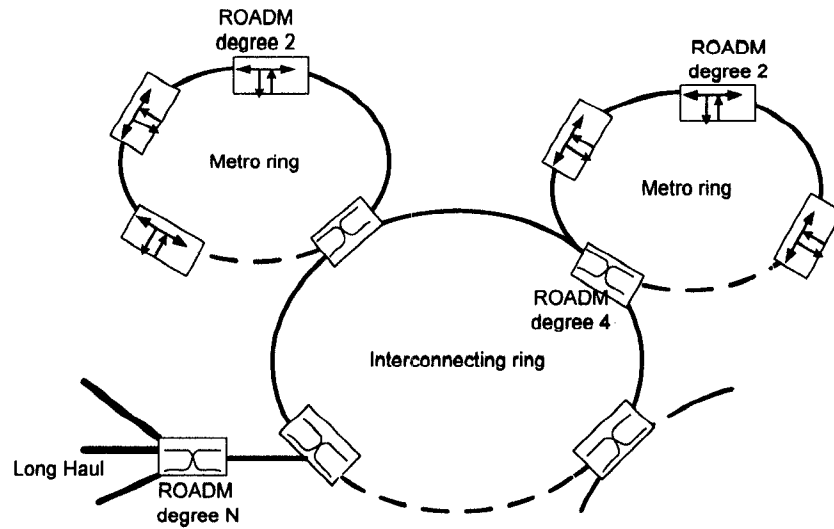


Fig. 6.10. Generic optical network consisting a metro rings, interconnecting ring, and long haul.

6.3.2 Simulation model: periodic add/drop

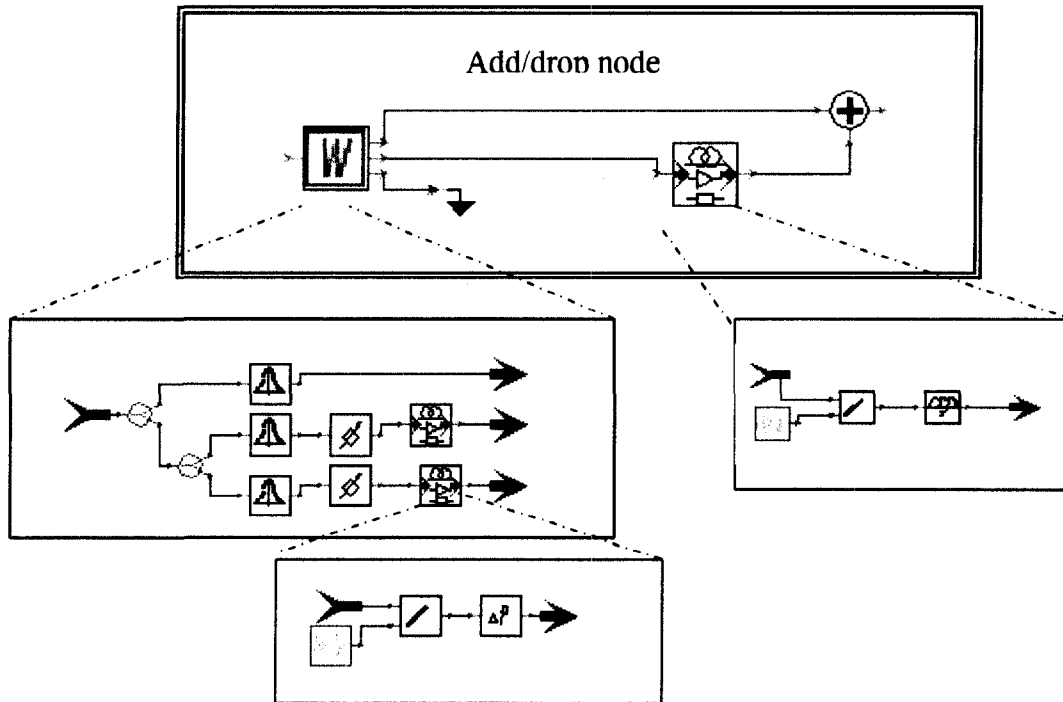


Fig. 6.11. The implementation of crosstalk sources in an add/drop node

The RCL model described in Sec. 6.2.3 is used, but the WSS node is modified to accommodate the local add and drop and the required node degree. The express and service

ports are modeled with the measured filter responses. Crosstalk sources that leak from service ports to express ports are set with a variable attenuator to set to the crosstalk power level of interest. As an example, an add/drop node with a single crosstalk source is shown in Fig. 6.11. The phases of the crosstalk sources are generated independently from random sources which outcomes are uniformly distributed over $-\pi$ to π . The bit streams of crosstalk sources are de-correlated to each other and to the main signal by applying random time delays. A constant state of polarization for all the crosstalk sources and the signal is assumed ensuring polarization matching to study the worst case scenario. Accordingly, the fiber is modeled as dispersive but it handles only a single state of polarization. Polarization filters used at the output of the EDFAs. The ASE noise accumulations are therefore smaller compared to that in the model, in Sec. 6.2.3, which employs no polarization filters for the noise. Random number seeds for the noise sources were kept at arbitrarily fixed values to produce equal ASE noise effects among simulations for fair comparisons. The BER estimation is performed using Gauss_ISI (inter symbol interference) by using the Gaussian statistics for the beat noises and taking into account the ISI due to dispersion or pulse broadening.

Each link contains two EDFAs, at the beginning and end of the link. The gains of the EDFAs are set such that the same power is transmitted at each node. The model conveniently assumes an equal link distance between the nodes.

6.3.3 Simulation results

6.3.3.1 The impact of fiber dispersion on the tolerance to WSS crosstalk

Initially, a metro ring network is modeled at a link distance of 75 km. The implementation of the node consists of a WSS for drop (or WSS for add) with a passive combiner for add (or splitter for drop). At each passing node there will be a single crosstalk addition to the main signal.

Fig. 6.12 plots the BER as a function of number of cascades for a WSS crosstalk of -40 dB with and with out fiber dispersion, calculated using the RCL model. Also shown are the cases for no dispersion and no crosstalk, which represents the ASE limit, and no crosstalk with a dispersion of 4.5 ps/nm-km, which represents the ASE and dispersion limit. In this model, the results show that the dispersion is the most limiting factor in the absence of any

crosstalk limiting the number of loops to 26 at a BER of 10^{-9} . When there is crosstalk, it can be seen that the fiber dispersion severely affects the tolerance to in-band crosstalk effect by leaving less room for crosstalk induced effects for a given system performance; at a BER of 10^{-9} , the number of loops drops to 17 (from 24) in the presence of fiber dispersion.

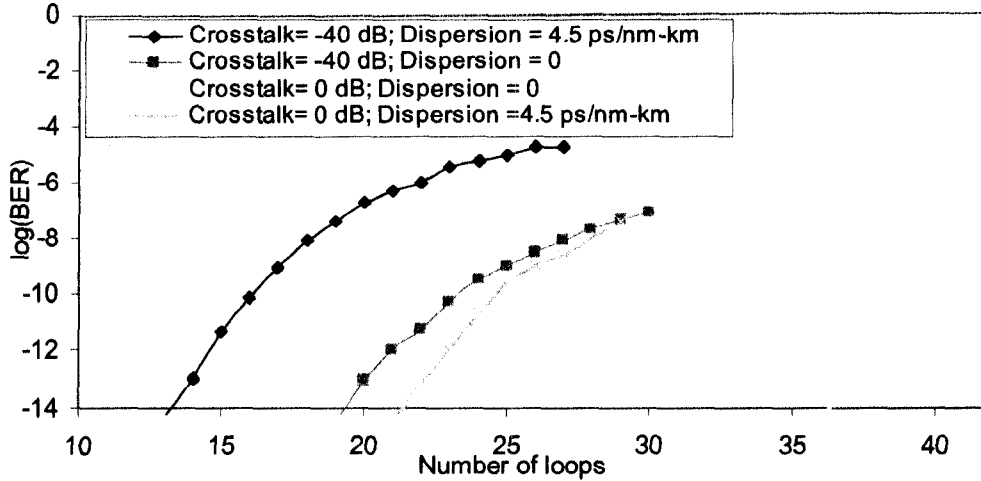


Fig. 6.12. BER as function of number of loops for a WSS crosstalk of -40 dB with and without fiber dispersion.

Fig. 6.13 shows the number of cascaded nodes for fiber dispersions of 4.56, 2.56, 0 ps/nm-km calculated at a BER of 10^{-9} for different WSS crosstalks. At low crosstalk values, fiber dispersion has a significant influence on the number of cascades, e.g. at a WSS crosstalk of -45 dB the number of cascades has dropped from 35 with zero dispersion to 26 and 18 for fiber dispersions of 2.56 and 4.56 ps/nm-km, respectively. At high crosstalk levels (> -30 dB) the dispersion effects make negligible influence as the crosstalk dominates in deteriorating the signal quality.

Any fiber dispersion left uncompensated, thus, puts stringent requirement on the WSS design for better crosstalk. For example., for 15 numbers of cascades, WSS crosstalk of -36 dB is adequate for zero fiber dispersion while a WSS crosstalk of -40 dB is required for fiber dispersion of 4.5 ps/nm-km.

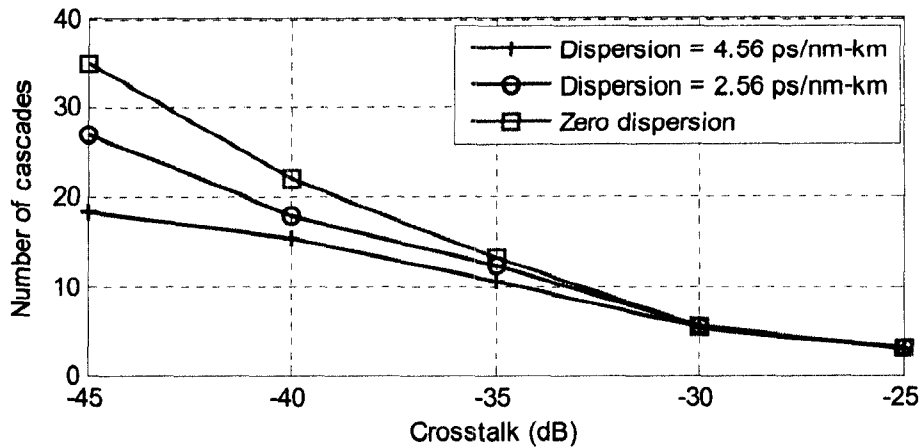


Fig. 6.13. Number of WSS cascades as a function of WSS crosstalk at varying fiber dispersion.

Fig. 6.14 shows the crosstalk induced power penalty calculated at WSS crosstalk of -45 dB as a function of fiber dispersion for a ring network with 16 nodes at a link distance of 75 km. Power penalty is calculated as additional power required at the receiver with crosstalk to that of zero crosstalk. At 2.5 Gb/s, power penalty increases slowly with increasing dispersion and remains below 0.6 dB for dispersions as high as 4 ps/nm-km. For a higher bit rate, 10 Gb/s, crosstalk induced power penalty increases rapidly for fiber dispersions above 0.5 ps/nm-km and to maintain a penalty of 1 dB, fiber dispersion should be limited to 1.2 ps/nm-km.

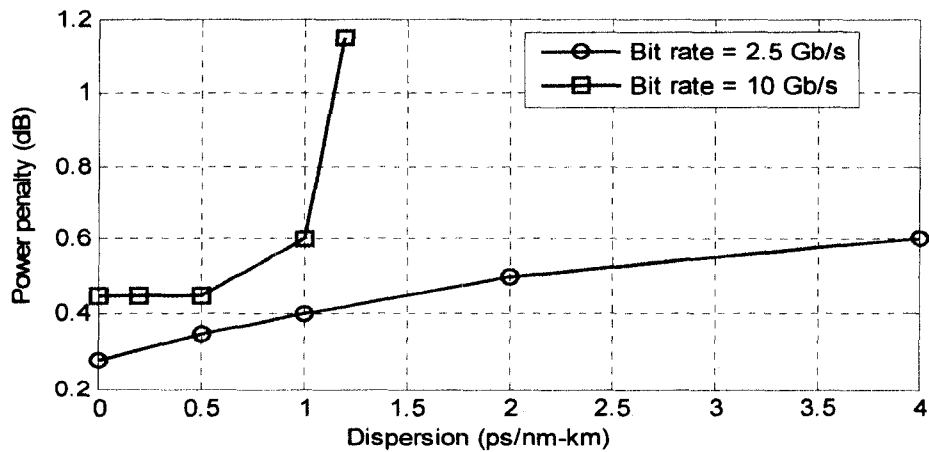


Fig. 6.14. The power penalty (due to crosstalk) calculated as function of fiber dispersion for a ring network with 16 nodes.

Another key application of the WSSs in optical networking is the core ring, which interconnects local rings as shown in Fig. 6.10. The diameter or the link distance of the core ring is usually larger than that of the access ring. Node implementation option of WSS for drop and combiners for add is considered. Fig. 15 shows the number of cascades as a function of WSS crosstalk for a BER of 10^{-9} for link distances of 75 and 150 km, with a fiber dispersion of 4.56 ps/nm-km. The loss of the 150 km link is assumed to be equal to that of 75 km in order to make a comparison of dispersion and crosstalk induced effects between the two cases while keeping the ASE noise unchanged. For a WSS crosstalk of -45 dB, 11 and 8 number of cascades are possible in the core ring for link distances of 75 km and 150 km, respectively.

When WSSs are used for adding either with passive splitting/dropping or with WSS for dropping the crosstalk doesn't scale with the node degree as it does in passive combining. Better crosstalk performance can be achieved by taking the advantage of the inherent nature of the WSS that could serve both as a wavelength blocker and a switch in adding (Sec. 5.4).

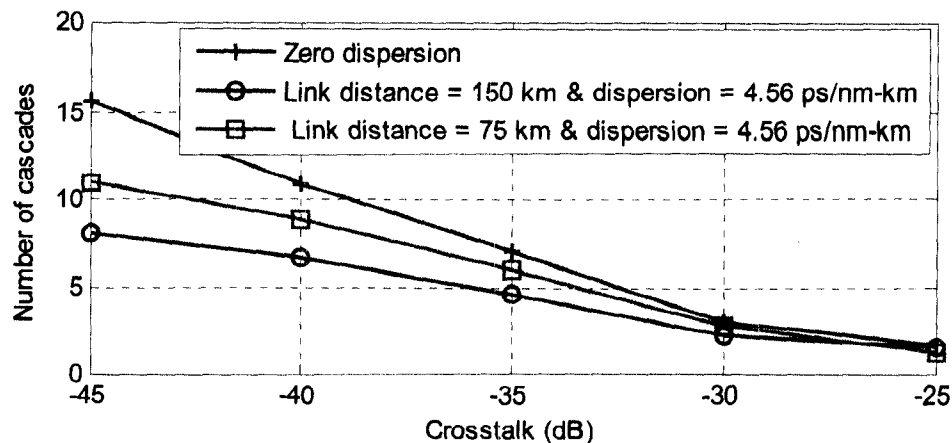


Fig. 6.15. Number of cascades as a function of WSS crosstalk.

6.3.3.2 Large degree WSS-based ROADM

A numerical model was developed to study the scalability of the large degree WSSs based ROADM. The basic block is a 1×9 WSS and is modeled with the measured filter responses and crosstalks at 1561.4 nm. In the drop configuration crosstalk of as high as -47.8 dB was observed among the drop ports. In the add configuration, crosstalks of -47 dB and -51 dB

were observed from two of the input ports while the crosstalk from the remaining 7 ports were below -60 dB. A single stage ROADM node with the same receiver settings as in Sec. 2.1 is considered (the ASE and dispersion effects are not considered). It is assumed that the power levels of the crosstalk source powers and the main signal powers are equal. Architectural options of WSS for drop with combiners for add and splitters for drop and WSS for add are considered. Fig. 6.16 shows the power penalty as a function of node degree (‘▲’, WSS with splitters) and ‘■’, WSS with combiners). It can be seen that node degrees of 150 can be achieved at 1 dB of power penalty by using WSSs for adding. The option of using combiners for add performs poorly with respect to crosstalk allowing a node degree of 36 at 1 dB of power penalty.

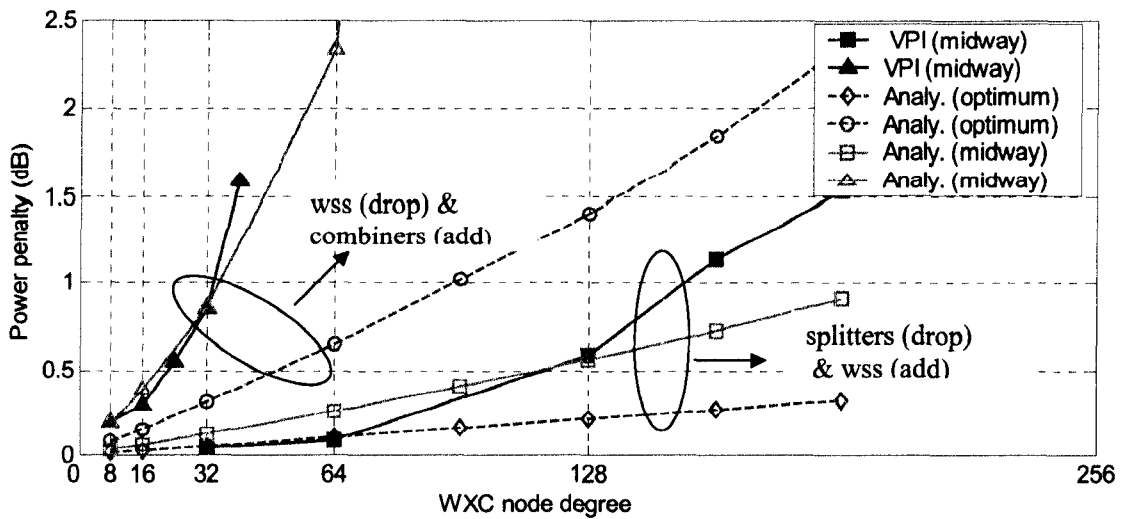


Fig. 6.16. Power penalty as a function of node degree of a single stage WSS-based ROADM node.

For comparison, the results from the analytical models (Sec. 5.5.1) are also shown in the same figure. Estimation using the analytical model with midway threshold (same as that in VPI), is in good agreement with that of VPI calculations, for both architectures. However, for large degrees, the analytical model under estimates the penalty. In the analytical model, an averaging of 0.5 is assumed for phase matching between the signal and crosstalk and for the ‘mark’ and ‘space’ density. However, in the VPI model, there is no such averaging, and more of a realistic system with random phases and ‘mark’ and ‘space’ densities are represented among the bit streams for the signal and crosstalk sources. Thus,

higher the number of interferes and/or the crosstalk per interferer the difference in estimation for power penalty increases between the two models.

6.3.3.3 The impact of channel filtering on the cascability

The shape of the pass band of a ROADM also influences the number of add/drop nodes that can be cascaded. In particular, flat-top pass bands are preferred as any small deviations in center frequency from the ITU grid can be tolerated with negligible penalties. The center frequency deviations from the ITU grid may occur at the transmitter or in the WSS, due to the design error in the center frequency of channel shape. To study the cascability of WSSs to center frequency detuning, an optical ring network with link distance of 75 km of NZ-DSF was considered. Since the WSS is a non-thermal device, in which the center frequency can not be altered, a tunable transmitter is needed. Due to the limited resources on the tunable transmitters, the above effect was analyzed only numerically using a VPI model.

The number of loops (or WSS cascades) as a function of center frequency detuning from the ITU grid of 192 THz, at a BER of 10^{-9} is shown in Fig. 6.17 (‘♦’), in the presence of fiber dispersion (4.56 ps/km-nm). It can be seen that frequency detuning of ± 20 GHz can be tolerated with negligible impact on the number of nodes that can be cascaded. Above ± 20 range, the number of cascades drops sharply. These results are as expected due to the fact that WSS shows a wide flat pass bands, 55 GHz of bandwidth at 0.5 dB, with a steep roll off. The key design aspect of the WSS is that the waveguide dispersion incurred in the incoming (MUX) path to the mirror is inverted and cancelled in the outgoing (MUX) path after the beam reflection in the MEMS, enabling wide flat-top channel shapes. The measured channel shape of WSS is shown in Fig. 6.18 and is compared with a channel shape measured from an AWG, which is made using silica on silicon, integrated planar lightwave circuit technology (iPLC). AWG shows a Gaussian channel shape, coinciding with theory, calculated with $\sigma = 0.034$. ROADMs constructed using iPLC mainly use AWGs for multiplexing and directional couplers for switching and often show Gaussian channel shapes.

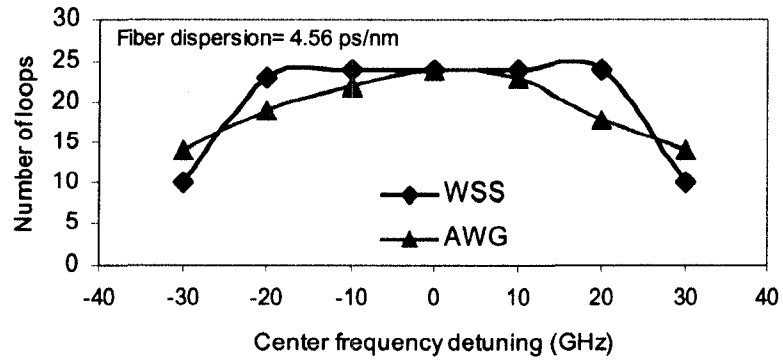


Fig. 6.17. Number of loops as function of center frequency detuning.

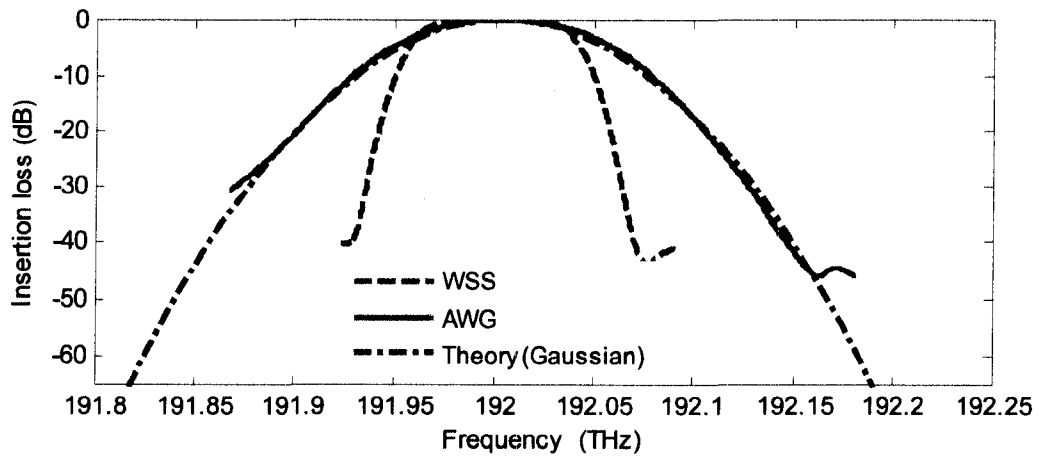


Fig. 6.18. The channel shapes of WSS (broken line) and AWG (solid line).

The cascability of the AWG calculated as function of center frequency detuning, also shown in Fig. 6.17 ('▲'), at a BER of 10^{-9} . The number of cascades gradually drops with center frequency detuning due to the smooth roll off of the channel shape.

6.4 Summary

The physical layer scalability of periodic add/drop optical ring networks constructed using WSS-based ROADMs was studied experimentally as well as theoretically. The models, experimentally and numerically, presented in this Chapter can be used to design add/drop networks by comparing different system configurations and system parameters for an optimized performance, for any given set of requirements.

Firstly, experimental set up of a re-circulating test-bed and its operation were described. The impact of ASE accumulation and dispersion on the number of recirculations

was investigated. It was found that, in the setup used in this work, the ASE accumulation dominates over the dispersion, and limits the number of cascades of 75 km of NZ-DCF links to 24. This is due to the high noise figure of the two EDFAs, 7.8 dB, used inside the loop. A numerical model of the re-circulating loop was also constructed and the simulation results obtained were verified with the experimental results with good agreement.

Secondly, the cascadability of periodic add/drop optical ring networks constructed using WSS-based RADM was studied in the presence of crosstalk, ASE, and fiber dispersion using the numerical model. The impact of fiber dispersion left uncompensated was investigated as functions of WSS crosstalk, fiber dispersion, varying number of node degree, and bit rates. For a given system performance, any fiber dispersion left uncompensated, demands for improved switch crosstalk compared to that with zero dispersion. The tolerance to switch crosstalk in the presence of fiber dispersion drastically drops for increasing bit rate and dispersion. The simulation results show that at the measured WSSs crosstalks, at 2.5 Gb/s, metro rings can be constructed with 18 periodic add-drop nodes at a link distance of 75 km and core rings that interconnects several metro rings can be constructed with 8 add-drop nodes at a link distance of 150 km for fiber dispersions as high as 4.6 ps/nm-km. At 10 Gb/s, a 16 node metro ring can be constructed at a link distance of 75 km by limiting the fiber dispersion as high as 1.2 ps/nm-km.

Thirdly, the crosstalk performance of a large degree WSSs based ROADM node, single stage, was studied numerically. Node degrees, up to 150, at 1 dB of crosstalk induced penalty can be constructed. Comparison of these results with that from analytical models revealed that the analytical model under estimate the switch performance to crosstalk due to many assumptions and simplification made in the closed-form crosstalk model.

Finally, the impact of center frequency detuning on the WSS cascadability was investigated numerically. It was found that, frequency detuning of ± 20 GHz can be tolerated with negligible impact on the number of cascades due to wide flat pass bands of the WSS.

7 Physical layer characterization of optical transport networks supporting heterogeneous switch architectures

The continuous and systematic increase of demand for wide spectrum of services will push the current limits on the optical transport layer in terms of transmission capacity and efficient bandwidth utilization. Optical networks employing WDM technology utilize the fiber bandwidth dividing into multiple wavelengths. Over the past few years, reconfigurable optical networks have been deployed with the successful realization of ROADMs. To date, the capability of ROADMs is limited to handle the signals at wavelength level in establishing wavelength paths in the network. The current transmission capacity in each wavelengths is 2.5 to 10 Gb/s and soon to be ready for 40 Gb/s [89]. The user traffic requirements are, however, in the range of 622 Mb/s to few Gb/s [90]. For efficient utilization of WDM channel bandwidth the traffic need to be handled in sub-wavelength granularities called time frames or packets with durations of few tens to few hundred nanoseconds. Accordingly, the network nodes should also be gradually upgraded to switch data in frames or packets. Complete migration from wavelength routing to packet switching will be highly challenging and an expensive proposition. However, handling high bandwidth slowing varying traffic using the ROADMs and highly varying low-bandwidth traffic using fast switches that can be added with the ROADMs in implementing a heterogeneous switch seems a reasonable approach in the near future. It is therefore of interest to explore architectural options and to study the physical layer performance of optical networks with heterogeneous switching nodes.

In this work, the physical layer performance of optical networks with heterogeneous switching nodes is investigated. Two network topologies are studied: optical star with a single stage switch for wide area applications and core rings for metropolitan networks. Heterogeneous switching node is implemented with two different switch technologies,

WSSs and SOA gates, to handle slow-wavelength switching and fast-packet switching, respectively.

7.1 Introduction

The next generation of optical networks is expected to employ heterogeneous switching architectures to improve the network utility [90], [91]. Analytical model of such networks with nodes constructed employing different traffic grooming capabilities has been reported with the aim of identifying the nodes to be upgraded when the resources are limited [90]. In another work, blocking performances of these networks has been analyzed under varying granularity levels [92]. In terms of physical layer performance of these optical networks, little or no work has been reported.

Considerable research has been carried out in accessing the scalability and physical layer performance of wavelength routed optical add/drop networks. Test beds with add/drop nodes constructed using various ROADM technologies, iPLC [93], MEMS [94], [19], wavelength blocker [24], and other [95] have been reported. Number of cascaded nodes of as high as 32 nodes for 16 channels at 10 Gb/s [19], and 16 nodes for 5 channels at 42.6 Gb/s [96] have been demonstrated in dispersion compensated fiber ring networks.

Over the last decade, there has also been a lot of progress made in the area of photonic packet switching with optical implementations of relevant building blocks. Unlike in wavelength switched interconnects, packet switched interconnects have to deal with certain functionalities including synchronization of incoming packets at various ports with the locally available clock reference and optical buffering (or delay lines) to resolve contention resolution of the packets. Yet, performing many of the controlling functionalities such as header processing and determining the routing of the packets is electronic since optical logic is too primitive a state to enable controlling with optics. In this work, the scope is limited to study the packet switched interconnect (the core of the switch with no other functional blocks) and to investigate the overall performance with other switches (ROADM) in a heterogeneous switched network.

Packet switching interconnects have been predominantly realized using SOA gates, which has achieved a stage of maturity and are available commercially from various vendors as single switch elements and up to 4x4 switches at competitive prices. The performance characterizations of a packet switched test bed deploying SOA based switch

fabrics have been reported for short reach interconnects with total fiber lengths limited to few hundred meters [97], [98]. In a separate work, the performance of a 12 x 12 switch, implemented by a cascade of 2 x 2 SOA blocks has been reported [99].

In long distance transmission networks, studies involving cascading effect of SOAs in optical networks have been limited to in-line amplifiers [100], [101]. In the context of optical transport networks, in which the nodes are upgraded with SOA switches, the packet switched signals experience additional impairments to that of wavelength switched signals. As a result, the margin of power penalty and power dynamic range requirements vary among channels at the receiver and limit the number of nodes traversed on light paths that carry both wavelength and packet level data.

In this work, the physical layer characteristic of a single stage and cascaded stages of heterogeneous switching node is assessed. Single stage switch is of interest for short reach networks and star topologies and the cascaded switching nodes are of interest in ring and mesh networks. The organization of this chapter is as follows. In Sec. 7.2, the architectures of the heterogeneous switching node are described. A brief review on the state of the art on SOA technology is given in Sec. 7.3 and the optical characterization of a commercially available general purpose SOA that was used in this work is presented in Sec. 7.4. Characterization of the heterogeneous switch in systems is given in Sec. 7.5. Finally, a summary of this work is given in Sec. 7.6.

7.2 Heterogeneous switch architecture

A possible realization of a heterogeneous switch is using WSS-based ROADMs for the wavelength switching and SOA gates for time slot switching, as shown in Fig. 7.1. The colorless port nature of the WSSs allows dropping any desired number of wavelengths to the drop port/ports that are directed to the SOA switch, which does the time domain switching of the optical packets to various ports that are directed towards the add ports of a WSSs (a) or to a passive combiner (b).

For the implementation SOA switch fabrics, two different granularities are considered, wavelength and time and time (wavelength striped). The SOA switch architecture that can handle packets with wavelength and time granularities is shown Fig. 7.2 (a), where each SOA gates packets/frames at a specified wavelength. Networks

supporting wavelength stripped optical packets has also been proposed to minimize component counts and management overhead. Fig. 7.2 (b) shows the SOA switch structure that switches packets in time domain regardless of grouping of wavelengths. Each SOA handles certain number of wavelengths that are grouped for transmission end to end.

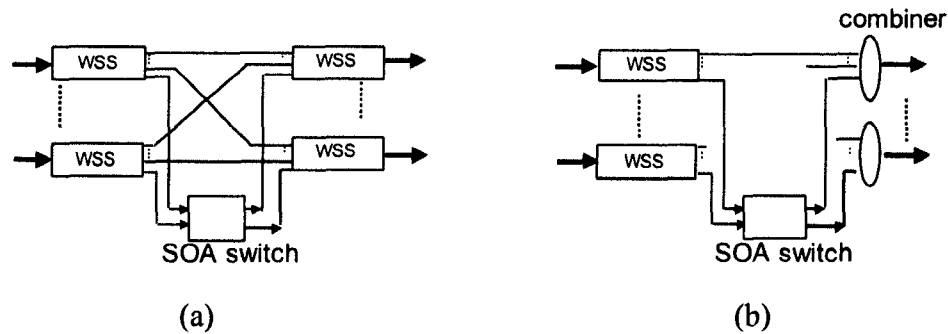


Fig. 7.1. Heterogeneous switch employing WSSs and SOA switch.

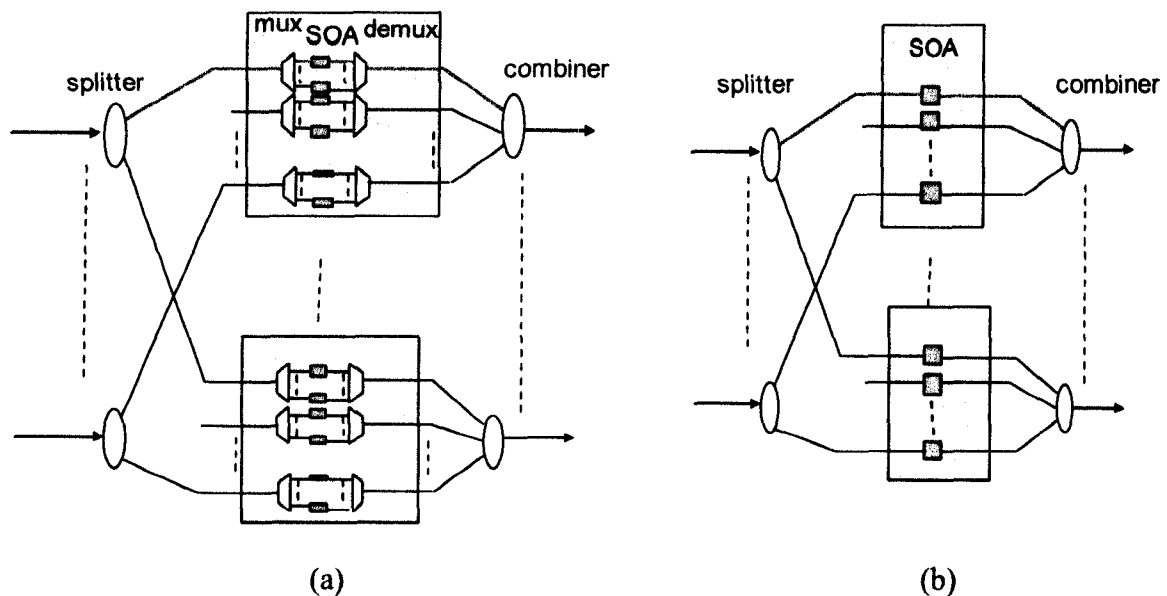


Fig. 7.2. SOA switch: (a) Structure that can handle wavelength and time domain switching; (b) Structure that can handle time domain (wavelength stripped) switching.

The optical characterization of WSSs and WSS-ROADMs has been reported in Chaps. 5 and 6. This work focuses on the performance characterization of SOAs, as stand alone device and as a switch integrated with WSS. For the switch, both scenarios single channel operation, Fig. 7.2 (a), and multiple channel operation, Fig 7.2 (b), are considered.

A review on SOA technology is given next, followed by the SOA characterization, given in Sec. 7.4.

7.3 SOA technology

The operation of SOAs is similar to that of lasers except that SOAs are single pass devices without reflecting facets. The optical gain is achieved through stimulated emission, caused by the recombination of electrons and holes. An external current source is used to inject the electron-hole pair. For SOA, the net gain is generally 10 to 25 dB. Thus, SOA operates at higher current densities than a laser.

7.3.1 SOA structure

The conventional structure of a SOA is a double heterostructure, shown in Fig. 7.3. A thin active layer of thickness $\sim 0.1 \mu\text{m}$ is sandwiched between p-type and n-type cladding layers. For optical gain at wavelengths in the range of $1.3 - 1.6 \mu\text{m}$, the substrate material mainly used for SOA fabrication is InP. In the active region quaternary compound $\text{In}_{1-x}\text{Ga}_x\text{As}_y\text{P}_{1-y}$ is used, where subscripts x and y indicate the fraction of In atoms that are replaced by Ga and the fraction of P atoms that are replaced by As, respectively.

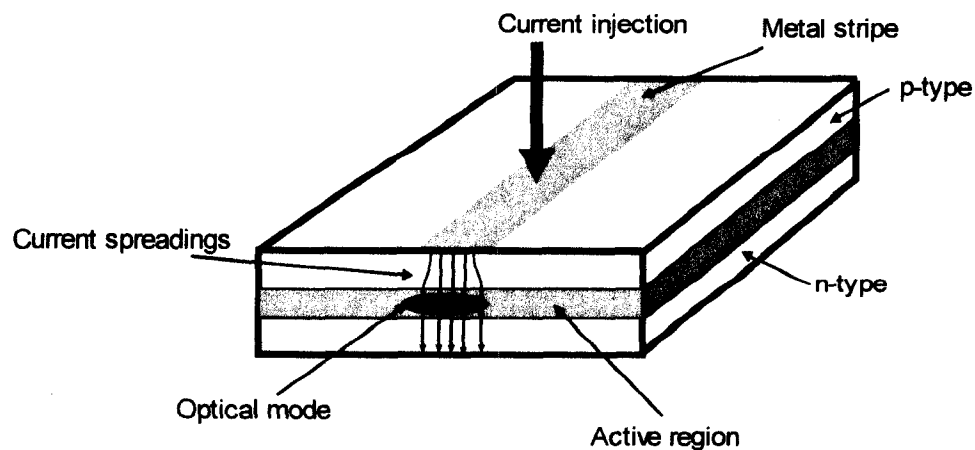


Fig. 7.3. Schematic of a double-heterostructure SOA.

For efficient device operation, the carrier confinement in the active region is necessary for two main reasons, to provide sufficient gain to the propagating light and to lower the bias current requirements. This is achieved by having an active region that has lower bandgap energy than the cladding regions. To confine the light propagation to the

active region, the refractive index of active region has to be higher than that of cladding layers. Indeed, lower bandgap energy materials have higher refractive indices, a good coincidence.

The attractive features of the SOA switches are optical gain, wide gain bandwidth (50 – 80 nm), and small footprint. A disadvantage of the SOAs is its gain dynamics when it is operated at gain saturation. The gain recovery time of SOAs, which is in the range of 200-600 ps, is an issue when signals at a bit period comparable to or shorter than the gain recovery time are input to the SOA. At high input powers, this creates signal waveform distortion (patterning effects) due to SOA gain saturation. Another disadvantage is polarization dependency due to the asymmetrical cross-section of the active region. In multi-channel applications, the total power increases with increasing number of channels. However, as the output power increases the SOA is driven into saturation and some nonlinear effects in the active region of the SOA, such as cross-gain modulation (XGM) and four wave mixing (FWM), begin to appear. While such non-linear effects of SOA are advantageous in all-optical functional applications, such as wavelength conversion and clock recovery, such effects cause additional penalties in packet switching applications.

Over the last decade, there has been a tremendous progress made in SOA technology, both in the device design and material processing techniques in improving SOA performance, such as fast gain recovery (quantum dot SOA), and high saturation output powers (gain-clamped and quantum-well SOAs).

7.3.2 Polarization issues and techniques for compensation

A drawback in the conventional design is that the SOA gain is dependent on the state of polarization of the input light. The asymmetry in the active region, where the thickness is much shorter than the width (0.1:1), results in unequal mode confinement factors between the two main modes, transverse electric mode, TE (field polarization along the junction plane), and transverse magnetic mode, TM (field polarization perpendicular to the junction plane). The gain difference between TE and TM modes can be a few dB.

Two major strategies to overcome the polarization dependency are square cross-sectional waveguide and strained layers. With square cross-sectional waveguides an equal confinement between TE and TM can be produced [103]. However, fabrication of such a

device, etching down the width as close to a thickness of 0.1 μm , is difficult and is not feasible for mass production. A better approach is to use strained layers in the active region. In an unstrained bulk material, the material gain will be equal between TE and TM modes. By growing strained layers in the active region, the material gains between the two modes can be adjusted to compensate for the differing confinement factors. Improvement in polarization sensitivities of <0.5 dB have reported in strained bulk region [104] and in strained quantum wells [105].

7.3.3 Multiple quantum- well (MQW) SOAs

An improved design of the SOA active region is incorporating multiple quantum wells to offer better characteristics compared to bulk devices. MQW are fabricated by stacking several quantum wells. Each quantum well consists of an active layer of thickness less than ~ 20 nm, sandwiched between two thin cladding layers. Compared to bulk, where an electron in the conduction band is free to move in three directions (3D), in a quantum well the electron is free to move only in two directions (2D) and confined in the direction along the stacking of wells.

The density of states of a quantum well has a staircase type dependency on energy whereas in bulk it is continuous function of energy. The reduced dependency on energy in the quantum wells leads to shorter gain recovery time, broader gain spectrum, and lower noise figure compared to bulk SOAs. The reduced loss coefficient in MQW also results in larger saturation output powers.

7.3.4 Quantum dot (QD) SOAs

In a QD-SOA, the electron motion is restricted in all three directions. In the active region few QD layers (~ 5) are grown, with each layer having a density of QDs $\sim 4 \times 10^{10} \text{ cm}^{-2}$ [106]. QD SOA offers several unique properties, including ultrafast gain recovery on the order of few ps, widest broadband gain, and the lowest noise figure among all the SOA structures. A disadvantage of QDs is that it requires very high drive currents, $\sim 2\text{A}$.

7.3.5 Gain-clamped SOAs (GC-SOA)

In a GC-SOA, the gain of the SOA is clamped to a fixed value regardless of any change in the input power. A lasing action, at a wavelength remote from signal wavelength, is produced in the SOA by using a wavelength specific feedback. This effect keeps the carrier density fixed such that any changes in the input signal leads to opposing changes in the lasing mode power. With GC-SOA, the linear region of the SOA can be extended at output powers up to ~15 dBm. But once saturation is reached, the power falls off rapidly.

A performance comparison of polarization insensitive (< 1dB) high performance SOA structures reported in the literature are given in Table 7.1.

Table 7.1. Comparison of main parameters from different SOA structures.

| SOA structure | Gain (dB) | Gain BW (nm) | Gain recovery time (ps) | Saturation output power (dBm) | NF (dB) | PDG (dB) | Drive current (mA) |
|---------------|-----------|--------------|-------------------------|-------------------------------|---------|----------|--------------------|
| Bulk | | | | | | | |
| [107] | 29 | 50 | - | 9 | - | 0.3 | 200 |
| [104] | 20 | 40 | - | 13 | 6 | 1 | 200 |
| GC | | | | | | | |
| [108] | 11 | 40 | 400 | 10 | 8 | 0.6 | 200 |
| MQW | | | | | | | |
| [109] | 17 | 40 | > 300 | 16.5 | 6 | 1 | 500 |
| [110] | 10 | 40 | > 300 | 22 | 6 | 0.6 | 600 |
| QD | | | | | | | |
| [106] | 25 | 90 | < 10 | 20 | 5 | < 0.5 | 2000 |

7.4 Characterization of SOA

7.4.1 SOA and driver unit

The SOAs used in this work is a commercial device from Kamelian (OPB-10-10-N-C-FA). It is primarily intended for use as an optical power booster in ROADM nodes to amplify data rates from Mb/s up to and beyond 40 Gb/s. SOAs are flexible in terms of other functionalities such as gating and switching. The SOA is fabricated using InP material. A buried hetrostructure design which uses a strained bulk active region is employed. Polarization dependency has been minimized by balancing out the differing confinement

factors and differing material gains between the modes and a PDG of <0.8 dB is achieved over the C-band. The SOA is housed within a standard 14-pin demountable butterfly package and pig-tailed with SM fibers at input and output.

An evaluation driver board (OPTOSCI, LDR250GKE), incorporating a current source and a thermo electric cooler, is used to mount and operate the SOA (Fig. 7.4). The board interfaces with the built-in driver unit and combines the computer control interface. Flexible device mounting options are provided through the use of user configurable wire jumpers. The board is also fitted with a custom modulation input with modulation bandwidth ranging from 18 Hz to 120 kHz (at 3dB).

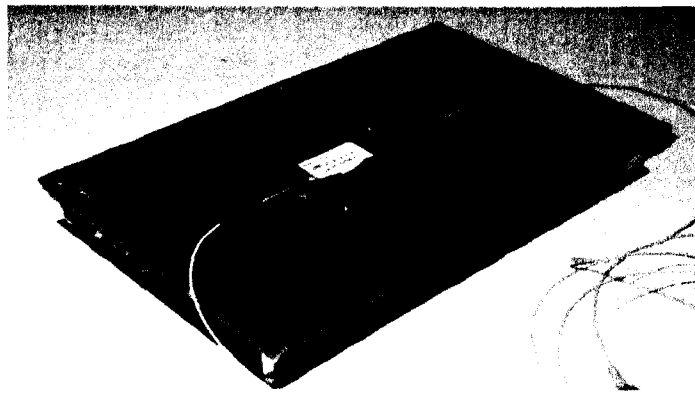


Fig. 7.4. SOA mounted on the evaluation board.

The measured gain and noise figure (NF) as a function of drive current at signal input power of -10 dBm at 1561.4 nm is shown in Fig. 7.5. At zero drive current, the SOA shows < -45 dB of isolation. The gain increases with increasing current and reaches to 10 dB and 12.8 dB at 64 mA and 200 mA, respectively. The noise figure of 6.4 – 6.9 is measured over the current range of 20 to 180 mA.

In switching applications, the SOA current needs to be modulated to pass or block the signal through the SOA. The gain of the SOA at 'ON' and 'OFF' states determines the extinction ratio of the bits at the output of the SOA. For extinction ratios of better than 20 dB, the off state current of the SOA needs to be limited to 3.5 mA for an 'ON' state gain of 10 dB.

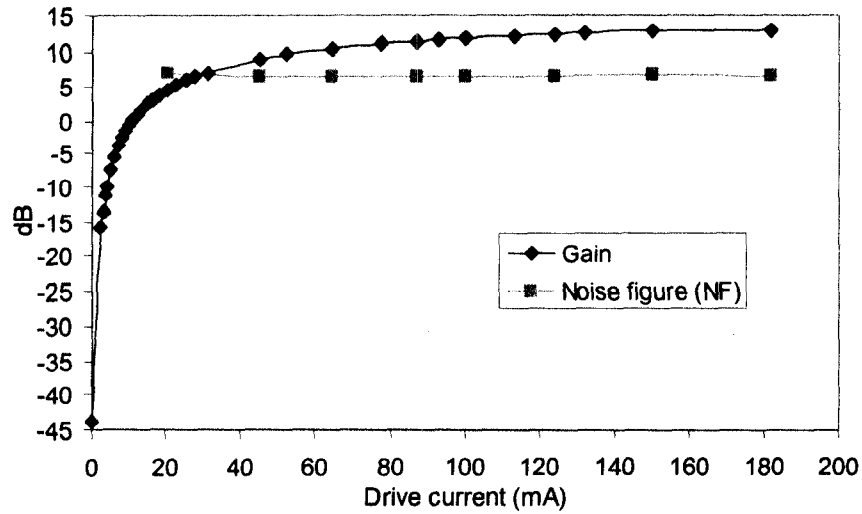


Fig. 7.5. SOA gain vs drive current at a signal input power of -10 dBm at a wavelength of 1561.4 nm.

The SOA gain as a function of wavelength is shown in Fig. 7.6(a). A gain variation of 2dB over the wavelength of 1540 to 1560 nm is measured. The ASE spectrum of the SOA is shown in Fig. 7.6 (b), showing the gain peak at 1456 nm. The gain peak wavelength is designed at off C-band to reduce the ASE accumulation in optical networks operating over C-band.

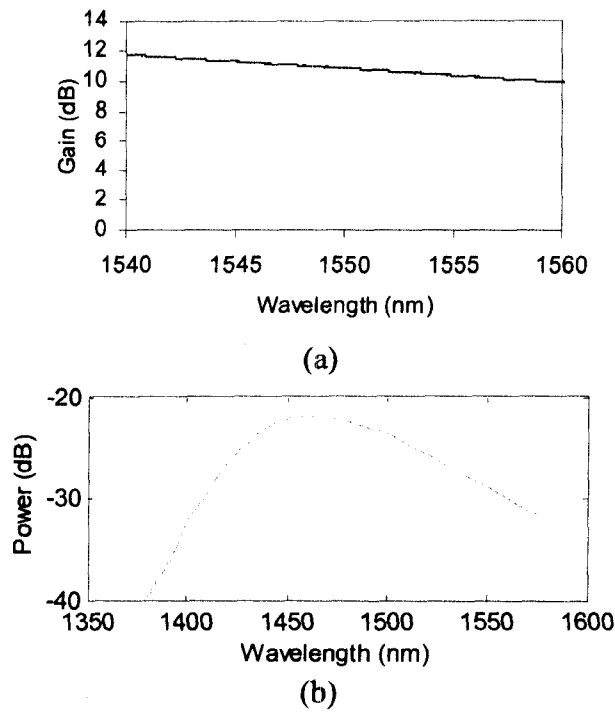


Fig. 7.6. SOA gain vs wavelength (a); ASE spectrum (b). The drive current for SOA is 80 mA.

The gain as a function of input power is shown in Fig 7.7 at a wavelength of 1561.4 nm at a drive current of 100 mA. Unsaturated gain is 10 ± 0.5 dB and the input power at 3 dB gain saturation is ~ 1 dBm.

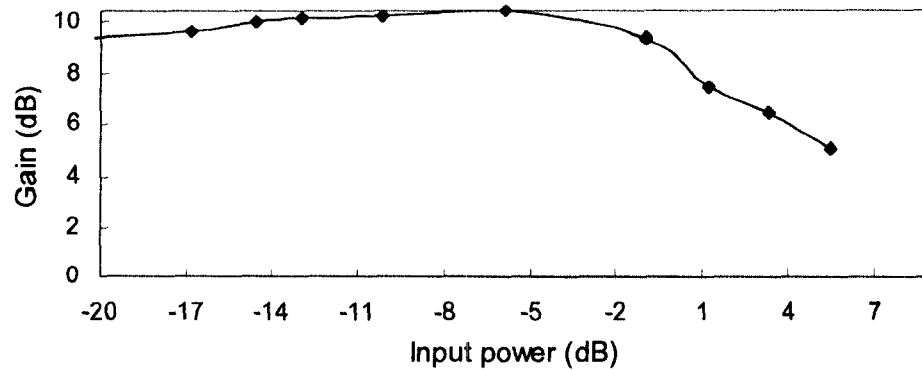


Fig. 7.7. Gain as a function of input power at a wavelength of 1561.4 nm at drive current of 100 mA.

7.5 Characterization of the heterogeneous switch in systems

The objective of the physical layer characterization is to fully assess the penalties incurred at the switch due to packet switching, understand the courses of them, and to find solutions to improve the performance of the switch. Two network topologies are studied. A single stage switch for short reach interconnects and a ring topology with varying number of nodes. A re-circulating loop test bed is used to emulate the cascaded switch effect in the ring networks.

The switch is initially tested under static routing conditions. In packet switched networks, since the switching is completed within the guard time that is allocated between adjacent packets, the transmission characteristics of the SOA gate can be studied under static operation. The SOA gates are kept at the ON stage by supplying a steady state current. Power penalties incurred due to the addition of SOA switch is assessed as a function of following parameters: input power levels at the SOA – the wider the input power dynamic ranges at the SOA, the larger the scalability of the packet switch; bit rates-relates to gain dynamics; and the number of wavelengths transmitted- higher the number of channels, the more the capacity of the switch.

7.5.1 Single channel configuration

Fig. 7.8 shows the experiment set up used. An externally modulated laser source at 2.5 Gb/s, at a wavelength of 1561.4 nm was used for the BER measurements. Variable optical attenuators, VOA1, VOA2, VOA3, are used to control the channel powers at the input to the switch, at the input of SOA, and at the receiver, respectively. The SOA current was set at 100 mA.

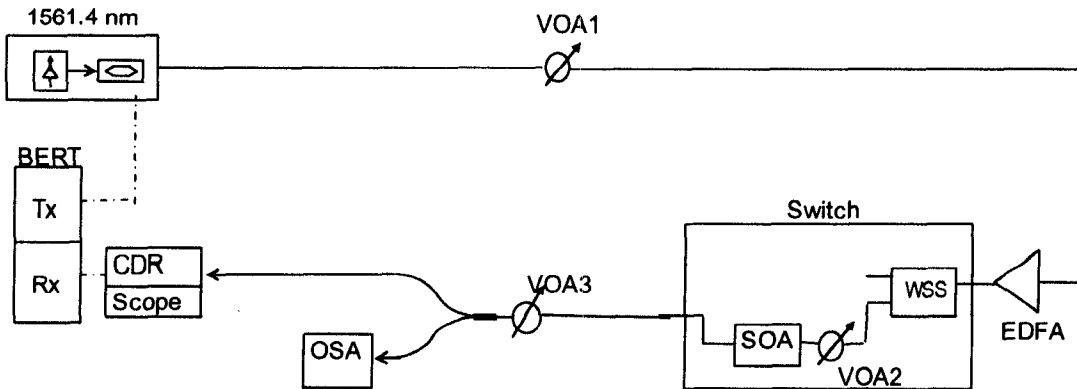


Fig. 7.8. Experimental setup for single channel operation.

7.5.1.1 The impact of gain compression and gain dynamics

The penalty incurred when the SOA was operated in various regions of the gain curve, near before saturation, in saturation and small signal were studied and compared to that of the wavelength path (through WSS, without the SOA). To understand the gain dynamics induced effects, a lower bit rate of 622 Mb/s is also studied in addition to the bit rate of 2.5 Gb/s. At 622 Mb/s, the bit duration is much higher than the carrier lifetime of SOA and the carriers get sufficient time to respond to variation in signal powers between ‘one’ and ‘zero’ compared to that at 2.5 Gb/s, at which the carrier lifetime and the bit duration becomes comparable and the amplifier gain tends to be constant between the power levels at ‘one’ and ‘zero’.

Fig. 7.9 shows the BER measured as a function of received power and the Table 7.2 lists the additional powers required at the receiver compared to that without the SOA, at a BER of 10^{-9} . The lowest penalty of 0.4 dB, at 622 Mb/s, is observed in the linear region. This penalty is due to the additional ASE from the SOA and it can be reduced by using a narrowband filter at the receiver, centered at 1561.4 nm. At the same input power, at a

higher bit rate, 2.5 Gb/s, an additional penalty of 0.4 dB is incurred due to the rapid carrier dynamics.

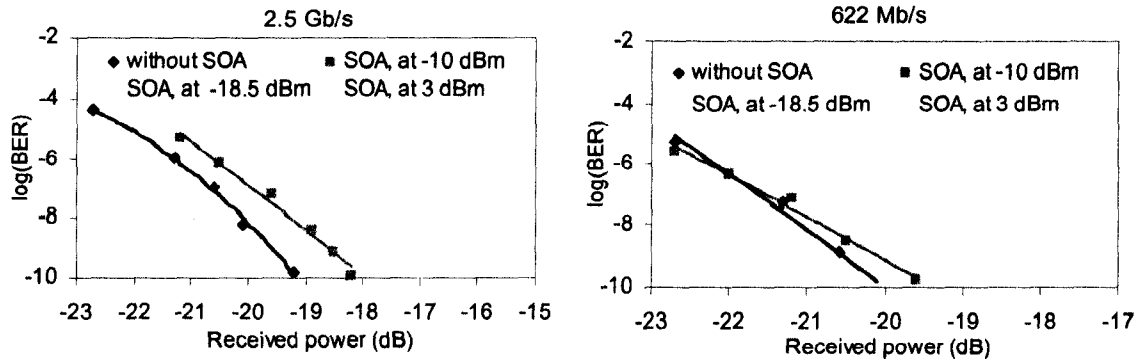


Fig. 7.9. Ber vs received power at 2.5 Gb/s (left) and 622 Mb/s (right) at different input powers.

Table 7.2. Power penalties incurred at different input powers for bit rates of 2.5 Gb/s and 622 Mb/s.

| Input power to SOA (dBm) | Penalty (dB) | |
|--------------------------|--------------|----------|
| | 2.5 Gb/s | 622 Mb/s |
| -10 | 0.8 | 0.4 |
| 3 | 1.6 | 1.6 |
| -18.5 | 3.0 | 2.6 |

In the saturation region, penalty of 1.6 dB is observed for both bit rates. Compared to the liner region, the penalty is higher in saturation due to gain dynamics and extinction ratio degradation. At 622 Mb/s, the penalty is mainly due to extinction ratio degradation and the resulting eye closure-‘one’ state sees a lower gain (saturated gain value) and ‘zero’ state sees higher gain (unsaturated gain). At 2.5 Gb/s, degradation of the eye is due to patterning effects since the carrier lifetime and bit duration become comparable. Fig. 7.10 shows the eye diagrams of the bits at the receiver for the input powers of -10 dBm (a) and 3 dBm (b) at bit rates of 2.5 Gb/s and 622 Mb/s. In the linear regime, replica of the input eye is seen. But, at 3 dBm input power, patterning effects are seen at both bit rates, comparatively larger at 2.5 Gb/s. The peaking at ‘one’ state occurs when a ‘one’ state is preceded by a ‘zero’ or consecutive ‘zeros’-unsaturated gain is seen at the raising part of the pulse and the gain then reaches the saturated value in the latter part of the pulse. While

for a series of consecutive 'ones', the gain remains at a saturated value, showing no peaking.

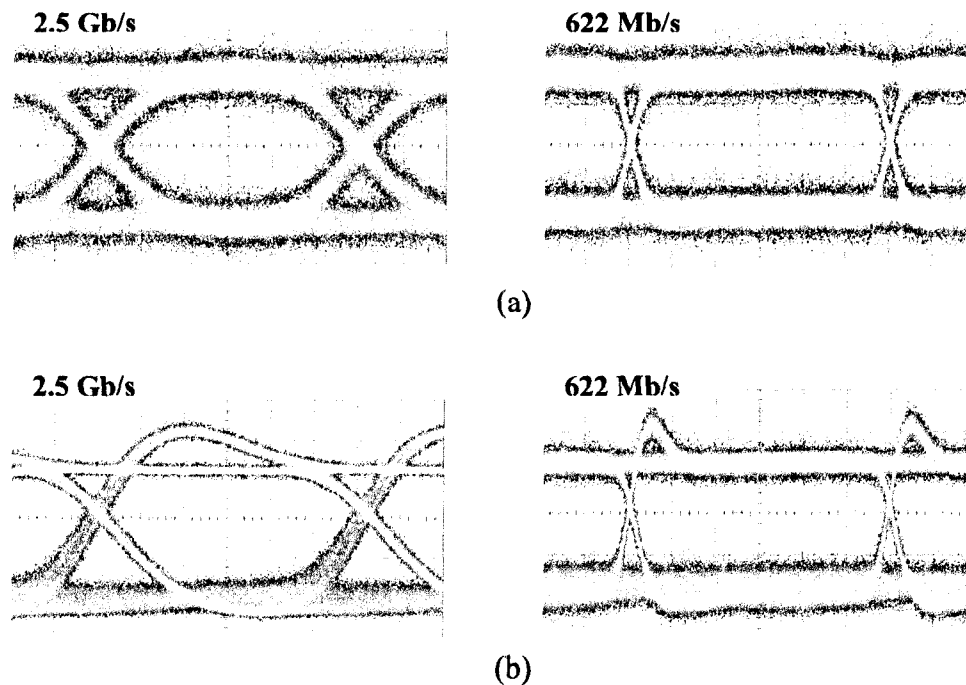


Fig. 7.10. Received eye diagrams at input powers of -10 dBm (a) and 3 dBm (b).

Highest penalty, of 3 dB (2.5 Gb/s) and 2.6 dB (622 Mb/s), are observed in the small signal regime due to the increased ASE noise level (reduction in OSNR of ~ 8.5 dB compared to that at -10 dB of input power).

7.5.2 Multi-channel systems

In the switch configuration, shown in Fig 7.2 (b), the SOA must operate in multi-wavelength condition to improve the switch throughput. The input power in multi-channel systems is high. However, the operation of the SOA must be ensured not to be deep in saturation in order to avoid patterning effects and any penalties due to the nonlinear effects in the SOA such as FWM and XGM.

For additional wavelengths, small form factor pluggable (SFP) transceivers that are driven by an FPGA are used (Fig. 7.11). The FPGA houses four transceivers, each transmitting 2.5 Gb/s PRBS data stream. Different seeds for bit generation are used to ensure bit de-correlation among the channels. All five channels are multiplexed using the

MUX and the built-in (channel wise) attenuation functionality was used to balance out the channel powers at the output of the Mux. A narrowband filter is used at the output of the switch to filter out 1561.4 nm for BER measurements. The SOA current was set at 100 mA.

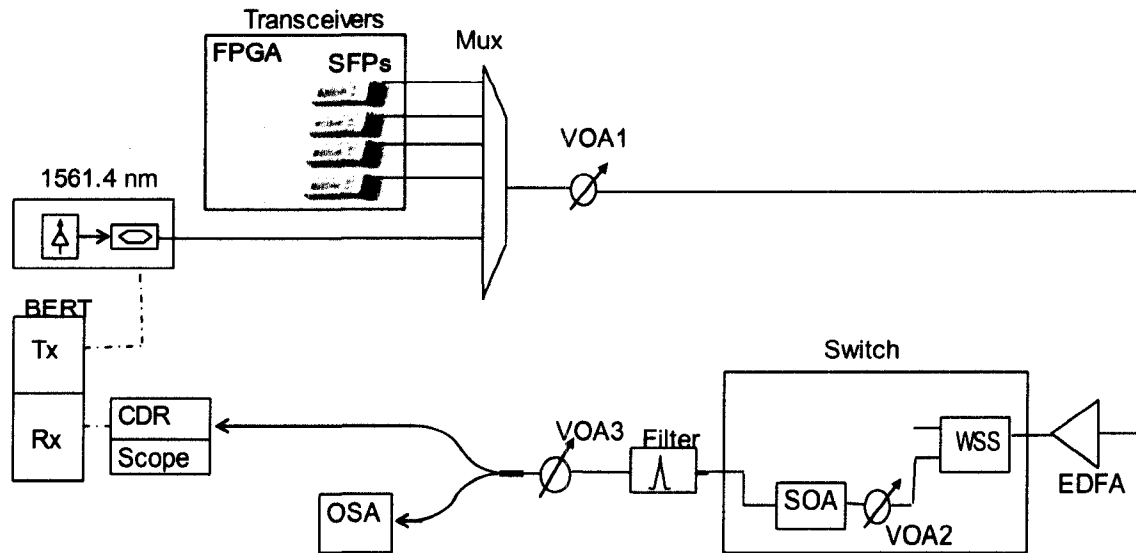


Fig. 7.11. Experimental setup.

7.5.2.1 FWM

FWM is a coherent nonlinear process by which optical signals at different wavelengths that are closely spaced mix to produce new signals at other wavelengths. The newly generated signals are at low power and they appear as crosstalks to the main signals if they are at the wavelengths of the main signals. The interference is worse if crosstalk and the main channels are polarization matched. The intensity of the crosstalk channels is a function of channel power and channel spacing.

Fig. 7.12 shows the spectrum at the output of the SOA, at a channel power of 1 dBm, at 100 GHz channel spacing (solid line) and 200 GHz (broken line). FWM rejection ratios of -33 dB and -36 dB are measured at 100 and 200 GHz channel spacings, respectively.

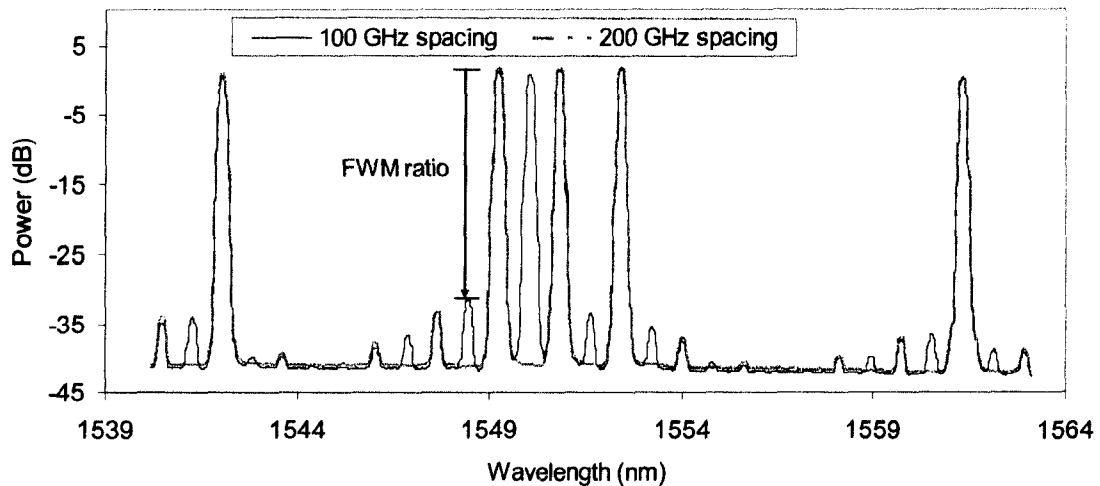


Fig. 7.12. Spectra of FWM at the output of SOA.

7.5.2.2 Cross gain modulation (XGM)

The broadening of the material gain spectrum of the SOA results in carrier density changes in the amplifier affecting all the input signals. Carrier density changes give rise to pattern effects and inter-channel crosstalk in multi-wavelength applications. The basic XGM is where two signals at different wavelengths, a CW (probe) and a strong modulated signal (pump), are input to an SOA, the pump modulates the SOA gain and the gain variations are experienced by the probe. This effect transfers the information encoded in the pump to the probe (inverted), useful mechanism to realize wavelength conversion of data channels in the optical domain. But, in switching applications, XGM imposes penalties due to inter-channel crosstalk.

To study the XGM effect in the SOA, the number of channels passed through the SOA varied while keeping the total output power at the SOA constant. Fig. 7.13 shows the BER measured as a function of received power for cases of single, two, and five channels systems. For the SOA total output power of 10 dBm, power per channel for one, two, and five channel cases are 10, 7, and 3 dBm, respectively. To estimate the impact due to XGM, required received powers, for a BER of 10^{-9} , were compared to that of a single channel system. For two channel systems, a penalty of 0.5 dB is seen due to XGM. But, as the number of channels increased to five, a gain of 1 dB is seen in the required power at the receiver. This indicates that inter channel crosstalk due to gain modulation effect and

patterning effects reduce due to the fact that the temporal power fluctuations in the SOA smooth out for higher number of channels.

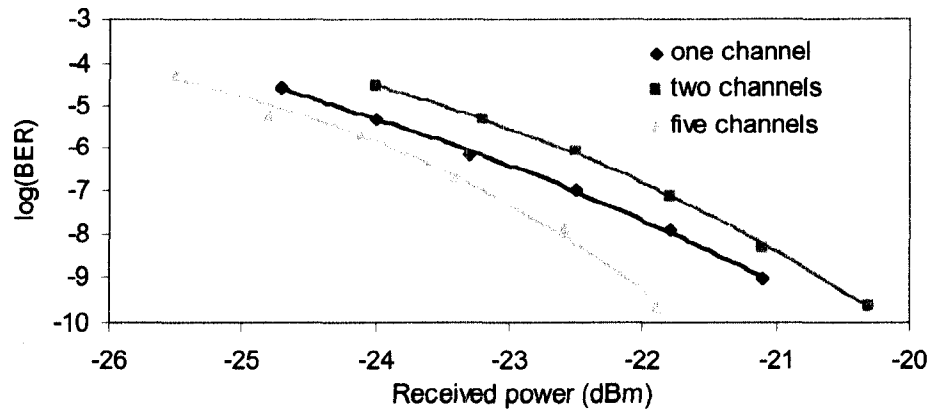


Fig. 7.13. BER vs received power measurements as a function of number of channels with SOA in saturation.

7.5.2.3 Penalty due to gain compression for multiple channel operation

The power penalty as function of increasing number of channels is measured in order to study any effects due to gain compression from increased total input power at the SOA. The experimental setup used is shown in Fig. 7.14. The numbers of channels that are sent to the SOA are selected using the WSS with appropriate mirror settings. A multiwavelength source, (Pletron TM 3050) that emits channel wavelengths at spacing of ~ 50 GHz over the range of 1543.83 nm – 1550.16 nm is used. Fig. 7.15 shows the spectrum at the input of the SOA with total number of channels of 15 at power level of -10 ± 2 dBm per channel. An external modulator (MOD2) is used to modulate the wavelength stream of the Peleton source and a fiber spool of 75 km with a total dispersion of 342 ps/nm was used to decorrelate the bit streams among different channels. The channel at 1561.4 nm was used for the BER measurements.

Fig 7.16 shows the penalty incurred and the SOA gain as a function of number of channels that are passed through the SOA, at a BER of 10^{-9} . The power penalty increases with increasing number of channels. For one channel the penalty is 0.2 dB, much lower than that obtained in Sec. 7.5.1 because of the narrowband filter used at the receiver. In the linear region (constant gain), increase in penalty is negligible (<0.1 dB) to increasing number of number of channels up to 3. As the number of channels increased above 3, the gain starts to saturates, and the penalty increases rapidly to 1.2 dB at five numbers of

channels. Further increase in number of channels results in gradual increase in power penalty and at 16 numbers of channels (total input power of 2 dBm) a penalty of 2.7 dB is seen. The major effect that contributes to the steady increase in penalty is gain saturation due to increase in total input power. Other possible effects are channel-to-channel crosstalk effect (XGM) due to the randomness in the input signal power and FWM when SOA in gain saturation. Observing the rate of increase in penalty in gain saturation, it can be seen that, when the number of channels are less (from 3 to 5 numbers of channels) contribution from XGM effect is higher compared to that for higher number of channels, in which case, the randomness in input power averages, resulting in lesser XGM effect.

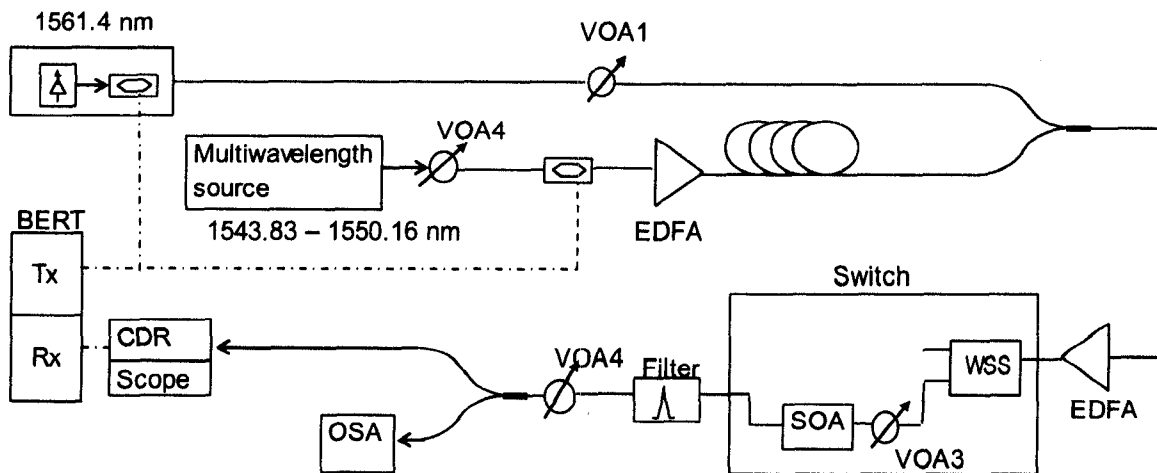


Fig. 7.14. The experimental set up used to measure the penalty due to gain compression in multi-wavelength operation.

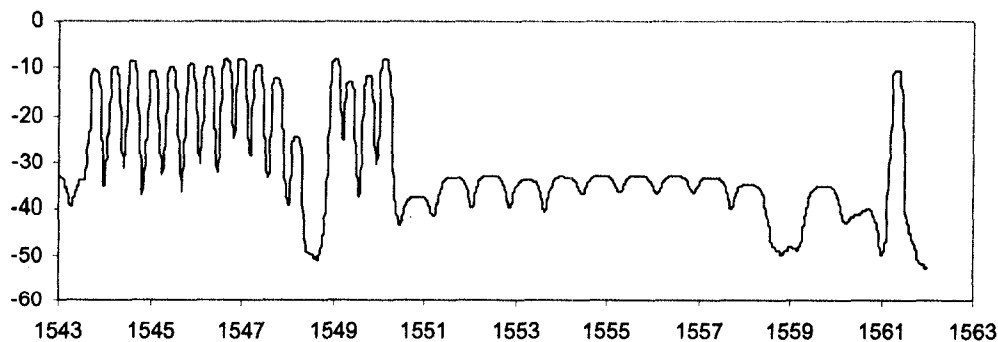


Fig. 7.15. Multi-channel input spectrum at the input of SOA.

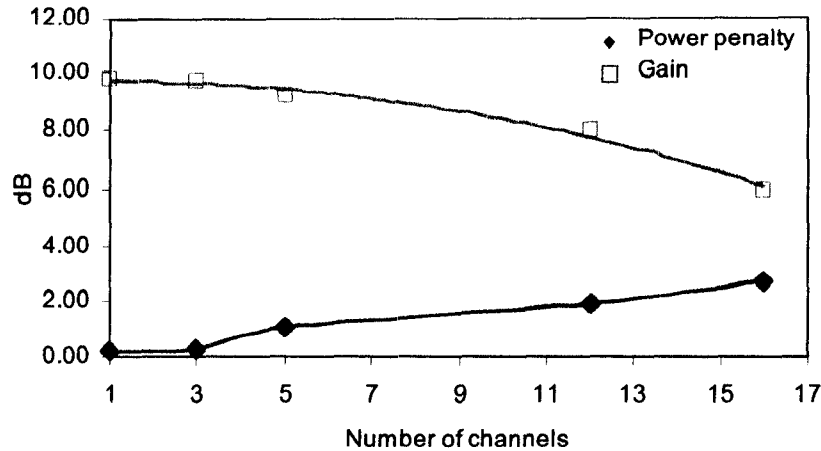


Fig. 7.16. Power penalty and the SOA gain as a function of number of channels.

7.5.3 Dynamic routing

Driving the SOA directly with electronic signal permits realization of controlled switching functionalities. An un-biased SOA, absorbs and blocks the signal passing through the SOA with an isolation of < -45 dB. The SOA becomes transparent (0 dB of loss) at a bias current of 11 mA (Fig. 7.5) and signal gain up to 11 dB can be realized at higher currents.

The experimental set up for dynamic switching is as shown in Fig. 7.8 and the detail on the generation of the modulating electrical signal is shown in Fig. 7.17. The transmitter was kept constantly transmitting the bits at 2.5 Gb/s. An FPGA was used to generate the modulating signal to the SOA and the triggering signal for the scope. The TTL signal at 3.3 V from the FPGA was converted to $+0.65/-0.65$ V peak-to-peak signal at 50% duty cycle using a signal conditioning circuit based on op-amp circuit with a bandwidth of < 500 kHz. The converted signal was then directed to the modulation input of the driver board. The modulation transfer function of the driver circuitry is -0.125 A/V. The SOA was biased at 70 mA. The 'ON' and 'OFF' state currents were therefore set at 150 and 0 mA, respectively. For every received packet, the measurements on received bits were carried out by leaving some guard time at the beginning and ending of the packet to account for slow rise and fall time of the drive electronics.

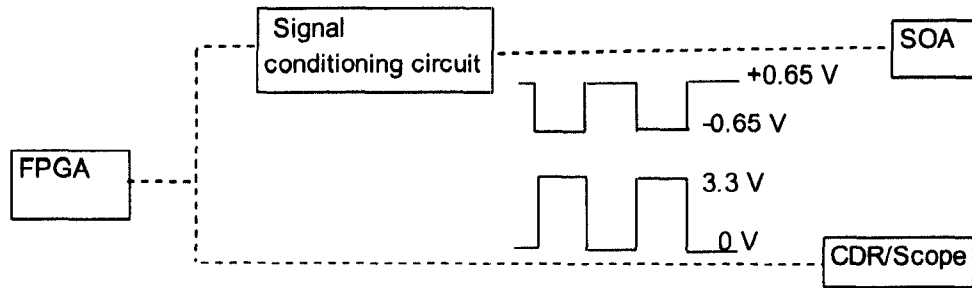


Fig. 7.17. 17. Details on drive electronics.

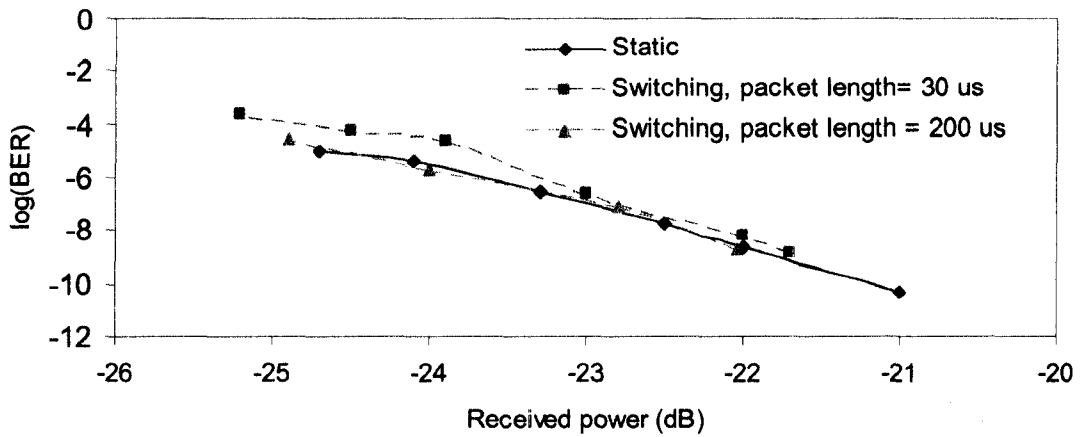


Fig. 7.18. BER as a function of received power for the SOA under static (solid line), and dynamic (broken lines) switching conditions.

Fig. 7.18 shows the BER measurements, carried out at the wavelength of 1561.4 nm, when the SOA was switched (broken lines) and not switched (solid line). Switching performance was measured at two different packet lengths, 200 and 30 μs. Negligible penalty (< 0.2 dB) is observed due to switching compared to that of static operation regardless of the packet length. The observed eye diagrams with SOA biased at 70 mA with no modulating signal and with the modulating signal at ‘ON’ and ‘OFF’ state are shown in Fig. 7. 19.

It should be noted that the SOA is capable to switch packets in lengths of few hundred ns, but the bandwidth limitations of the drive electronics (driver board and the signal conditioning circuit) limited the packet length for measurements in this experiment to 30 μs.

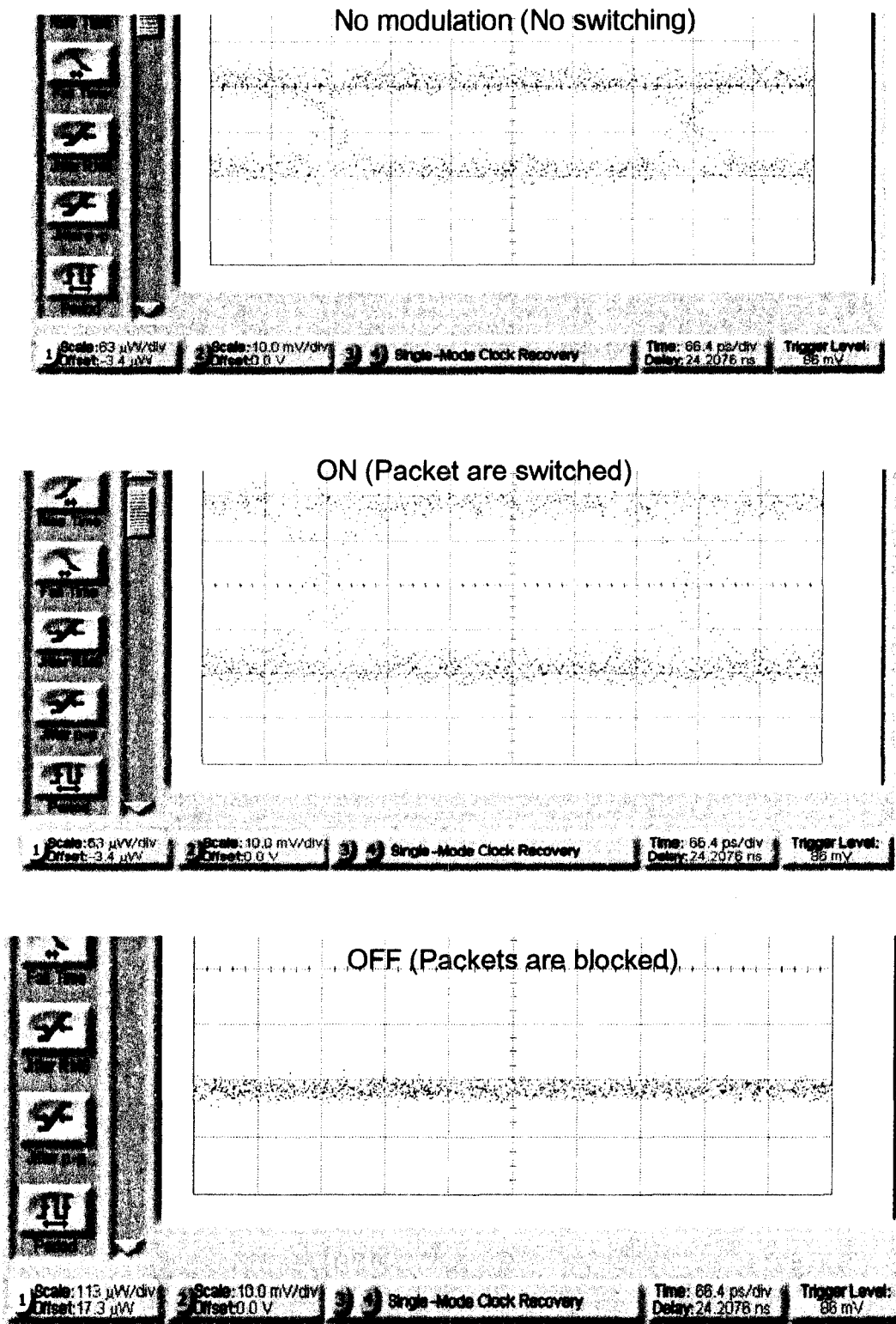


Fig. 7.19. Received eye diagrams for SOA.

7.5.4 The effect on cascading of SOA gates in periodic networks

The impact of accumulation of physical layer impairments due to cascading of the switch was investigated using the re-circulating testbed described in Chapter 6, Sec. 6.2. Fig. 7.20 shows the switch configurations that were used in characterizing static routing of wavelength and packet paths. A total of five wavelength channels were considered at the transmitter, as shown in Fig. 7.8. The BER measurements were made at the wavelength of 1561.4 nm.

Fig. 7.21 shows the number loops for the wavelength path for varying loop input powers for a single channel ('♦'), at a BER of 10^{-9} . As seen, the number of loops circulated is optimal (26) at -10dBm of input power and over the power range of -15dBm to -6 dBm the number of loops circulated remain > 23 . At a loop input power of -13.5 dBm/channel, when the number of channels increased to two (total power -10.4 dBm) and five (total power -6.5 dBm), the numbers of loops that can be circulated are 25 and 23, respectively, also shown in Fig. 7.21. The results indicate that the cascadability of the wavelength path shows a good tolerance to loop input (total) power range of ~ 11 dB, -17 dBm to -6dBm.

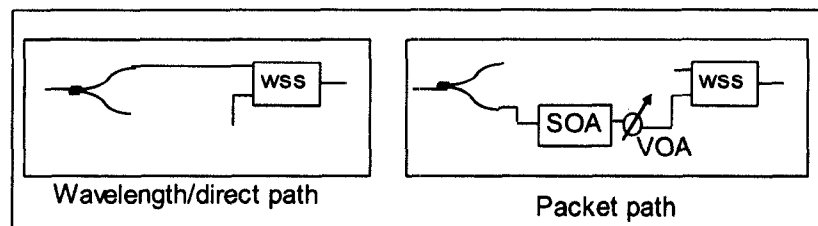


Fig. 7.20. Switch configurations for characterizing the wavelength and packet paths.

At a loop input power of -13.5 dBm, the number of circulations for the packet path, were measured for varying input power at the SOA. A VOA was used to vary the input power to the SOA. Fig. 7.22 shows the number of circulations, at a BER of 10^{-9} for an input power range of -17 dBm to -7dBm (shown in '▲') at the SOA. The number of loops gradually drops from 18, at -17 dBm, to 15, at -11 dBm. The drop in number of loops (or the signal quality) is mainly due to additional ASE noise accumulations from the SOA and its carrier dynamics. For power level above -10 dBm, number of loops starts to drop sharply

and is limited to 5 at a power of -7 dBm due to the additional degradation from gain saturation induced effects of the SOAs at high input powers.

When the number of channels passed through the SOA were increased to two the cascability is lesser by ~ 2 (shown in '□') at low input powers and fast decay in number of loops is observed at a lower power per channel, -13 dBm, compared to that of single channel system. For a five channel system (shown in '◆'), the cascability is 14 loops at low signal power per channel, -17 dBm, and beyond that a sharp decay is observed as the input power per channel is increased.

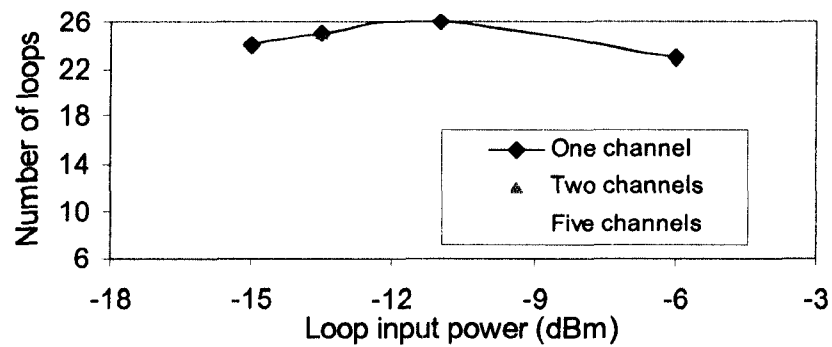


Fig. 7.21. Number of loops as a function of loop input power (per channel) of the wavelength path.

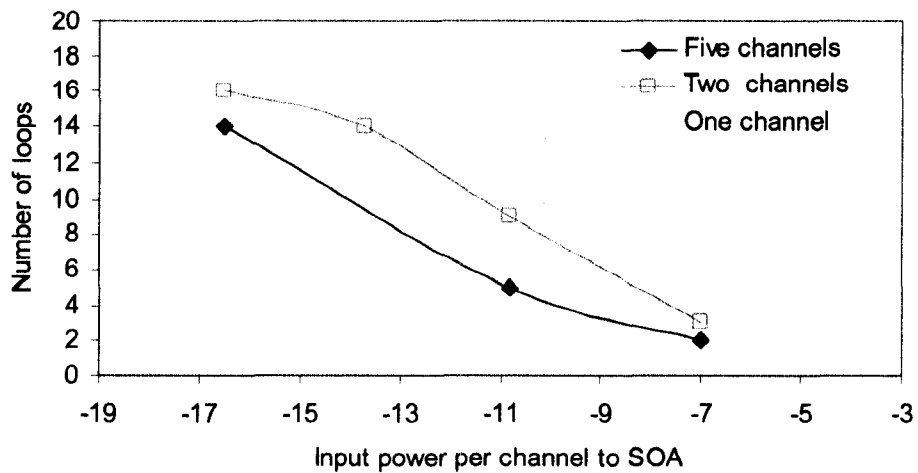


Fig. 7.22. BER as a function of number of loops for the packet path.

For the packet path, the decay in signal quality or the loops cascaded is very sensitive to total input power level, power per channel and number of channels, at the SOA input. Because, deeper the SOA is driven into saturation the more severe is the extinction

ratio degradation due to gain dynamics and, in addition, in multi-channel systems, the larger is the impact due to XGM and FWM effects. The eye diagrams of a five channel system are shown in Fig. 7.23, at loop input power of -13.5 dBm/channel, for both wavelength path and the packet path at the number of loops of 25 and 5, respectively. The channel power at the SOA input was -7dBm (total input power of 0 dBm). In the packet path, the noise accumulations in the 'one' state are severe, even at only 5 loops, due to ASE, gain compression, and inter-channel crosstalk effects from the SOA.

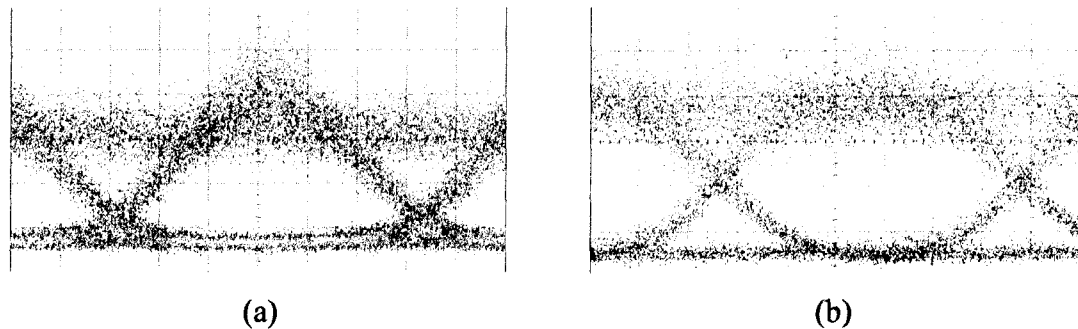


Fig. 7.23. Eye diagrams: (a) wavelength path, five channels, at 22 loops; (b) packet path, five channels, at 5 loops.

7.5.5 Summary and discussion on switch characterization

In a single stage configuration, the switch shows the best performance with penalties of < 0.2 dB for the packet path (compared to wavelength path) if the SOA is operated in the linear gain region. In the small signal region, the ASE noise deteriorates the signal quality while in the saturation region, the gain dynamics of the SOA degrades the extinction ratio of the signal. For a signal channel operation, input power dynamic range of > 20 dB can be obtained, for the packet path, with penalties of less than 3 dB. For multiple channel operation, signal degradation arises mainly due to operation of the SOA in gain saturation due to high total input powers. The penalty incurred can be limited to 2.5 dB for 16 channel systems at typical input power per channel of ~ -10 dBm. For few numbers of channels (≤ 3) the inter-channel crosstalk due to XGM dominates. For higher number of channels gain compression and crosstalk due to FWM dominate and the crosstalk due to XGM becomes negligible.

For cascading of the switch in a periodic ring network, the wavelength path shows a good tolerance (> 22 cascades) to input power dynamics and number of channels. However,

for the packet path, the cascability is strongly influenced by the number of channels and channel per power. For a five channel system, the number of cascades of 10 can be achieved with channel power as high as -13 dBm. Once the SOA enters to gain saturation, the cascability drastically drops with increasing input power, due to gain dynamics and inter-channel crosstalk and crosstalk due to FWM.

For packet switching applications in DWDM systems, there are various techniques that have been reported to improve the non-linear effects of the SOA in gain saturation. To minimize the XGM and FWM effects, different encoding schemes, such as return-to-zero (RZ) differential quadrature phase-shift keying (DQPSK) and polarization multiplexed RZ-DQPSK are proposed [111] to overcome the temporal power variations and crosstalk from FWM generated channels, which are seen in systems using conventional ON-OFF keying. In another scheme, Manchester-encoding has been proposed to suppress the XGM, for signal powers as high as 18 dBm, in conventional SOAs [112]. For minimizing the FWM effects, unequal channel spacing schemes on the ITU grid can be employed for the channels allocated for packet switching [113].

In these experiments, the switch was characterized by considering single port (single incoming fiber) being active. Though the impact of most of the impairments can be investigated with single port being active, studying the impact due to crosstalk from other ports requires full implementation and lighting of all ports of any given switch dimension. Due to limited resources, the penalty measurement on crosstalk was not carried out. However, an analytical study on crosstalk induced performance of SOA switches was presented in Chapter 3.

7.5.6 Performance comparison between SOA switch structures

A comparison between the two SOA switch structures in terms of main parameters is given in Table 7.3. The switch that can support wavelength and time domain performs better over all in terms of impairments as each SOA handles a single wavelength. But, it requires a higher number of SOAs compared to the time domain switch.

Table 7.3. A comparison between the two SOA switch structures.

| | SOA Switch supporting wavelength and time domain, Fig 7.2 (a) | SOA switch supporting time domain, Fig. 7.2 (b) | Comments |
|--------------------------|---|---|---|
| Loss (dB) | $2(3 \log_2 N + L_m) - G$ | $2(3 \log_2 N) - G$ | N - SOA switch dimension L_m - multiplexer loss G - gain of the SOA |
| Number of SOAs | $N^2 W$ | N^2 | W - number of wavelengths |
| Impairments due to SOA | ASE, patterning effects | Gain saturation, XGM, FWM, ASE | |
| Input power range to SOA | Good (> 20 dB) | Low* (10 dB) | For penalty < 3dB * Function of wavelengths |
| Impact due to crosstalk | Negligible** | Moderate*** | ** Second order effect *** First order effect |

7.6 Summary

The implementation options of a heterogeneous switch capable of routing at wavelength and packet levels were reported. The physical layer performances of the switch to various impairments were experimentally quantified for single stage and cascaded stages. The operating regions, in terms power levels and number of channels were summarized for given penalty margins.

The switch was implemented by adding SOA gates to the wavelength switch (WSS), to realize fast packet switching on predetermined wavelengths. Initially, the state-of-the art on SOA technology was given briefly and the possible impairments faced by using the SOA were addressed. The optical properties of a commercial SOA, gain as functions of drive current, input power, and wavelength and noise figure were measured and reported.

The optical performance of the switch (WSS+SOA) was then carried out for single stage network (star). The switch performs well if the SOA is operated in the linear region. However, when the SOA is pushed to gain saturation due to high input powers the packet path incurs considerable penalties due to gain dynamics and pattern effects, in single wavelength operation and gain compression, XGM, and FWM effects in multi-channel operation. For a total input power, in the range of -16 to 2 dBm, penalties for the packet

path of < 2.5 dB can be obtained. When tested under dynamic packet switching, a negligible penalty (< 0.2 dB) was measured compared to that of static operation of the SOA.

To emulate a periodic ring network, the switch was tested in a re-circulating loop. The wavelength path showed a good tolerance (> 22 cascades) to input power dynamics and number of channels while, for the packet path, the cascadability was found to be strongly influenced by the number of channels and channel per power. For a five channel system, the number of cascades of 10 can be achieved with channel power as high as -13 dBm. The cascadability dropped drastically once the SOA entered gain saturation due to the rapid accumulation of ASE and non-linear effects of the SOA.

Finally, the performance of the two switch structures that support wavelength and time domain and time domain were compared. The structure that support wavelength and time domain performs better overall in terms of power dynamic, inter-channel crosstalk, and in-band crosstalk.

8 Conclusions and future directions

8.1 Conclusions

With the exponentially growing demand for the bandwidth, the communication industries are pushed with the need to expand the emerging optical network, with increasing capacity and scale. Optical switches play a major role in tackling this demand efficiently and cost effectively. Many optical switching technologies have been explored but only a few have succeeded stepping out the laboratories and finding practical applications. This thesis has focused on investigating the scalability of three such potential switches, directional coupler (DC) switches, wavelength selective switches (WSS), and semiconductor optical amplifier (SOA) gates by exploring and assessing the performance of different architectural options. Further, the performance aspects and the scalability of optically switched networks was also studied to investigate the fundamental limitations due to physical layer impairments to direct for optimal operating conditions under a given set of network configurations and parameters.

Firstly, integrated electro-optic DC-based switches that are very attractive due to its fast switching times and compactness were addressed. Study of scaling limitations due to impairments has been poorly addressed by ignoring some sources of impairments in the switch and using closed-form models with limited insights. For more accurate representation, a numerical model was developed, in this thesis, taking into account all possible impairments, including the ASE from the loss compensating amplifier, with the aim of optimizing the switch performance in terms of various parameters. It was shown that the receiver threshold setting has an impact on switch crosstalk and ASE induced power penalties and it can be optimized to relax the crosstalk requirement by ~ 6 dB. A tutorial on a DC switch design example considering different structural options was also presented.

Next, WSS, the key element in building flexible and degree upgradeable ROADMs, which are essential for the design and deployment of future optical transport networks, was considered. Multi-degree node implementations options of WSS-based ROADMs were

analyzed in terms of switch crosstalk and it was shown through experimental investigation that for a given node degree and functionality, the number of WSS required per ROADM can be reduced by half –instead of using pair of WSSs for adding and dropping, one could use splitter (for dropping) and a WSS (for adding) without trading off significant crosstalk accumulations compared to that with pairs of WSSs. To minimize crosstalk, one could take advantage of the inherent nature of the WSS that could serve both as a wavelength blocker and a switch in adding. To address the pay-as-you grow approach, a modular architecture to implement a large degree ROADM node using currently available WSSs has also been proposed. The scalability of the proposed architecture with respect to in-band crosstalk was also studied by making use of the crosstalk measurements carried out in an 8 x 8 ROADM. The results indicate that node degrees of 150 can be achieved at 1 dB of power penalty.

Thirdly, to update and extend the switching granularity to a finer level, time slots or packet, multi-granularity switch was studied in order to improve bandwidth utilization in current wavelength add/drop networks. The switch was implemented by adding SOA gates to the wavelength switch (WSS), to realize fast packet switching on predetermined wavelengths. For the implementation of the SOA switch fabrics, two different granularities were considered, wavelength and time and time (wavelength striped), and the physical layer performances of the switch to various impairments were experimentally quantified.

In a single stage configuration, the switch shows the best performance with penalties of < 0.2 dB for the packet path (compared to wavelength path) if the SOA is operated in the linear gain region. However, when the SOA is pushed to gain saturation due to high input powers the packet path incurs considerable penalties due to gain dynamics and pattern effects, in single channel operation and gain compression, XGM, and FWM effects in multi-channel operation. For a total input power, in the range of -16 to 2 dBm, penalties for the packet path of < 2.5 dB can be obtained. When tested under dynamic packet switching, a negligible penalty (< 0.2 dB) was measured compared to that of static operation of the SOA.

The remaining part of the thesis work was devoted to study the scaling limitations of optical networks with cascaded switches and links due to the effect of combined and accumulated impairments. To emulate periodic add/drop networks experimentally, an optical re-circulating loop (RCL) was used. The loop consisted of 75 km of non-zero

dispersion shifted fiber (NZ-DSF), EDFAs, and WSS, with power splitters and fast switches for the control and operation of the loop. NZ-DSF shows a reduced dispersion profile of < 5 ps/nm-km in the C-band and is mainly used in cost sensitive metro networks to benefit from the exclusion of expensive in-line and post dispersion compensation. The measurements were carried out at a bit rate of 2.5 Gb/s.

Initially, transmission measurements were carried out to find out the influence of ASE noise and dispersion on the cascability limit on the number of loops, by setting the WSS in passing through without any adding/dropping. It was found that, the ASE accumulation dominated over the dispersion, and limited the number of loops cascaded to 24, due to the high noise figure of the EDFAs (7.8 dB). The experimental results were verified with the results from numerical and analytical models to confirm the accuracy of the experimental results.

Next, the cascability of periodic add/drop optical ring networks constructed using WSS-based ROADM was studied in the presence of crosstalk, ASE, and fiber dispersion. Due to limited resources and the complexity involved in accurately setting up the experiments to investigate crosstalk induced penalty in RCL, a numerical study was conducted. The experimentally verified numerical model was used with necessary modifications to represent a generic network model consisting of metro and interconnecting rings with varying node degrees. The impact of fiber dispersion on the WSS crosstalk was investigated as functions of bit rates, node degrees, and dispersion. The results showed that at 2.5 Gb/s, the fiber dispersion left uncompensated did not impose stringent crosstalk requirements compared to that with zero dispersion. At measured WSS crosstalk, metro rings can be constructed with 18 periodic add-drop nodes at a link distance of 75 km and core rings that interconnect several metro rings can be constructed with 8 add-drop nodes at a link distance of 150 km for fiber dispersions as high as 4.6 ps/nm-km. The tolerance to WSS crosstalk, however, drastically drops at 10 Gb/s with dispersion (link distance). To implement a 16 node metro ring, at a link distance of 75 km, the fiber dispersion should be limited to a value of 1.2 ps/nm-km.

Finally, the cascability of the multi-granularity switch was tested using the recirculating loop. The wavelength path showed a good tolerance (> 22 cascades) to input power dynamics and number of channels while, for the packet path, the cascability was

found to be strongly influenced by the number of channels and channel per power due to the rapid accumulations of ASE and nonlinear effects of the SOA in gain saturation. For a five channel systems 10 cascades can be achieved with channel power as high as -13 dBm. Comparing the two switch structures that support wavelength and time domain and time domain, the former performs better overall in terms of power dynamic, inter-channel crosstalk, and in-band crosstalk due to single channel operation.

8.2 Original contributions

Based on the above mentioned work (Sec. 8.1), the following original contributions to the field of fiber optic networks and systems were made:

- Cost effective structure for multi-degree WSS-based ROADM node, which optimizes the performance due to switch crosstalk, for add/drop metro networks was identified and reported for the first time¹.
- A new modular architecture for large degree ROADM nodes by using the currently available WSS as building blocks for future networks to offer benefits such as pay-as-you-grow was reported¹.
- Numerical study and the results involving the performance of cost sensitive metro add/drop networks in the presence of fiber dispersion and its impact on the tolerance to switch crosstalk were presented for the first time².
- The characterization of the physical layer performance of cascaded multi-granularity switching nodes, implemented with WSS and SOA was reported for the first time.
- An improved numerical model to study the design and performance optimization of directional coupler switches was presented³.
- For AAPN: suitable architectural options for the implementation of core switch at various port counts were suggested⁴.

¹ R. Shankar, T. J. Hall, M. Florjańczyk, A. Vukovic, and H. Hua, "Multi-degree ROADM based on Wavelength Selective Switches: Architectures and Scalability," *Optics Communications*, Vol. 279, 2007, pp. 94-100

² R. Shankar, J. Couturier, K. Hinzer, and T. J. Hall, "Scalability analysis in terms of crosstalk in NZ-DSF ring networks constructed with WSS based ROADM," *Proc. of SPIE*, Vol. 6796, 2007

³ R. Shankar, T. J. Hall, "Performance Analysis of Directional Coupler Based Switches Using Statistical Modeling," *IEEE-CCECE*, Ottawa, Canada, May 7-10, 2006

⁴ R. Shankar, T. J. Hall, "Core Switch Architectures for the Agile All-Photonic Network: Performance Evaluation with Crosstalk," *IEEE-INDICON*, India, December 12-14, 2005

8.3 Future directions

Future directions for the continuation of this work could be as follows:

1. Repeating the re-circulating loop experiments at a bit rate of 10 Gb/s to investigate the scaling limitations due to impairments and their impact on the tolerance to switch crosstalk.
2. Constructing a double re-circulating loop to investigate non-periodic (links and add/drop) networks and the implementation of appropriate switch control software codes.
3. Implementing the current drivers for the SOA with increased bandwidth for switching of packets in lengths of few tens of ns and constructing an 8 × 8 SOA switch prototype, including control plane, and fully assessing the signal impairments.
4. Carrying out the above experiment (3) for increased number of wavelengths and at varying channel spacing, 50, 100, and 200 GHz to investigate the influence of channel spacing on the impairments due to inter channels and studying on optimum channels allocation schemes for packet switching to minimize FWM effect of the SOA.
5. Studying of using different modulation formats for signal transmission to minimize the penalty incurred due to temporal gain variations of the SOA.

References

- [1] Y. Inada et. al, "32 /spl times/ 40-Gb/s dense WDM transmission over 3000 km using "double-hybrid" fiber configuration," *IEEE Photonics Technology Letters*, Vol. 14, No 9, 2002, pp. 1366-1368.
- [2] T. McDermott and T. Brewer, "Large-scale IP router using a high-speed optical element," *Journal of Optical Networking*, Vol. 2, No. 7, 2003, pp. 229-240.
- [3] J. Gripp, "Optical switch fabrics for terabit-class routers and packet switches," *Journal of Optical Networking*, Vol. 2, No. 7, July 2003, pp. 243-254.
- [4] D. Breuer, "Network upgrade from telecom operators view," *Optical Fiber Communication Conference 2007*, paper OThS7.
- [5] B. P. Keyworth, "ROADM subsystems & technologies," *Optical Fiber Communication Conference 2005*, paper OWB5
- [6] D. K. Hunter, I. Andonovic, "Approaches to optical Internet packet switching," *IEEE Communications Magazine*, Vol. 38, No. 9, 2000, pp. 116-122.
- [7] G. I. Papadimitriou, C. Papazoglou, A. S. Pomportsis, Optical switching: switch fabrics, techniques, and architectures *Journal of Lightwave Technology*, Vol. 21, No. 2, 2003, pp. 384- 405.
- [8] G. V. Bochmann et al, "The Agile All-Photonic Network: An Architectural Outline," in *Proc. Biennial Symp. On Comm.*, Kingston, Canada, May, 2004.
- [9] A. Stavdas, "Scheme for performing statistical multiplexing in the optical layer," *Journal of Optical Networking*, Vol. 4, No. 5, 2005, pp. 237-247.
- [10] C. Guillemot, "Transparent Optical Packet Switching: the European ACTS KEOPS Project Approach," *IEEE/OSA Journal of Lightwave Technology*, Vol. 16, No. 12, 1998, pp. 2117-2134.
- [11] D. K. Hunter, "WASPNET - a Wavelength Switched Packet Network," *IEEE Communications Magazine*, Mar. 1999, pp. 120-129

- [12] A. Carena, M. D. Vaughn, R. Gaudino, M. Shell, and D. J. Blumenthal, "An optical packet experimental routing architecture with label swapping capability," *IEEE/OSA Journal of Lightwave Technology*, Vol. 16, No. 12, 1998, pp. 2135-2145
- [13] L. Dittman, et al., "The European IST Project DAVID: a viable approach toward optical packet switching. Architecture and performance of AWG-based optical switching nodes for IP networks," *IEEE Journal of Selected Areas in Communications*, Vol. 21, No. 7, Sep. 2003, pp. 1026-1040.
- [14] E. L. Goldsten, L. Eskildsen, and A. F. Elrefaie, "Performance Implications of Component Crosstalk in Transparent Lightwave Networks," *IEEE Photonics Technology Letters*, Vol. 6, No. 5, May 1994, pp. 657-660.
- [15] E. L. Goldstein and L. Eskildsen, "Scaling Limitation in Transparent Optical Networks Due to Low-Level Crosstalk," *IEEE Photonics Technology Letters*, Vol. 7, No. 11, 1995, pp. 93-94.
- [16] T. Y. Chai, T. H. Cheng, Y. Ye, and Q. Liu, "Inband Crosstalk Analysis of Optical Cross-Connect Architectures," *IEEE/OSA Journal of Lightwave Technology*, Vol. 23, No. 2, 2005, pp. 688-700.
- [17] Y. Jianjun, P. Jeppesen, "Improvement of cascaded semiconductor optical amplifier gates by using holding light injection," *IEEE/OSA Journal of Lightwave Technology*, Vol. 19, No. 5, 2001, pp. 614 – 623.
- [18] R. Ramaswami, and K. N. Sivarajan, "Optical Networks, A practical perspective," Morgan Kaufmann, 2002.
- [19] T. Ducellier, A. Hnatiw, M. Mala, S. Shaw, A. Mank, D. Touahri, D. McMullin, T. Zami, B. Lavigne, P. Peloso, and O. Leclerc, "Novel High Performance Hybrid Waveguide-MEMS 1x 9 Wavelength Selective Switch in a 32-Cascaded Loop Experiment," *Proc. Conf. ECOC*, 2004.
- [20] B. P. Keyworth, "ROADM Subsystems & Technologies, *Optical Fiber Communication Conference 2005*, paper OWB5.
- [21] L. Eldada, "40-Channel Ultra-low-power compact PLC-based ROADM subsystem," *Optical Fiber Communication Conference 2006*, paper NThC4.
- [22] A. K. Dutta, N. K. Dutta, and M. Fujiwara, WDM Technologies : Optical Networks, Elsevier Academic press, 2004.

- [23] K. A. Williams, "Integrated semiconductor-optical-amplifier-based switch fabrics for high-capacity interconnects, *Journal of Optical Networking*, Vol. 6, No. 2, 2007, pp. 189-199.
- [24] M. Vasilyev, "Transparent ultra-long-haul DWDM networks with "broadcast-and-select" OADM/OXC architecture," *Journal of Lightwave Technology*, Vol. 21, No. 11, 2003, pp. 2661-2672.
- [25] X. Ma, and G. S. Kuo, Optical switching Technology comparison: optical MEMS vs other technologies, *IEEE Communication Magazine*, special issue on optical networking, Nov. 2003, pp. s16-s23
- [26] S.Araki et al., "Highly scalable optoelectronic packet-switching fabric based on wavelength-division and space-division optical switch architecture for use in the photonic core node," *Journal of Optical Networking*, Vol. 2 No. 7, 2003, pp. 213-228.
- [27] A. Jourdan, F. Masetti, M. Garnot, G. Soulage, M. Sotom, "Design and implementation of a fully reconfigurable all-optical for high capacity multiwavelength transport networks," *Journal of Lightwave Technology*, Vol. 14, No. 6, 1996, pp. 1198-1206.
- [28] G. R. Hill et. al., "A transport network layer based on optical network elements, *Journal of Lightwave Technology*, Vol. 11, No. 5/6, 1993, pp. 667-679.
- [29] N. Kataoka et. al., "Field trial of data-granularity-flexible reconfigurable OADM with wavelength-packet-selective switch, *Journal of Lightwave Technology*, Vol. 24, No. 1, 2006, pp. 88-94.
- [30] S. Okamoto, A. Watanabe, K.-I. Sato, "Optical path cross-connect node architectures for photonic transport network, *Journal of Lightwave Technology*, Vol. 14, No. 6, 1996, pp. 1410-1422.
- [31] C. Develder et al," Multistage Architectures for Optical Packet Switching Using SOA-Based Broadcast-and-Select Switches," *Optical Fiber Communication Conference 2003*, Vol. 2, pp. 794-795.
- [32] J. Cheyns et. al., Clos lives on in optical packet switching, "*IEEE Communication Magazine*, Feb. 2004, pp. 114-121.
- [33] A. Stavdas et. al, "An OXC Architecture suitable for High Density WDM wavelength Routed Networks, "*Photonic Network communications*, Vol. 1, 1999, pp. 77-88.

- [34] P. DeDobbelaere, K. Falta, K. S. Gloeckner, S. Patra, "Digital MEMS for optical switching", *IEEE Communication Magazine*, Vol. 40, No. 3, Mar. 2002, pp. 88-95
- [35] G. I. Papadimitriou; C. Papazoglou, C.; A. S. Pomportsis, "Optical switching: switch fabrics, techniques, and architectures", *Journal of Lightwave Technology*, Vol. 21, No. 2, Feb. 2003, pp. 384-405.
- [36] P. J. Duthie, M. J. Wale, "16 x 16 Single chip optical switch array in Lithium Niobate," *Electronics Letters*, Vol. 27, No. 14, 1991, pp. 1265-1266.
- [37] T. Goh et. al, "Low loss and high extinction ratio strictly nonblocking 16x16 thermo-optic matrix switch on 6-in wafer using silica-based planar lightwave circuit technology, *Journal of Lightwave Technology* , Vol. 19, No. 3, 2001, pp. 371-379.
- [38] W. A. Crossland, et. al., "Holographic optical switching: the "ROSES" demonstrator," *Journal of Lightwave Technology*, Vol. 18, No. 12 , 2000, pp. 1845-1854.
- [39] K. Noguchi, "Optical free-space multichannel switches composed of liquid-crystal light-modulator arrays and birefringent crystals, *Journal of Lightwave Technology*, Vol. 16, No. 8, 1998, pp. 1473-1481.
- [40] E. Almstrom et. al, "Experimental and analytical evaluation of packaged 4x4 InGaAsP/InP semiconductor optical amplifier gate switch matrices for optical networks, *Journal of Lightwave Technology*, Vol. 14, No. 6, Jun 1996, pp. 996-1004.
- [41] W. van Berlo et. al, Polarization-insensitive, monolithic 4x4 InGaAsP-InP laser amplifier gate switch matrix, "*IEEE Photonics Technology Letters*, Vol. 7, No. 11, 1995, pp. 1291-1293.
- [42] F. Dorgeuille et. al, "1.28 Tb/s throughput 8 x 8 optical switch based on arrays of gain clamped semiconductor amplifier gate arrays," *Optical Fiber Communication Conference 2000*, paper PD18-1.
- [43] J. S. Barton et. al., "2.5- Gb/s Error-free wavelength conversion using a monolithically integrated widely tunable SGDBR-SOA-MZ transmitter and integrated photodetector, "*IEEE Photonics Technology Letters*, Vol. 16, No. 6, 2004, pp. 1531-1533.
- [44] S. Murata, A. Tomita, J. Shimizu, and S. Suzuki, " THz optical frequency conversion of 1 Gb/s signals using highly nondegenerate four-wave mixing in an InGaAsP semiconductor laser," *IEEE Photonics Technology Letters*, Vol. 3, Nov 1991, pp. 1021-1023.

- [45] M. W. K. Mark and H. K. Tsang, "Polarization-insensitive widely tunable wavelength converter using a single semiconductor optical amplifier," *Electronic letters*, Vol. 36, No. 2, Jan. 2000, pp. 152-153.
- [46] C. Joergensen, S. L. Danielsen, K. E. Stubkjaer, M. Schilling, K. Daub, P. Doussiere, F. Pommerau, P. B. Hansen, H. N. Poulsen, A. Kloch, M. Vaa, B. Mikkelsen, E. Lach, G. Laube, W. Idler, and K. Wunstel, "All-optical wavelength conversion at bit rates above 10 Gb/s using semiconductor optical amplifiers," *IEEE Journal of Selected Topics on Quantum Electronics*, Vol. 3, No. 5, 1997, pp. 1168-1180.
- [47] M. L. Masanovic et al, "Widely Tunable Monolithically Integrated All-Optical Wavelength Converters in InP," *Journal of Lightwave Technology*, Vol. 23, No. 3, 2005, pp. 1350-1362.
- [48] H. Takahashi, K. Oda, and H. Toba, "Impact of Crosstalk in Arrayed-Waveguide Multiplexer on Optical Interconnection," *Journal of Lightwave Technology*, Vol. 14, No. 6, 1996, pp. 1097-1105.
- [49] T. Y. Chai et al, "Crosstalk Analysis for Limited-Wavelength-Interchanging Cross Connects," *IEEE Photonics Technology Letters*, Vol. 14, No. 5, 2002, pp. 696-698.
- [50] T. McDermott and T. Brewer, "Large-scale IP router using a high-speed optical switch element," *Journal of Optical Networking*, Vol. 2, No. 7, 2003, pp. 229-240.
- [51] N. Sahri et al., "A highly integrated 32-SOA gates optoelectronic module suitable for IP multi-terabit optical packet routers," *Optical Communication Conference 2001*, Washington D.C, Vol. 54, PD32-1.
- [52] L. Mason et al, " Topological Design and Dimensioning of Agile All Photonic Networks," *Computer Networking*, 2005, Accepted for publication.
- [53] R. A. Spanke, V. E. Benes, "N-stage planar optical permutation network," *Applied Optics*," Vol. 26, No. 7, 1987, pp.1226-1229.
- [54] M. Jinno et al., "Advanced optical transmission and switching technologies for next generation wavelength-abundant IP/Optical networks", *TERENA conference*, June 2005.
- [55] K. Okamoto, "Fabrication of 128-channel arrayed-waveguide grating multiplexer with 25 GHz channel spacing," *Electronic Letters*, Vol. 32, No. 16, 1996, pp. 1474-1475.

- [56] F. Ebisawa et al, "High-Speed 32-Channel Optical Wavelength Selector Using PLC Hybrid Integration," *Optical Communication Conference 1999*, ThB1-1, pp. 18-20.
- [57] C. Develder et al, "Multistage Architectures for Optical Packet Switching Using SOA-Based Broadcast-and-Select Switches," *Optical fiber Communication Conference 2003*, Vol. 2, pp. 794-795.
- [58] H. Takahashi et al, "Transmission characteristics of arrayed waveguide $N \times N$ wavelength multiplexer," *IEEE Journal of Lightwave Technology*, Vol. 13, 1995, pp. 447-455.
- [59] D. Wolfson et al., Detailed experimental investigation of all-active dual-order mode Mach-Zehnder wavelength converter", *Electronics letters*, Vol. 36, No. 15, July 2000, pp. 1296-1297.
- [60] J.E. Watson et. al., "A low-voltage 8 x 8 Ti:LiNbO₃ switch with a Dilated-Benes Architecture," *Journal of Lightwave Technology*, Vol. 8, No. 5, 1990, pp 794-801.
- [61] C. Burke, M. Fujiwara, M. Yamaguchi, H. Nishimoto, and H. Honmou, "Studies on a 128-line space-division switch using LiNbO₃ switch matrices and optical amplifiers," in *Photonics switching*, OSA Proceeding series, Washington, D.C., Vol. 8, 1991, pp. 2-6.
- [62] E. J. Murphy et. al., "16 x 16 strictly nonblocking guided-wave optical switching system", *Journal of Lightwave Technology*, Vol. 14, No. 3, 1996, pp 352-358.
- [63] I. Sawaki et. al "Rectangularly configured 4 x 4 Ti: LiNbO₃ matrix switch with low drive voltage," *IEEE Journal of Selected Areas in Communication*, Vol. 6, No. 7, 1988, pp 1267-1272
- [64] H. S. Hinton, "Photonic switching using directional couplers," *IEEE Communications Magazine*, Vol. 25, No. 5, 1987, pp. 16-26.
- [65] Chin-Tau Lea, "Bipartite graph design principle for photonic switching systems," *IEEE Transactions on Communications.*, Vol. 38, No. 4, 1990, pp. 529-538.
- [66] J. W. Goodman, "Fan-in and fan-out with optical interconnections," *Optica Acta*, Vol. 32, No. 12, 1985, pp. 1489-1496.
- [67] G. A. Bogert, "Ti:LiNbO₃ intersecting waveguides," *Electronics Letters*. Vol. 23, 1987, pp. 72-73.

- [68] K. Aretz, H. Bulow, "Reduction of crosstalk and losses of intersecting waveguide," *Electronics Letters*, Vol. 25, No. 11, 1989, pp. 730-731.
- [69] C. Clos, "A study of nonblocking switching networks," *The Bell Systems Technical Journal*, March 1953, pp. 406-424.
- [70] H. Okayama, A. Matoba, R. Shibuya, and T. Ishida, "Optical switch matrix with simplified N X N tree structure," *Journal of Lightwave Technology*, Vol. 7, No. 7, 1989, pp. 1023-1028.
- [71] R. A. Saponke, "Architectures for Guided-wave optical space switching systems," *IEEE Communication magazine*, Vol. 25, No. 5, 1987, pp. 42-48.
- [72] R. Shankar and T. J. Hall, "Characteristics and Scalability Study on Technologies for Fast Optical Switches," Technical Report, Agile All-Photonic Networks (AAPN), University of Ottawa, May 2004.
- [73] S. D. Dods, T. B. Anderson, "Calculation of Bit-Error Rates and Power Penalties Due to Incoherent Crosstalk in Optical Networks Using Taylor Series Expansions," *Journal of Lightwave Technology*, Vol. 23, 2000, pp. 1828-1836.
- [74] F. Liu, C. j. Ramussen, and J. S. Pedersen, "Experimental Verification of a New Model Describing the Influence of Incomplete Signal Extinction Ratio on the Sensitivity Degradation due to multiple Interferometric Crosstalk", *IEEE Photonics Technology Letters*, Vol. 11, 1999, pp. 137-139.
- [75] T. Y. Chai et al, "Crosstalk Analysis for Limited-Wavelength-Interchanging Cross Connects," *IEEE Photonics Technology Letters*, Vol. 14, No. 5, May 2002, pp. 696-698.
- [76] E. L. Goldstein, L. Eskildsen, C. Lin, and Y. Silberberg, "Polarization Statistics of Crosstalk-Induced Noise in Transparent Lightwave Networks," *IEEE Photon. Technol. Lett.*, Vol. 7, Nov., 1995, pp 1345-1347.
- [77] R. Ramaswami and P. A. Humblet, "Amplifier Induced Crosstalk in Multichannel Optical Networks," *Journal of Lightwave Technology*, Vol. 8, Dec. 1990, pp. 1882-1896.
- [78] M. Mezhoudi, R. Feldman, and R. Goudreault, "The value of multiple degree ROADMs on metropolitan network economics, in *Optical Fiber Communication*

- Conference*, 2006 OSA Technical Digest Series (Optical Society of America, 2006), paper NThA4.
- [79] B. Basch, R. Egorov, and S. Gringeri, "DWDM System Architecture and Design Trade-Offs," in *Optical Fiber Communication Conference*, 2006 OSA Technical Digest Series (Optical Society of America, 2006), paper NThC2.
- [80] S. D. Robinsion, "How ROADM Technology is Simplifying Network Management," in *Optical Fiber Communication Conference*, 2005 OSA Technical Digest Series (Optical Society of America, 2005), paper NThP2.
- [81] P. A. Boneafant and M. L. Jones, "OFC 2003 Workshop on Wavelength Selective Switching Based optical Networks," *Journal of Lightwave Technology*, Vol. 22, 2004, pp. 305-309.
- [82] E. B. Basch, R. Egorov, S. Gringeri, and S. Elby, "Architectural Tradeoffs for Reconfigurable Dense Wavelength-Division Multiplexing Systems," *IEEE Journal of Selected Areas in Communication*, Vol. 12, 2006, pp. 615-626.
- [83] T. Zami, B. Lavigne, and E. Balmerfrezol, "Crosstalk analysis applied to Wavelength Selective Switches," in *Optical Fiber Communication Conference*, 2006 OSA Technical Digest Series (Optical Society of America, 2006), paper OFP4.
- [84] Y. Shen, K. Lu, and W. Gu, "Coherent and Incoherent Crosstalk in WDM Optical Networks," *Journal of Lightwave Technology*, Vol. 17, No. 5, 1999, pp. 759-764.
- [85] H. K. Kim and S. Chandrasekhar, "Dependance of In-Band Crosstalk Penalty on the Signal Quality in Optical Network Systems," *IEEE Photonics Technology Letters*, Vol. 12, No. 9, 2000, pp. 1273-1274.
- [86] C. Caspar, M. Konotzer, F. Schmidt, E. Schulze, B. Strebels, and C. M. Weinert, "Influence of Cascaded Crosstalk Sources on Transparency Length," *IEEE Photonics Technology Letters*, Vol. 12, No. 6, 2000, pp. 737-739.
- [87] V. Mikhailov, "Investigation of high-speed wavelength-division-multiplexed (WDM) optical fiber transmission systems and devices using recirculating loop techniques," PhD thesis, University College London, 2003.
- [88] J. Couturier, "Development of an FPGA Optical Transceiver Interface for a Bandwidth Provisioning Switch Prototype and an Optical Recirculating Loop Controller" M. Sc. Thesis, University of Ottawa, 2008.

- [89] A. Girard, A. sundstrom, D. Kallgren, and M. Soderberg, "Network link readiness for 40 Gb/s transport, *Optical Fiber Communication Conference 2007*, paper NWC5
- [90] R. Srinivasan, A. K. Somani," Analysis of optical networks with heterogeneous grooming architectures," *IEEE/ACM transactions on networking*, vol. 12, No. 5., 2004, pp. 931- 943.
- [91] H. T. Mouftah, P. -H. Ho, *Optical Networks: Architecture and Survivability*, Kluwer Academic Publishers, 2003
- [92] R. Srinivasan, A. K. Somani," A generalized framework for analyzing time-space switched optical networks," *IEEE Journal of Selected Areas in Communication*, Vol. 20, No. 1., 2002, pp. 202- 215.
- [93] M. -F. Huang et. al., "Add/drop applications in fiber ring networks based on a reconfigurable optical add/drop multiplexer in a re-circulating loop, *Optics Communication*, Vol. 267, 2006, pp. 113-117.
- [94] V. Kaman, X. Zheng, S. Yuan; J. Klingshirn, C. Pularla; R.J. Helkey; O. Jerphagnon, J.E. Bowers "Cascadability of large-scale 3-D MEMS-based low-loss photonic cross-connects, *IEEE Photonics Technology Letters*, Vol. 17, 2005, pp. 771-773.
- [95] M. Macchi, "Design and demonstration of a reconfigurable metro-regional WDM 32 x 10 Gb/s system scaling beyond 500 km of G.652 fiber," *IEEE Journal of Selected Areas in Communication*, 2005, paper OTuP2.
- [96] B. Clouet et. al., "Cascadability study of 16 1 x 9 wavelength selective switches with 5x42.6 Gb/s CS-RZ channels, *Proc. Conf. ECOC*, 2005, paper We4.P.117.
- [97] T. Lin; K. A. Williams, R. V. Penty, I. H. White, M. Glick, "Capacity Scaling in a Multihost Wavelength-Striped SOA-Based Switch Fabric," *Journal of Lightwave Technology*, Vol. 25, No. 3, 2007, pp. 655-663.
- [98] K. A. Williams , G. F. Roberts , T. Lin , R. V. Penty , I. H. White , M. Glick and D. McAuley "Integrated optical 2," *IEEE Journal of Selected Topics in Quantum Electronics*, Vol. 11, No. 1, 2005, pp. 78-85.
- [99] O. Liboiron-Ladouceur , B. A. Small and K. Bergman "Physical layer scalability of WDM optical packet interconnection networks," *Journal of Lightwave Technology*., Vol. 24, Jan. 2006, pp. 262-270.

- [100] L. H. Spiekman , J. M. Wiesenfeld , A. H. Gnauck , L. D. Garrett , G. N. van de Hoven , T. van Dongen , M. J. H. Sander-Jochem and J. J. M. Binsma “Transmission of 8 DWDM channels at 20 Gb/s over 160 km of SMF using a cascade of SOA,” *IEEE Photonics Technology Letters*, Vol. 12, Jun. 2000, pp. 717.
- [101] Y. Yan et. al, “Error-free transmission of 32 x 2.5 Gb/s DWDM channels over 125 km using cascaded in-line semiconductor optical amplifiers, *Electronics letters*, Vol. 35, No. 21, pp1863-1864, Oct. 1999.
- [102] G. P. Agrawal, “Fiber-Optic Communication Systems,” Wiley Interscience, 1997
- [103] P. Doussiere et. al., “1.55 um polarization independent semiconductor optical amplifier with 25 dB fiber to fiber gain”, *IEEE Photonics Technology Letters*, Vol. 6, 1994, pp. 170-172.
- [104] C. Michie et.al., “Polarization-Insensitive SOAs Using Strained Bulk Active Regions,” *Journal of Lightwave Technology*, Vol. 24, No. 11, 2006, pp. 3920-3927.
- [105] M. Silver et. al., “Design and ASE characteristics of 1550-nm polarization-insensitive semiconductor optical amplifiers containing tensile and compressive wells”, *IEEE Journal of Quantum Electronics*, Vol. 36, 2000 pp 118-122.
- [106] T. Akiyama, M. Sugawara, Y. Arakawa, “ Quantum-dot semiconductor optical amplifiers”, *Proceedings of the IEEE*, Vol. 95, No. 9, Sep. 2007.
- [107] J. -Y. Emery et. al., “High performance 1550 nm polarization-insensitive semiconductor optical amplifier based on low-tensile-strained bulk GaInAsP,” *Electronics Letters*, Vol. 33, No. 12, June 1997, pp. 1083-1084.
- [108] F. Dorgeuille et. al., “Fast optical amplifier gate array for WDM routing and switching applications, “*Optical Fiber Communication Conference*, 1998., Feb. 1998, pp. 42 – 44.
- [109] A. Borghesani et. al., “High saturation power (>16.5 dBm) and low noise figure (<6 dB) semiconductor optical amplifier for C-band operation, *Optical Fiber Communication Conference*, March 2003, Vol. 2, pp. 534 – 536.
- [110] Tanaka, S.; Tomabechi, S.; Uetake, A.; Ekawa, M.; Morito, K.,”Record high saturation output power (+20 dBm) and low NF (6.0 dB) polarisation-insensitive MQW-SOA module,” *Electronics Letters*, Vol. 42, No. 18, 2006, pp. 1059 – 1060.

- [111] P.S. Cho, Y. Achiam, G. Levy-Yurista, M. Margalit; Y. Gross; J.B. Khurgin, "Investigation of SOA nonlinearities on the amplification of DWDM channels with spectral efficiency up to 2.5 b/s/Hz, *IEEE Photonics Technology Letters*, Vol. 16, March. 2004, pp. 918-920.
- [112] Y. Shibata, Y. Yamada, K. Habara, and N. Yoshimoto, "Semiconductor laser diode optical amplifiers/gates in photonic packet switching, "*Journal of Lightwave Technology*, Vol. 16, No. 12, 1998, pp. 2228-2235.
- [113] A. Bogoni, L. Poti, "Effective channel allocation to reduce inband FWM crosstalk in DWDM transmission systems", *IEEE Journal of Selected Topics in Quantum Electronics*, Vol. 10, 2004, pp 387-392.